ON THE DESIGN AND FUNCTIONALITY OF A SOLAR CHIMNEY, *SOLAR PRESSURE-STAGED WIND TUNNEL* ELECTRIC POWER GENERATING PLANT AND AN INTEGRATING SPHERE CALORIMETER.

BY

RECCAB OCHIENG MANYALA

A thesis submitted in fulfilment of the requirements for the degree of Doctor of Philosophy in Physics

DEPARTMENT OF PHYSICS

MASENO UNIVERSITY

ABSTRACT

The design and application of solar chimney and *solar pressure-staged wind tunnel* electric power generating plants involve the understanding of parameters which affect their operations and utilization. The size and dimensions of the systems are crucial factors for their power outputs in addition to environmental factors such as terrestrial radiation, wind speed and weather conditions. It is important to know how these factors are likely to affect the operation of full-scale systems under normal operational conditions prior to the actual design. The design and modelling offer a possibility to forecast how the system would operate before implementation. These processes give rise to systematic analysis and allow for material and parameter selections for the development of the perceived designs.

This thesis documents a study of three experimental designs for Renewable Energy Technology (RET). The first two experiments comprise a study of the design and simulation of a solar chimney and a *solar pressure-staged wind tunnel* electric power generating plant both of which can be useful for rural areas of developing countries. A study of the parameters that affect the operation of a model solar chimney and a *solar pressure-staged wind tunnel* electric power plant under various conditions was also carried out. The dimensions and conditions under which full-scale designs would operate were investigated for power output optimization purposes.

Although solar chimney electric power plants have been investigated theoretically and experimentally by a number of researchers working in the area of renewable energy, literature on models for use in rural areas of developing countries is rather scanty. To the best of our knowledge, no literature exists for models of solar pressure-staged wind tunnel power generating plants apart from one which gives a brief theory of the system in

comparison to the solar chimney electric power generating plant, hence the interest in the two systems.

Our work comprised the modelling of a sturdy solar chimney electric power generating plant that can be used in the rural areas. The study looked at the minimum dimensions that would maximize the power output in addition to other parameters such as temperature, air density and air velocity inside the chimney. Simulations were carried out to determine the values of the said parameters that would maximize the power output for minimum dimensions. The calculations showed that the power that can be generated by a solar chimney of specific dimensions depends on a threshold temperature ratio (τ) arising from the difference between the collector surface temperature and the temperature of the turbine $(T_s - T_H)$ and the difference between the air mass temperature under the roof and the collector surface temperature $(T_m - T_s)$. Our work showed that there exists a threshold, $\tau = 2.9$, for which an appreciable electric power $(\geq 10^3\ \text{W})$ can be generated by a sturdy and physically viable solar chimney with dimensions $L = 150\text{m}, H = R = 1.5\text{m}$ where L is the length of each side of the collector, H is the height of the turbine from the collector and R is the radius of the turbine vanes. A solar chimney with the foregoing dimension can comfortably serve a good number of households (about 50) in a typical rural setting.

The second aspect of the study looked at the design of a *solar pressure-staged wind tunnel* electric power plant. Our investigations show that the main parameters influencing appreciable power production are the size of the turbine vanes and the wind velocity inside the tunnel. It is shown that if the minimum area swept by the turbine vanes is $10{,}000\ \text{m}^2$ then the wind velocity must be about 7.5ms^{-1} in the tunnel so as to

provide approximately 10 kW of electric power. This requires that the diameter of the tunnel be approximately 100 meters. This result offers an opportunity to estimate the size of turbines for any desired electric power requirement and output for a *solar pressure-staged wind tunnel* electric power plant.

Solar selective surfaces/ absorbers are crucial in solar energy applications hence the knowledge of absorptance are of fundamental importance for materials used in solar thermal applications. The third aspect of this work was therefore dedicated to the design of a calorimeter based on the principle of an integrating sphere for the determination of thermal absorptance, α and emittance ε, of opaque bulk materials. A transient technique based on sample heating and cooling histories was employed to determine absorptance and emittance for copper and aluminium. Arrays of four thermocouples used as temperature sensors on the sample within the integrating sphere were interfaced to a thermal card on a Fluke-2286/5 data logger. Two of the thermocouples measured the average ambient temperature inside the sphere whereas the other two thermocouples were used to obtain an average value of the sample temperature. The data was used to calculate the absorptance and emittance of the samples.

The use of "integrating sphere calorimeter" configuration resulted in much simpler heat balance equations within the enclosure as opposed to other methods which rely on convective and radiative heat transfer coefficients. The equations used in our work were tested experimentally giving rise to thermophysical values which were in good agreement with values obtained using other methods

CHAPTER ONE

1.0 INTRODUCTION

This chapter gives background information, the basis and scope of the thesis, it further provides the motivation and objectives of the research as well as the significance of the study.

1.1 General introduction

Human beings, as long as they have existed on this earth, have used both the sun and fire as means of survival as outlined by Buti and Perlin [1]. Many cultures throughout history have considered the sun as a kind of deity, as the giver of light and life, the source of plenty, the enemy of darkness and evil. Around the world the sun is represented in art of many kinds, often associated with gods or royalty who derived power from its mystique. Today we understand more fully that the sun is the source of all life on our planet. The sun has power to create photosynthesis, which makes plants grow, which in turn feeds all life, including human beings. The earth's rotation around the sun initiates day and night; the varying tilt of the earth towards the sun is responsible for the seasons. The sun evaporates moisture from the seas, watering the land portions of the earth. Without the sun, all life would soon perish - small wonder that it has been worshipped, studied, and pondered on, and that humankind has tried through the ages to utilise its powers for many purposes.

Early solar study efforts include the success of early people in using the sun's energy to heat and cool living spaces. In ancient Greece, population growth was decimating forests; wood fuel was used heavily in small braziers to heat houses. It has been found that the ancient technology made use of the sun's heat. Excavations of

classical Greek cities show that nearly all the houses, even entire cities, were oriented to the south, permitting maximum heat in cold weather, while large overhangs prevented heat from entering the houses in the summer months. Similarly the Romans considered the sun in planning human dwellings. Solar energy was used for greenhouses and cold frames, at least by the wealthy. Even "sun-right" laws were enacted to protect householders from other houses that might interfere with their sunlight.

By the first century A. D., the invention of glass made it possible to turn some rooms into veritable "solar furnaces", using the "heat trap" principle, the basis of solar box cookers. It is in light of the foregoing that modern science has embraced the view of finding ways of using the sun more effectively as a source of energy after seeing the decline in production of the best known source of energy (fossil fuels). Other factors such as environmental issues have accelerated the search for more environmentally user friendly sources of energy [2].

The development of renewable energy sources, defined as energy from resources that are not depletable or are naturally replenished when used at sustainable levels, has been a major topic of research and study all over the world for many years. Renewable energy resources are normally taken as hydropower, solar, wind, biomass, ocean, and landfill gas. In addition to these renewable resources, fuel cell technology is included because fuel cells provide potentially significant, long-run environmental and economic benefits to the world, can be powered with renewable energy, need support for commercialisation, and have market barriers similar to barriers for renewable energy development.

There is need to develop renewable energy resources which are cheap and easily available for both domestic and commercial purposes. Many equipment and gadgets have

been designed and implemented for production and use with many renewable sources. This has been done in order to curb the problem of global energy shortage due to the fast rate at which one of the most efficient forms of energy (fossil fuels) is being depleted. Governments and nations all over the world are spending millions of dollars and many valuable resources in search of cheaper and renewable energy sources because of the enormous economic implications of future fuel shortage. However, the solution to the global energy shortage is far from being achieved because the efficiencies of renewable energy sources are low and require huge investments in terms of research, equipment and time.

It has been estimated by McMullan *et. al* [3] that 370×10^6 MW of energy is available from wind and wave power of the earth's surface, although a substantial portion of this will be dissipated over oceans or in inaccessible regions of the land mass. Thus, there is power available in the wind capable of making a contribution to the world's energy requirements provided that it can be harnessed in an economic and environmentally acceptable way.

Renewable energy sources can be derived from resources that are regenerative or for all practical purposes cannot be depleted. Hence, renewable energy sources are fundamentally different from fossil fuels, and do not produce as many greenhouse gases and other pollutants as fossil fuel combustion [4]. Some of these renewable energy sources have shown promising results on large economic scales. Attempts have been made to use many of these energy sources in large scales but with very little success. Various technologies have been develop and are still being developed to solve some of the problems associated with renewable energy sources.

The majority of renewable energy technologies (RET) are directly or indirectly powered by the sun. The relationship between RET and solar energy is shown schematically in Fig.1-1 [5] The earth-atmosphere system is in equilibrium such that heat radiation into space is equal to incoming solar radiation, the resulting level of energy within the system can roughly be described as the earth's "climate." The hydrosphere (water) absorbs a major fraction of the incoming radiation.

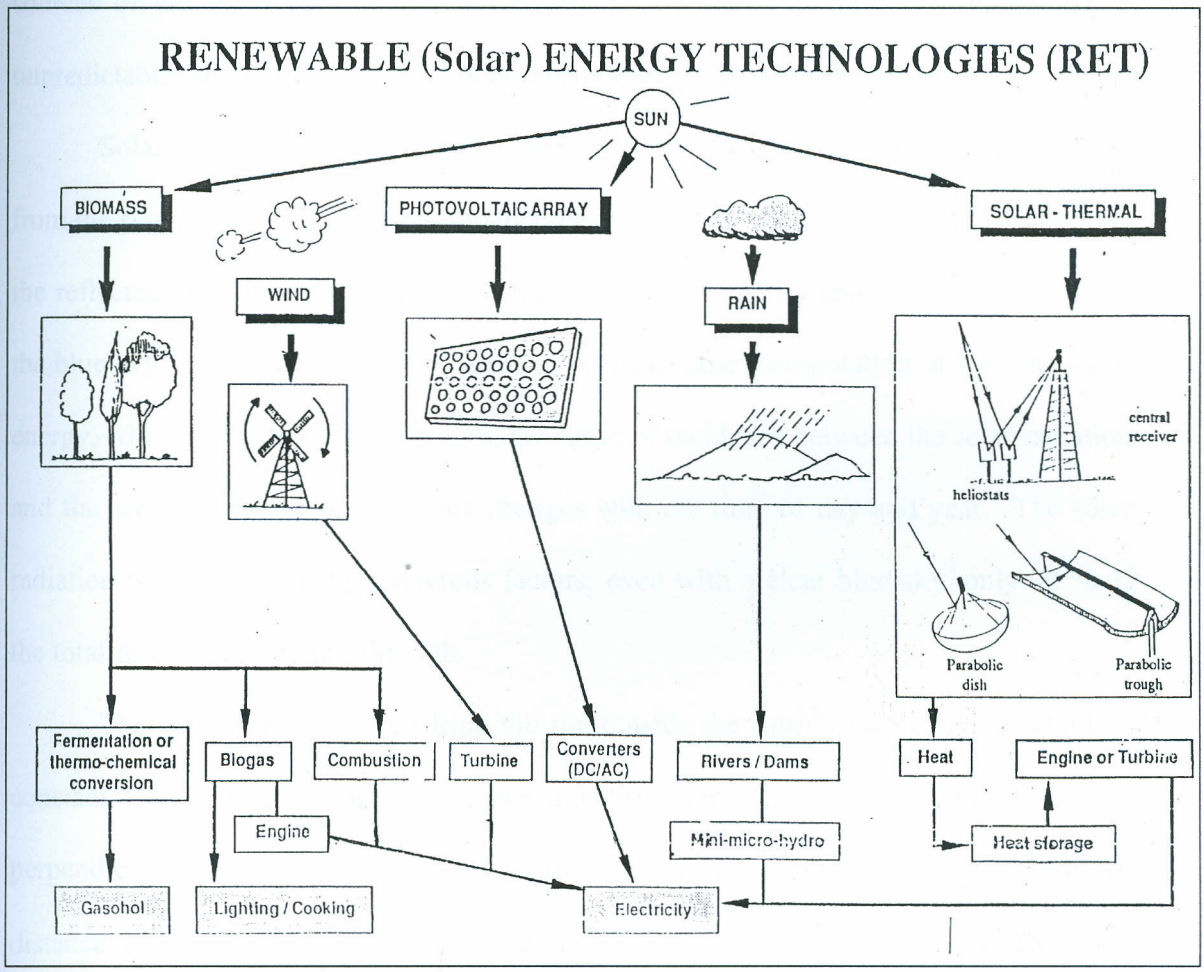

Fig.1-1. *Relationship between renewable energy technologies (RET) to solar energy [5].*

Most radiation is absorbed at low latitudes around the equator, but this energy is dissipated around the globe in the form of winds and ocean currents. Wave motion may

play a role in the process of transferring mechanical energy between the atmosphere and the ocean through wind stress. Solar energy is also responsible for the distribution of precipitation, which is tapped by hydroelectric projects, and for the growth of plants used to create bio fuels.

Other sources of energy, called conventional sources of energy, are mainly fossil fuels (coal petroleum and natural gas), and nuclear energy [6]. These conventional sources of energy have a life time and therefore reliance on them for future use is unpredictable; another reason why attention has shifted to renewable energy sources.

Solar radiation (also called insolation) consists of the radiation that comes directly from the sun as well as the radiation that comes indirectly. Indirect radiation includes: (1) the reflected radiation of an area, particularly areas covered by snow, (2) radiation from the blue sky, and (3) other diffuse radiation. For the exact computation of the amount of energy, which falls on a particular area, the angle of incidence between the solar radiation and the area is decisive because this changes with the time of day and year. The solar radiation is also reduced by numerous factors; even with a clear blue sky, only 90 % of the total solar radiation gets through.

The energy flux received from the sun outside the earth's surface is essentially a constant. The energy from the sun, per unit time, received on a unit area of surface perpendicular to the direction of propagation of the radiation at the mean earth-sun distance, outside the atmosphere is called the solar constant denoted by the symbol G_{sc}. The value of the solar constant has been a subject of extensive investigation. Prior to 1982, it was considered to be equal to $1353\,\mathrm{Wm^{-2}}$ before the standard value of $1367\,\mathrm{Wm^{-2}}$ was adopted by the World Radiation Centre (WRC) [7]. The value of

1367 Wm^{-2} with an uncertainty of 1% is normally used after allowing for immediately reflected incident radiation. A further loss is caused by the absorption of some fraction into the atmosphere so that under the most favourable conditions in desert areas, a maximum of 1000 Wm^{-2} is available. It is this quantity which is usually referred when considering solar power as the ultimate "free" and renewable energy source.

Unfortunately the value of 1000 Wm^{-2} is reduced considerably when averaged over 24 hours of the day to allow for periods of darkness and also when averaged over the year to allow for the greatly reduced amounts available in the winter. It is estimated that the solar output from the sun is about 3.5×10^{15} TW out of which some 1.8×10^{5} TW fall on the earth's surface. Some 30% of this is reflected as short-wave radiation, while a further 45% is converted to heat. The remaining 4×10^{4} TW manifests itself in the evaporation of water, in wind and waves and in photosynthesis. In theory, about 25% of the solar radiation reaching the earth is usable by plants, though in practice even the most efficient crop, sugar cane uses only some 1.4% of the available solar radiation during the year and the conversion efficiency for a forest is about 0.5% [8]. By far, the greatest impact of solar radiation at the earth's surface is in the evaporation of lakes, rivers and seas.

When the sun heats half of the earth, the other half, which is not heated, acquires a temperature less than the one which is heated. Thus, there is an imbalance in atmospheric temperature created. Cold air masses then rush to replace the warm air masses, an action, which causes wind to blow. The ultimate driving force of wind is the solar radiation, which generates pressure differences, which are the sources of wind.

Wind has been defined differently by various researchers and authors. The definitions, however, have the same meaning in one way or another. Moran and Morgan [9] define wind as nothing other than atmospheric circulation. Bansal *et. al.,* [10] however, define wind as air movement caused by the acceleration of air particles due to pressure differences in the atmosphere whereas Lutgens and Tarbuck [11] define wind simply as a result of horizontal difference in air pressure. Physics show that wind results from the expansion and convection of air as solar radiation is absorbed on earth [12]. We can therefore say that wind refers to the air movement as a result of air pressure differences. This movement is such that it is from a region with high pressure to one with low pressure. Wind can also be perceived as a result of nature's attempt to balance inequalities in pressure.

Generally, wind speeds follow patterns, which can repeat daily and seasonally. Regionally and globally, wind speed patterns can repeat but in most cases the repetition may take place after a long period of time. Since the patterns change frequently, the wind speed changes hourly, daily, monthly and annually. It is therefore necessary to have accurate data on types of wind patterns and factors affecting wind speed in order to determine indicators of high wind potentials to properly and appropriately utilise and plan for wind energy as a resource.

Average natural annual wind speeds vary from 0.5 to 18 ms^{-1} with the lower figure quoted by Iyer [13] for Dibrugarp in Assam, reputed to be the calmest place on earth. Putman [14] gives a five year average of 15 ms^{-1} at the summit of Mt. Washington at a height of 1920 m in the United States of America.

To be used for economic purposes, the average wind speed should lie between about 6.5 and 11.5 ms^{-1} giving an output power of between 100 and 500 Wm^{-2}.

Measurement of wind speed is complicated due to the fact that wind speed is not a scalar quantity but a three-dimensional vector parameter. Caused by larger scale pressure differences, its meeting with objects create small scale pressure differences accompanied by many complicated directional changes and separation of flows of air "parcels" (eddies). This behaviour has to be taken into account when measuring wind speed. The behaviour, through complicated interactions between the device and airflow affect measurements by the device.

Wind speed is measured by using anemometers. Several types of anemometers exist. These include the cup counter anemometer, the mechanical wind recorder (Woelfe type), the Dine pressure anemometer, the NAK FER W-6(OTA 15-M) totalizing anemometer and hot wire anemometer. Strip chart recorder, data loggers and magnetic tapes are used as auxiliaries to record or store data. Among these instruments, the cup counter anemometers are commonly used in weather stations in Africa. The Woelfe anemograph as it is sometimes called, is used to record instantaneous wind speed and direction. It consists of a wind vane, which serves to sense the wind direction and a set of three rotating cups, which measure the wind run. The difference in pressure causes the cups to move. The connection of all the three cups is such that each is connected independently to worm recording rollers via separate shafts, wheels and gears. The recording rollers trace separate curves on a continuous strip cart. Wind run and direction can be evaluated from the strip charts. The mechanical clock wound once per month by hand drives the strip chart. A calibrated "ladder rule" supplied by the manufacturer is used to evaluate hourly wind speed from average skewness of the trace. The wind

direction rollers trace a band on the strip chart. The average wind speed is estimated from the traced band.

The reliability of instruments differs from one to the other. Strip chart recorders for instance, have a long performance record although they cannot be considered extremely reliable [15]. However, their typical problems include the failure of chart drives, failure of chart marking mechanisms and paper jams.

Wind speed varies with height above ground level and terrain roughness. This is called *wind shear*. The variations occur within the height of local obstruction as well as in high winds [12]. A number of investigators have done work in determining the potential of wind as a source of energy for electric power generation mostly in Europe and Asia. Neil and Suruders [16] have given a thorough survey of wind development in the U.K, whereas Justus *et. al.*, Doran and Verhalek, Sedafain, Gupta, Hafzulla *et al.*, Satin and Sen, Kitagawa and Nomura, Sfestos, [17, 18-24] have developed general formulas and techniques of measuring or estimating wind speed and wind power density.

Incecik and Erdogmus, Özederm and Turkeli [25, 26] have specifically dealt with wind potential on the western coast of Anatoalia and wind energy potential estimation and micrositting on Izmir Institute of Technology Campus, Turkey respectively.

Oludhe and Ogallo [27] investigated the vertical characteristics of wind power densities at 24 sites in Kenya. The surface (10 m) wind power were independently extrapolated to 15, 20, 25, 30, 50, and 70 meter levels using the power law, logarithmic wind power formula and the Weibull distribution.

There is, however, inadequate data for Africa to carry out accurate predictions of wind energy. Low wind speeds prevail in many sub-Saharan African countries, particularly the land-locked nations. South Africa, North Africa and the Red Sea coast

have some of the highest wind potential in the region. Wind speeds of 7.2–9.7 ms^{-1} have been recorded around Cape Point and Cape Alguhas in South Africa. The North African coast is another attractive wind speed region and large scale wind power generation projects aiming to exploit this abundant energy source are now under way in Morocco. Kenya has a few wind generators such as the one at Ngong with a capacity of 0.35 MW which has been operating effectively as was reported by Kenya Power and Lighting Company in their 1994 annual report. There has been very little dissemination of wind turbines for electricity generation in sub-Saharan Africa, partly because of the low wind speeds and partly because of high costs. The problem is compounded by the low level of technical skills and lack of awareness of the potential of the technology. Few projects have been undertaken in sub-Saharan Africa, and there is only limited experience of wind energy for grid connected or mini-grid electricity generation. In comparison with other parts of the world, Africa has seen little development of modern wind turbines and most of its wind machines (found in eastern and southern Africa) are used for water pumping, rather than for electricity generation. Wind pumping supplies water for household use, irrigation and for livestock. South Africa and Namibia possess large numbers of wind pumps. In South Africa alone, an estimated 300,000 wind pumps are in operation [28].

1.2 Basis and scope of this work

1.2.1 Motivation

Supplying modern energy services to more than 2 billion people who still use traditional solid fuels and lack access to electricity is probably one of the most pressing problems facing humanity today. The amount of energy needed to satisfy the basic needs of rural populations around the world is relatively small, and appropriate technologies are

available. However, widening access to modern energy services is limited by the extreme poverty found particularly in the least developed countries. Living standards in rural areas can be significantly improved by promoting a shift from direct combustion of biomass fuels (dung, crop residues, and fuel wood) or coal in inefficient and polluting stoves to clean, efficient liquid or gaseous fuels and electricity. The aim of this work was to design a solar chimney, a *solar pressure-staged wind tunnel* electric power generating plant and study thermophysical properties of materials used as collectors to maximize the power production of these systems.

The focus to harness "free" energy from the sun has seen developments in many areas of renewable energy technology. The use of direct energy from the sun on a much bigger scale has been tried, however, the main problem of the mode of conversion employing solar thermal selective materials and solar concentrators, has been the low efficiency of these systems.

In developing technologies to convert the sun's energy directly into electricity, materials with certain thermophysical properties (specifically absorptance and emittance) are necessary. Methods for the determination of thermophysical properties of opaque bulk materials employ mostly the steady-state and transient techniques. Transient technique for determination of thermophysical properties of materials have been used in absorption calorimeters [29, 30, 31, 32]. These methods are based on various assumptions on the geometrical configurations of the sample chambers as well as the heat transfer mechanisms. Solar radiation and solar simulators have been employed in determining thermophysical properties of opaque materials. Electron beam probes and electric pulses have also been used for the determination of emittance at microscopic scales by some researchers.

Due to the high cost of materials for setting up experiments on solar chimney and *solar pressure-staged wind tunnel* electric power generating plants, we have used modelling technique as a means of study but used experimental technique to study absorptance and emittance of some opaque bulk materials using an integrating sphere calorimeter without ports.

1.2.2 Statement of the research problem

To construct a viable solar electric power generating plant capable of providing energy to fifty (50) households require appropriate design criteria and conditions. In this work we set out to provide designs of certain power generating plants and study thermophysical properties, specifically absorptance and emittance, of some opaque bulk materials which can be used as a selective surface in the said power generating plants.

1.2.3 Objectives of the research

The objectives of the study were:

(i) to design a single channel solar chimney electric power generating plant particularly suitable for rural settings in developing countries;

(ii) to design a *solar pressure-staged wind tunnel* electric power generating plant which can accommodate several channels;

(iii) to carry out studies of a suitable integrating sphere calorimeter which may be used to determine the parameters necessary for the maximization of power output of both the solar chimney and *solar pressure-staged wind tunnel* electric power generating plants.

1.2.4 Significance of the study

The first two aspects of the study involved modelling whereas the third aspect was experimental. The limitation to construct models in the first two aspects of the study was due to high cost of materials and lack of resources in terms of finances.

1.3 Thesis organization

In chapter two we give a comprehensive literature review of renewable energy sources in general and specifically present reviews on the solar chimney, *solar pressure - staged wind tunnel* electric power generating plant and solar thermal systems. A review of the availability of solar radiation and wind in addition to methods and techniques used for their measurements is presented.

The study of solar energy application, absorption and emittance from surfaces involves the knowledge of the spectral properties of surfaces. In chapter three we present thermodynamic considerations of the radiation properties of surfaces as well as the theory of solar chimney, *solar pressure-staged wind tunnel* electric power generators and the theory of thermophysical properties of some opaque bulk materials.

In chapter four we present the experimental work on the design, modelling, simulations and experiments as set out in the three aspects of our study. The design of a solar chimney capable of serving fifty (50) households in a rural setting is presented. We also present a model and simulation of a *solar pressure-staged wind tunnel* electric power generator for different electric power output capacities as well as a new experimental set-up for the determination of thermophysical properties of some opaque materials.

In chapter five, the results and discussion of our work as carried out on the three aspects of the study are presented; and finally, in chapter six, we draw conclusions on the

accomplished work and propose a possible direction for future work and give some recommendations on methods and techniques for the optimum utilisation of renewable energy technologies (RET).

CHAPTER TWO

2.0 LITERATURE REVIEW

2.1 Solar chimney technology

The history of the use of solar energy dates back to the Greek, Roman and Chinese empires when all explored the use of curved mirrors, which they found could concentrate the sun's rays in a manner that would cause nearly any object to explode in flames. This technology is referred to by Buti and Perlin [1] as the start of the current solar cooking movement. Interestingly, the use which was perceived by the Greeks, Romans and Chinese for this device was military - could they focus the burning mirror, as example, on an enemy warship? Burning mirrors were also used for less venal purposes, such as lighting altar fires and torches for sacrificial parades, but almost no other applied use was found. The idea, now seen in concentrating solar cookers, is in use in many parts of the world today.

A more direct route to solar cooking came from extensive efforts to harness the sun for horticulture. Though found in Roman times in wealthy households, it was not until the sixteenth century when glass became common and cheap enough to be used for horticulture. Travel and trade on a global basis had seen the transport of tropical plants and fruits to northern countries, creating a desire for these products, which could not be raised in northern climates. First the Dutch and Flemish, then French and English built greenhouses for this purpose, heated only by the sun. Substantial horticultural activity focused on tropical flora and food crops, all raised under glass, in greenhouses huge in scale. Using southern exposure and insulation as needed, the greenhouse movement later inspired the use of "conservatories" or "sun rooms" in homes, as well. The principle of the greenhouse, the so-called "solar heat trap", was further utilised in what is thought of

as the very first attempt to use solar energy to cook. Many scientists of the era, and laypersons as well, knew about the use of glass to trap heat, but Horace de Saussure, a French-Swiss scientist, wondered why that commonly understood phenomenon had not led to additional applied use. In 1767, he built a miniature greenhouse with five glass boxes one inside the other, set on a black tabletop. Fruit placed in the innermost box cooked nicely - and a new technology was born [1]. De Saussure continued his experimentation, using other materials, adding insulation, cooking at different altitudes, etc. This European scientist, exploring solar energy nearly 300 years ago, is widely considered to be the father of today's solar cooking movement. Others followed his lead, including the Briton, Sir John Herschel, and American Samuel Pierpont Langley, later head of the Smithsonian, both of whom conducted experiments with the hot box, the forerunner of today's box cooker, probably still the most common design in use. A French mathematician named Augustin Mouchot, working almost a century later, was eager to ensure that the learning of the past was not to be lost. He was more interested in practical application than in the number of interesting but not very useful solar devices which were appearing. With the newly discovered potential of the sun (whistles, water movers, talking statues, etc.), he began a search to use the sun's energy efficiently enough to boil water for steam engines, a venture that was not successful. His second project was more successful; he combined the heat trap idea with that of the burning mirror, creating an efficient solar oven from an insulated box, which when further modified by adding reflecting mirrors, even became a solar still. Eventually, Mouchot did create an effective steam engine, but it was too large to be practical; he turned back then to the cooking challenge and developed a number of solar ovens, stills, pumps, and even electricity. Mouchot's work was, however, short circuited by the advent of improved coal mining

methods and hence lower cost of fuel. His work, also, was caught in the situation of replacement by cheap fuels, rendering solar usage unnecessary and thus impractical for the time. Late in the 19th century, other pioneers in the development of solar thermal (heat generating) technologies include Aubrey Eneas, an American who followed up on Mouchot's work and formed the first solar power company, building a giant parabolic reflector in the Southwest United States of America. Frank Shuman formed the Sun Power Company in Cairo to promote solar driven water pumping system, and later a parabolic concentrator generating electricity. Other solar innovations have followed: motors and engines, hot water heaters, photovoltaic lighting, and even crematoria. But throughout history, as in Greece and Rome and the Mouchot story, progress has repeatedly been interrupted by fluctuations in availability or cost of alternative fuels for all the above purposes [1, 28].

In the last two decades or so, however, attention has turned back to the old technology of using solar energy for a number of applications. More specifically, the emergence of solar chimney technology has seen many investigators designing solar chimneys that are not only more efficient, but combines several technologies for the production of electricity because of apparent environmental and economic issues.

Recent work on solar chimney includes: "The potential of solar chimney for application in rural areas of developing countries" by Onyango and Ochieng [33] and "Solar chimney for power generation in rural areas" by Padki and Sherif [34]. Other works of note are "A mathematical model for solar chimneys" by Padki and Sherif [35] and "Solar chimney for medium to large scale power generation" by Padki and Sherif [36]. Likewise to the best of our knowledge, no literature exists for models of *solar pressure-staged wind tunnel* power generating plants apart from the work by Conte [37]

which gives a brief theory of the system in comparison to the solar chimney electric power generating plant, hence the interest in these two systems.

The solar chimney electric power system depicted in Fig. 2-1 combines three familiar techniques: the hot air collector, the chimney and the turbine generators.

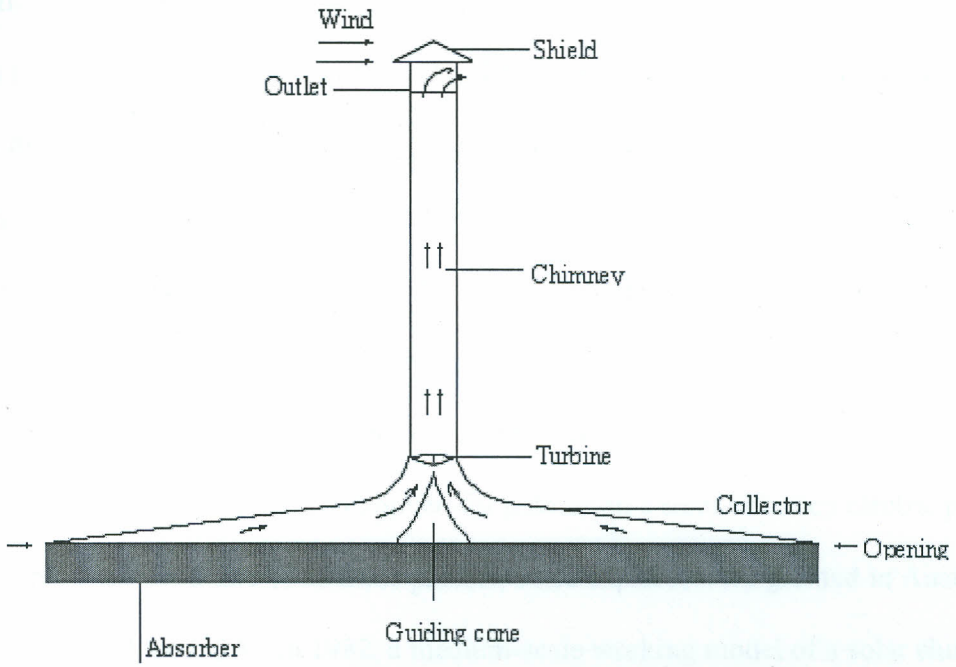

Fig. 2-1. *A schematic model of solar chimney electric power generating plant*

A solar up draught tower (also known as a solar chimney, a term avoided by many proponents due to its association with fossil fuels) is a relatively low-technological solar thermal power plant where air passing under a very large agricultural glass house is heated by the sun and tunnelled upwards towards a convection tower. It then rises naturally and is used to drive turbines, which generate electricity.

As opposed to the solar tower an energy tower is an alternative proposal to the solar updraft tower. In an energy tower, water is sprayed at the top of the tower and evaporation of the water causes a downdraft by cooling the air thereby increasing its

density, driving wind turbines at the bottom of the tower. It requires a hot arid climate and large quantities of water (seawater may be used) but does not require the large glass house of the solar updraft tower.

A solar chimney electric power plant works on the principle that in the collector, solar radiation is used to heat an absorber (ordinarily soil or water bags) on the ground, which in turn heats a large volume of air. The hot air then rises up the chimney due to the pressure difference between the chimney base and the surroundings of the chimney top, driving turbine generators to generate electricity.

In 1903, Spanish Colonel Isidoro Cabanyes first proposed a solar chimney power plant in the magazine "La energía eléctrica" [38]. One of the earliest descriptions of a solar chimney power plant was written in 1931 by a German author, Hanns Günther [39]. Beginning in 1975, Robert E. Lucier applied for patents on a solar chimney electric power generator; between 1978 and 1981 these patents, since expired, were granted in Australia, Canada, Israel, and the USA. In 1982, a medium-scale working model of a solar chimney power plant was built under the direction of German engineer Jörg Schlaich [40-42, 43, 44, 45, 46] in Manzanares, Ciudad Real, 150 km south of Madrid, Spain; the pilot project was the result of collaboration between the Spanish Government and the German designers, Schlaich Bergermann and Partner. The chimney had a height of 195 metres and a diameter of 10 metres, with a collection area (greenhouse) of 46,000 m^2 (about 11 acres, or 244m diameter) obtaining a maximum power output of about 50 kW. During operation, optimisation data was collected on a second-by-second basis. This pilot power plant operated for approximately eight years, but "*encountered severe structural instability close to the tower due to induced vortices*", and was decommissioned in 1989. Since then, more and more researchers have studied this solar power technology. In

1983, American scientist Krisst built a courtyard solar power set up with an energy production of 10 W. Its collector had a diameter of 6 m, while the chimney was 10 m high [47]. In 1985, a micro-scale model with a 2-meter high chimney and a 3.5-cm radius having a base collector area of 9 square meters was built by Kulunk in Turkey [48]. In 1997, a solar chimney power demonstration model was built by Pasurmarthi and Sherif in Florida, and considerable theoretical and experimental research of their performance was done [49]. In 2002, a trial solar chimney power system was built in China under the support of local government. The system had a collector 10 m in diameter and a chimney 8m tall.

Even though work has been done on solar chimney, there are very few works in literature on electric power generating models in size to the work presented in this thesis. The systems discussed in literature are either too large or describe models and systems whose functions are not for power production. The Manzanares prototype by Schlaich [43, 45, 46, 50] provides the reference to almost all solar chimney power plants being built or being studied presently. Fundamental investigations of the Manzanares plant were reported by Haff *et al.* [41]. The investigators presented a brief discussion of the energy balance, design criteria and cost analysis of the system. In a later study Haff [42], presented preliminary test results of the plant. Castillo [51] presented a new chimney design with a new structure of the chimney building supported by a hot-air balloon.

More recently Ong [52] proposed a simple mathematical model of a solar chimney in which the physical model is similar to the Trombe wall. One side of the chimney is provided with a glass cover, which with the other solid walls of the chimney form a channel through which the heated air could rise and flow by natural convection. Openings provided at the bottom and top of the chimney allow room air to enter and leave

the channel. Steady state heat transfer equations are set up in this model to determine the boundary temperatures at the surface of the glass cover, the rear heat absorbing wall and the air flow in the channel using a thermal network system. The analysis gives the thermal performance of the solar chimney as determined from the glass, wall and air temperatures, air mass flow rate and instantaneous heat collection efficiency of the chimney. Though this model of a solar chimney is useful, it cannot be used for power generation, however, it may be applied successfully to building ventilation since its concept is based on the Trombe wall which utilises a glazed vertical side-wall of a building to absorb and re-circulate warm air for passive heating of the building.

A theoretical model of a solar chimney power plant, which is expected to provide power from remote villages in north-western China, has been analysed and reported by Dai *et. al.,* [53]. The investigators have shown that the chimney height, diameter of the solar collector, ambient temperature, solar irradiance and efficiency of the wind turbine are parameters which influence the performance of power generation. The solar chimney power plant model analysed by Dai *et. al.*[53] with a chimney 200 m high and a diameter of 10 m housed on a solar collector of radius of 500 m with the turbine sitting at a height of 2.5 m above the ground inside the chimney is expected to produce 110~190 kW electric power on a monthly average all year. When this model is scaled down to the size of the model in our work whose base area is 22500 m^2 and a turbine of 3.0 m in diameter sitting at 1.5 m above the ground inside the chimney, the power it would produce is approximately 5 kW, a value closely comparable to our result if we use an efficiency of more than 50% in our model.

A more detailed presentation closer to the work given in this thesis has been provided by Benardes and Weinrebe [54]. The investigators have developed an analysis for solar

chimneys aimed at particularly providing comprehensive analytical and numerical models, which describe the performance of solar chimneys. The model was developed to estimate the power output of solar chimneys as well as to examine the effect of various ambient conditions and structural dimensions on the power output. Their results showed that the height of the chimney, the factor of pressure drop at the turbine, the diameter and the optical properties of the collector are important parameters for the design of the solar chimney. Bernardes and Weinrebe [54] have concluded in their work that the mathematical model developed was validated with the experimental data from the Manzanares solar chimney prototype. They have also found out that the power output of a solar chimney electric power generating plant can be increased by increasing the chimney height, the collector area and the transmittance of the collector.

The common features of these prototypes are low-efficiency and high-cost. Accordingly, small scale and even middle scale power plants do not provoke interests at all without any advantage over solar concentrating power systems. However, the conversion efficiency of a solar chimney thermal power plant increases with the height of the chimney, not linearly, but exponentially [55].

For commercial solar chimney power plants to produce energy economically, not only a large collector area is necessary for collecting a large amount of solar energy, but also a high gigantic chimney. Since the driving force is proportional to the height, a taller chimney is needed. Furthermore, higher conversion efficiency for larger scale solar chimney thermal power systems will simultaneously produce a reduction of the energy cost. Therefore, since 1990, there have been several proposals to build large-scale solar chimney thermal power plants, some in vast desert regions in a number of countries.

In the 1990s, a program for a solar chimney power plant with an energy production of 100 MW was proposed to be constructed in a desert, in Rajasthan, India. When the project was about to be implemented, it was realised that the programmed height was too high to assure security to a potential raid due to the nuclear competition between India and Pakistan. It was also realised that the construction cost was exorbitant and the program was finally cancelled [55]. Recently, EnviroMission Limited, an engineering company with office base in Australia planned to build a 200 MW commercial plant in Australia with a solar chimney 1000 m high [56]. This was, however, downsized to a 50 MW plant to have a solar chimney about 480 m high [37].

2.2 *Solar pressure-staged wind tunnel* electric power plant technology

In the year 2001 Conte [37] proposed an electric power generating plant similar to that tested in Spain by Schlaich [46]. Conte called his electric power plant *wind from the sun* electric power plant. In this work, we call this type of power pant *solar pressure-staged wind tunnel power plant* because of its operational principles. The proposed system by Conte employs the same three basic principles used in the solar chimney electric power plant but with slight modifications. The proposed system should turn the sun's light into heat just like the solar chimney. The heat produced, is then absorbed by the air above a thermally selective material (solar collector) heating it and thus creating a low-pressure region over it. Due to the pressure difference between the centre of the collector and its perimeter, wind flows from the high-pressure region through a horizontal tunnel housing wind turbines that are turned by the wind's kinetic energy to produce electricity. This system is different from the solar chimney electric power plant in that it has no chimney but a long horizontal large tunnel hosting generators. Instead of a large

greenhouse like glass roof, the system only has a collector made of dark material that absorbs the heat from the sun to heat the air above the collector.

Conte's [37] proposal outlines the theory of operation of *the solar pressure-staged wind tunnel* power plant. Although the operation is almost similar to that of the solar chimney power plant, there are many questions that have been left unanswered since such a system has not been built and tested. The questions that are of interest to physicists and engineers are: whether the pressure difference will be large enough between the tunnel and the collector to produce significant air velocity and whether the system can produce enough power to be economical. Other questions of interest are: how much power the system can generate and how large an area is required for an economical system. In this work we model such a system to answer some of these questions.

Conte [37] in his paper concludes that the technology of *solar pressure-staged wind tunnel* power plant is unproven and that the system has not been built and tested to a large enough scale to determine how much power would be produced. However, he states that in a small-scale test, an area of 36 square feet (Radius $r = 3.385\,\text{feet}$) or $L = 6$ feet was covered with black ceramic. The ceramic in direct sunlight increased in temperature as much as 40° C. The test was done at 42 degrees latitude in the month of August at a place where the solar radiation for that particular place and time was estimated to be about 5.5 kWh/m^2. In places like Africa where solar radiation values are higher, theoretically, the temperature of the collector should attain higher temperatures.

According to Conte [37], the wind velocity (u) in the wind tunnel depends mainly on the total pressure difference (Δp_{tot}) from one end of the air tunnel to the other. Air density (ρ) involved is a much less significant factor. The available power from the

wind (P_1), per square meter of cross-sectional area depends on the cube of the wind velocity (u^3) and the density (ρ).

2.3 Solar thermal technology

All systems, which harness and use the sun's energy as heat, are called solar thermal systems. These include solar water heaters, solar air heaters, solar stills, solar crop driers and solar space heat systems and water desalination systems.

Many dwellings in cold climates need heated air for comfort and hot water for washing and other domestic purposes. Large volumes of water are used to process heat in industry for heating fluids to "low" temperatures ($<100^0$C). In hot dwellings of hot climates, the heat from the sun is used for a number of purposes such as drying some foods and crops in addition to other uses.

Instead of using solar energy to heat, it can also be used to cool. A mechanical device capable of doing this is the *absorption refrigerator*. All refrigerators depend on the surrounding giving up heat to evaporate a working fluid. In a conventional electrical (or compression) refrigerator, the working fluid is recondensed by heat exchange at elevated pressure applied by a motor. In an absorption refrigerator, the required pressure rise is obtained from the difference in vapour pressure of the refrigerant between (1) a part containing the refrigerant vapour above a concentrated solution of refrigerant liquid (the generator), and (2) a part containing refrigerant vapour above a dilute solution (the absorber). Instead of an external input of work, as in a compression cycle, the absorption cycle requires an external input of heat. This heat is applied to the generator in order to

maintain its temperature at a level such that the vapour pressure there equals the saturation pressure in the condenser.

A suitable combination of chemicals is water as refrigerant and lithium bromide as absorbent. The heat can be applied either by a flame, by waste heat or by solar energy. Although systems are commercially available for use with flat plate collectors, operating at approximately 80^0C, they suffer from high mechanical complexity and low efficiency.

A better way to cool buildings in hot climates is again to use passive designs which, either harness the natural flows of cooling air (in humid areas), store coolness from night time or winter (in dry areas) or in some cases automatically generate a cooling flow by convection. A comprehensive account of relevant design principles, with examples can be found in the 'Manual of Tropical Buildings" [58]. The foundation literature which covers the performance of buildings in solar admittance includes Kittler [59], Cole [60], Burberry [61], Adelard *et. al.* [62], Gan and Awbi [63], Shaviv [64], Yezioro and Shaviv [65], Taheri and Shafie [66].

The main part of a solar heating system is the collector, where solar radiation is absorbed and energy is transferred to the fluid or the item in the process. The most common collectors are classed as *flat plate collectors*. Flat plate collector is the most widely used simple and effective means of collecting solar energy for applications that require heat at temperatures below 80^0C [67]. Flat plate solar collectors have been used successfully for more than 50 years for domestic and industrial water heating, space heating and drying. Flat plate solar collectors absorb both beam and diffuse radiation, and therefore still function when beam radiation is cut off by cloud. This advantage together with their favourable cost, means that flat plate collectors are preferred for

heating to temperatures less than about 100^0C. Even though the flat plate solar collectors have one common property of being flat, the simpler collectors are designed to hold all the water or the fluid to be heated. The more refined collectors heat only a little fluid at a time. If the fluid is required for use later, it is accumulated in a separate storage tank a procedure which allows for the reduction of heat loss from the system as a whole.

A typical flat plate collector consists of an absorber plate, one or more transparent cover(s), thermal insulation, heat removal system and an outer casing.

An absorber plate is generally a sheet of metal of high thermal conductivity like copper which is normally coated with black paint or given a special coating (called selective coating) so that it absorbs the incident solar radiation efficiently and minimises loss of heat by radiation from the collector plate.

A glass plate of good quality, which is transparent to incoming solar radiation to act as cover, is fixed about $2-4$cm above the absorber plate. This prevents convective heat loss from the absorber plate and prevents infrared radiation from the plate escaping to the atmosphere (green house effect). If the plate temperature under normal operation is expected to be higher than 80^0C, two glass plates separated from each other may be used.

The absorber plate rests on a $5-15$cm thick bed of glass wool or any other good thermally insulating material of adequate thickness, which is also placed along the sides of the collector plate to cut down heat loss by conduction.

The most common method of removing heat from the collector plate is by fixing tubes, called risers at spacing of about $10-25$cm. Good thermal contact between the tube and plate is very important for efficient operation of the collector hence the tubes

could be soldered, spot welded, tied with wires or clamped to the plate. These risers are connected to larger pipes called headers at both ends so that heat removal fluid can enter from the lower header and leave from the upper header. This configuration of absorber plate is called the fin type and is most commonly used. The heat removal fluid, usually water or oil, flows through these tubes to carry away the heat received from the sun. In another type of collector, heat removal fluid flows between two sheets of metal sealed at the edges, the top acting as the absorber plate.

All parts of the collector are kept in an outer case usually made of metal sheets. The case is made air tight to avoid considerable loss of heat from the collector plate to the ambient. The collector, is finally placed on a stand so that the absorber plate is correctly inclined to the horizontal and receives maximum amount of heat from the sun during a particular season or the entire year.

Flat plate solar collectors may be divided into two main classifications based on the type of heat transfer fluid used. Either liquid or gases (most often air) is used in collectors. Liquid heating collectors are used for heating water and non-freezing aqueous solutions and occasionally for non-aqueous heat transfer liquids such as thermal oils, ethylene glycol, etc. Air-heating collectors are used for heating air used for solar dying or space heating.

More advanced studies both experimental and theoretical have been carried out on flat plate solar collectors. Accurate modelling of solar collector system using a rigorous radiative model applied for the glass cover, which represents the most important component, was recently reported by Maatouk and Shigenao [68].

2.4 Thermophysical properties of opaque bulk materials

The most common methods for the determination of thermophysical properties of opaque bulk materials employ the steady-state [69, 70] and transient [30, 71] techniques. Transient technique for determination of thermophysical properties of materials in absorption calorimeter have also been reported [31, 72]. These methods are based on various assumptions on the geometrical configurations of the sample chambers as well as the heat transfer mechanisms which mostly use Laser-Vacuum techniques for spectral values. Some researchers have used solar radiation [73, 74], solar simulators [32] and electric pulses [69, 75], for probing the sample while electron-beam probe has also been used for the determination of emittance at microscopic scales [76]. Work on the absorption and thermal emission of electromagnetic radiation by a rough surface was recently reported [77] where numerical simulation of the absorptivity of a grating was used to explore the validity of the ray tracing approach.

Developments for the dynamic technique have been reported by Kola *et. al.* [31]. Although Otieno *et al* [29, 30] used an experimental set-up based on the principles as used in our work which employs an integrating sphere, there exist marked differences in the geometry of the calorimeters and consequently the mathematical analysis used in both cases.

An integrating sphere is an apparatus with an interior cavity (typically spherical) having a highly reflective, optically diffuse white surface. The simplest integrating sphere design contains two apertures, one which admits light and another which serves as a measurement port where the amount of light on the surface of the sphere can be measured. An integrating sphere has the property that at any point on the inner surface of the sphere the illumination is essentially independent of the direction and location of the

incident beam as well as the size of the beam. The inner surface is uniformly illuminated throughout, except at the point of direct illumination. Integrating spheres are used in calorimetry for the precise determination of color for a sample under test [78].

In one method and system to measure surface characteristics of a specimen using an integrating sphere, the implementation involves receiving at a receiver optical radiation reflected or scattered from a specimen. A measure of surface characteristics is then provided by processing a signal representing the received optical radiation which includes the specular components that are spatially encoded by wavelength according to chromatic aberration. Both color and surface effects of a specimen can be measured simultaneously using a single spectrophotometric instrument. In an alternative embodiment, the size of a port opposite a receiver is varied, and for each port size, the receiver receives a corresponding optical radiation signal representing optical radiation reflected by the sample. These optical radiation signals are processed to provide a measure of the specimen surface characteristics [79].

The apparatus (the integrating sphere calorimeter) used in our work is different considerably in form and operation from any previously reported work. It has no standard detection ports, or sample ports. This makes the sphere simple to operate without interfacing it with any expensive optical crystal detectors. The only opening in the sphere is an entrance window that allows the radiation into the chamber.

The dynamic technique employed in the work ensures that the heated sample attains a steady final temperature and allows for the formation of a simple heat transfer equation within the enclosure. Certain assumptions based on the geometry of the calorimeter used in our work have been made [80]. The complications of convective and radiative heat transfer terms in the equations of heat exchange formed are avoided by

coating the inside of the integrating sphere with white paint of barium sulphate ($BaSO_4$) whose reflectivity is greater than 98 percent for wavelengths between 400-1500 nm and greater than 95 percent for wavelengths between 250-2000 nm [81].

Other techniques [82-84] which have been used in the measurement of absorptance and emittance of opaque bulk materials, especially commercial copper and aluminium provide heat balance equations in which the mass of the sample, the area of the sample and the convective terms are present. The calculations of the convective coefficients are not very easy to solve for because they are both time and temperature dependent.

In our work we use a portless integrating sphere calorimeter, which makes the heat balance equation within the sphere simple and gives the explicit expression of the ratio of absorptance to the emittance. The ratio is a function of steady state temperatures (ambient and sample) within the enclosure and varies directly as the difference between the fourth powers of these temperatures.

CHAPTER THREE

3.0 THEORY AND THEMODYNAMICS GOVERNING RADIATION

Our work depends entirely on radiation properties such as absorptance, emittance and reflectance of different surfaces. The concept of a blackbody as a perfect radiation absorber or emitter is basic to the study of radiation energy transfer. Additional properties of a blackbody, which are, rarely thought of are zero surface reflection and complete internal absorption of radiation. As a perfect absorber it serves as a standard of comparison for bodies emitting radiation. However, only a few surfaces such as carbon black and gold black come close to a blackbody in their ability to absorb radiant energy. The blackbody derives its name from the fact that good absorbers of incident visible light do indeed appear black to the eye which is in fact not a good indicator of absorbing ability in the wavelength range of thermal radiation. A surface coated with white oil-based paint is a very good absorber of infrared radiation emitted at room temperature; however, the same surface is a poor absorber of visible light.

3.1 Kirchoff's law

Kirchhoff's law states that for a surface in thermal equilibrium, the hemispherical absorptance is equal to the hemispherical spectral emittance. Duffie and Beckman have given a comprehensive discussion and proof of Kirchhoff's law [7, 85]. However, essential results can be derived from elementary thermodynamics. First, we note that the absorptance depends on the wavelength distribution of the incident intensity. Using expressions of equations which define absoptance and emittance in terms of absorbed and incident radiation, we can obtain the absorptance of the surface. On the other hand the

hemispherical absorptance and emittance are equal under conditions of thermodynamic equilibrium, hence one can write

$$\alpha(\lambda,\theta,\phi)=\varepsilon(\lambda,\theta,\phi). \tag{3.1}$$

The equality of other forms of the absorptance and emittance can be deduced in a similar manner. For example, if the surface does not exhibit dependence on the azimuth angle, then we obtain the most general form of Kirchhoff's law, that is

$$\alpha(\lambda,\theta)=\varepsilon(\lambda,\theta). \tag{3.2}$$

If, in addition, we neglect the dependence on the polar angle we can write,

$$\alpha(\lambda)=\varepsilon(\lambda). \tag{3.3}$$

Finally, if the surface does not exhibit wavelength dependence, then we have

$$\alpha=\varepsilon. \tag{3.4}$$

3.2 Planck's law

The spectral distribution of the energy emitted by a radiating body is governed by the Planck's equation, *viz*,

$$I_b(\lambda,T)=\frac{c_1\lambda^{-5}}{e^{c_2/\lambda T}-1}, \tag{3.5}$$

where $I_b(\lambda,T)$ is the spectral emissive power at the wavelength λ while $c_1=3.7814\times10^{-16}\,\mathrm{Wm}^2$ and $c_2=1.4388\times10^{-2}\,\mathrm{mK}$ are constants (Figure 3-1).

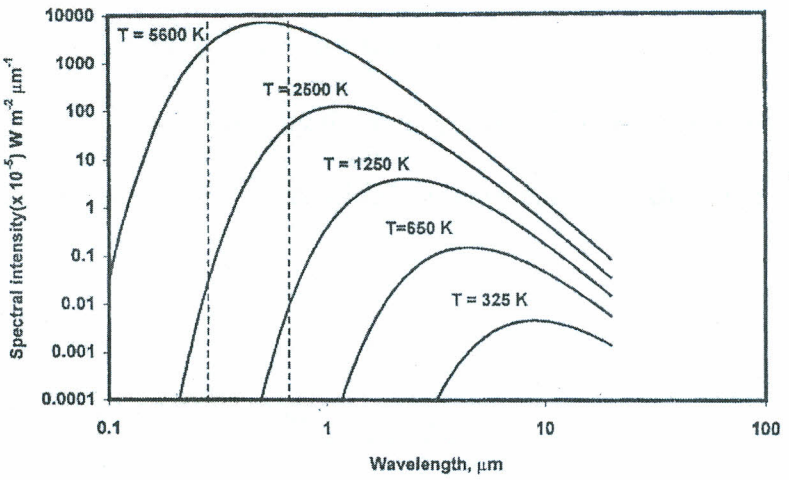

Figure 3-1. *Blackbody spectral radiation intensity at various temperatures plotted on a log-log scale. The dashed lines show the visible region.*

For a non-blackbody, Eq. (3.5) becomes

$$I(\lambda,T)=\varepsilon(\lambda)I_b(\lambda,T)=\varepsilon(\lambda)\frac{c_1\lambda^{-5}}{e^{c_2/\lambda T}-1}, \tag{3.6}$$

where $\varepsilon(\lambda)$ is the emissivity of the surface.

3.3 Wien's law

If Eq. (3.5) is integrated, one can obtain the wavelength λ_{max} corresponding to the peak emission, given by Wien's formula

$$\lambda_{max}=\frac{2898}{T}(\mu\text{m.K}), \tag{3.7}$$

where λ_{max} is in microns and T is the absolute temperature. About 75% of the emitted energy lies at wavelengths above λ_{max}. A comprehensive treatment of the spectral properties of thermal radiation is given in, for example Duffie and Beckman [7].

Extraterrestrial solar radiation corresponds more or less to a blackbody radiation at a temperature of about 5,800K. Thus, for the sun, the peak emission is at 0.5μm. If allowance is made for the absorption by the atmosphere, it is found that the solar radiation reaching the earth is almost entirely confined to wavelengths in the range $0.3-2.5\mu$m (Figure 3-2).

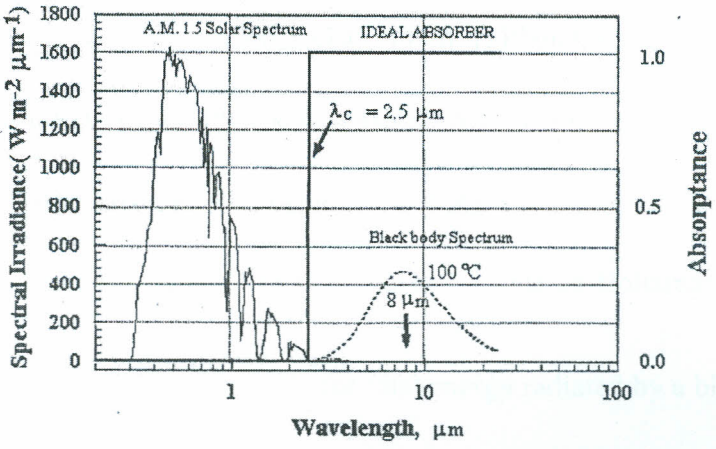

Figure 3-2. *Spectral distribution of: (a) Air Mass 1.5 solar spectrum, and (b) blackbody spectrum at* 100^0C. *The spectral absorptance of an ideal solar absorber is shown.*

Eq. (3.6) implies that an object at room temperature emits almost all of its radiation at wavelengths much longer than those in the solar spectrum. For example, the peak of emission for an object at 373K is $\lambda_{max} = 8\mu$m. This means that the solar radiation and the radiation of bodies at ordinary temperatures lie in well-separated wavelength regions. This is illustrated in Figure 3-2. The solid curve reproduces a typical spectrum for the solar irradiance at the ground. Specifically, the curve gives the Air Mass (AM) 1.5 spectrum [248] corresponding to clear sky conditions with the sun being 41.8^0 above the horizon. It is seen that most of the solar radiation comes at wavelengths $\lambda < 3\mu$m.

3.4 The Stefan-Boltzmann equation

The Stefan-Boltzmann law and the Wien displacement law are contained in the Planck law and thus may be derived from Eq. (3.5). The Planck equation gives the energy density of a blackbody. The intensity of the emitted radiation is equal to $c/4$ times this energy density. Thus, multiplying Eq. (3.5) by $c/4$ and integrating from $\lambda = 0$ to $\lambda = \infty$ we can calculate the energy radiated by a blackbody. Using Planck's first radiation constant $c_1 = 2\pi hc^2 = 3.7405 \times 10^{-16}\,[\mathrm{Wm}^2]$, Planck's second radiation constant $c_2 = hc/k = 0.0143879\,[\mathrm{Km}]$, Planck's constant $h = 6.626076 \times 10^{-34}\,[\mathrm{Js}]$, Boltzmann's constant $k = 1.38066 \times 10^{-23}\,[\mathrm{J/K}]$, velocity of light in vacuum $c = 299792458\,[\mathrm{m/s}]$, $T =$ emitter temperature [K] and Stefan-Boltzmann's constant $\sigma = \dfrac{2\pi^5 k^4}{15c^2h^3} = 5.6697 \times 10^{-8}\,[\mathrm{W/m^2K^4}]$, the total energy radiated by a blackbody can now be written as

$$w_b = \frac{c}{4}\int_0^\infty \frac{8\pi ch\lambda^{-5}}{e^{ch/\lambda kT} - 1}\,d\lambda\,. \tag{3.8}$$

If we let $x = ch/\lambda kT$, we obtain

$$w_b = \frac{2\pi k^4 T^4}{c^2 h^3}\int_0^\infty \frac{x^3}{e^x - 1}\,dx\,. \tag{3.9}$$

The definite integral is equal to $\pi^4/15$; therefore,

$$w_b = \sigma T^4\,. \tag{3.10}$$

Real surfaces emit less than blackbodies and Eq. (3.8) may be rewritten as

$$w = \varepsilon w_b = \varepsilon\sigma T^4\,, \tag{3.11}$$

where ε is less than unity and is called the hemispherical emittance. Since every surface that emits is also an absorber, it receives radiation from its surroundings. Thus the net radiation loss is given by

$$\Delta w = \varepsilon\sigma\left(T^4 - T_S^4\right), \tag{3.12}$$

where T_S is the temperature of the surrounding. In arriving at Eq. (3.12) we have assumed that Kirchhoff's law (Eq. (3.4) is valid for the surface under consideration even though the surroundings and the surface are not at an equilibrium temperature.

3.5 Beer-Bourger-Lambert law

Because of its usefulness in estimating and calculating the amount of radiation that can be obtained at a particular site on the earth's surface, we now discuss the law relating the change in radiation intensity as it passes through the atmosphere. This law expresses the change in radiation intensity I_λ due to the absorption of the radiation. Let us consider a parallel beam of radiation with intensity I_λ passing through an absorbing medium. The intensity of radiation after traversing a layer of thickness ds in the direction of the propagation is $I_\lambda + dI_\lambda$, and

$$dI_\lambda = -k_{\lambda a} I_\lambda \rho ds, \tag{3.13}$$

where ρ is the density of the medium and $k_{\lambda a}$ is the absorption coefficient (absorption cross section in units of area per unit mass) for radiation of wavelength λ. Integration of this Eq. (3.13) between $s = 0$ and $s = s_1$ yields the emergent intensity $I_\lambda(s_1)$ so that

$$I_\lambda(s_1) = I_\lambda(0)\exp\left(-\int_0^{s_1} k_{\lambda a}\rho ds\right), \tag{3.14}$$

where $I_\lambda(0)$ is the intensity at $s=0$. When the medium is homogeneous, $k_{\lambda a}$ is independent of s, and Eq. (3.14) then expresses the Beer-Bourger-Lambert law [62]. A similar law is valid for the scattering of parallel beam passing through the atmosphere. In this case, we must use a scattering coefficient $k_{\lambda s}$. When absorption and scattering occur simultaneously, we may write $k_\lambda = k_{\lambda a} + k_{\lambda s}$, where k_λ is called the extinction coefficient. The transmissivity τ_λ of the atmosphere at a given wavelength is then given by

$$\tau_\lambda = I_\lambda / I_{\lambda 0} = \exp\left(-\int_0^\infty k_\lambda \rho ds\right), \tag{3.15}$$

where k_λ is the extinction coefficient along a slant path ds in the direction of propagation through the atmosphere. If the zenith angle of the sun is Z, $ds = dz \sec Z$ and Eq. (3.15) can be written as

$$\tau_\lambda = I_\lambda / I_{\lambda 0} = \exp\left(-\sec Z \int_0^\infty \rho k_\lambda dz\right) = \exp(-\sec Z \psi), \tag{3.16}$$

where the quantity

$$\psi = \int_0^\infty k_\lambda \rho dz \tag{3.17}$$

is called the optical depth or optical thickness.

For normal incidence $(Z=0)$ and when $\psi = 1$ we find $\tau = e^{-1} = 0.37$ which implies that the initial intensity I_λ is decreased by 63%. If $\psi = 2$ we find $\tau = e^{-2} = 0.14$ or a decrease in intensity of 86%. During normal atmospheric conditions, the optical depth is much less than unity, but for very thick, dark clouds, it can be greater than unity.

3.6 Selective Surfaces

Selective surfaces are used in solar thermal absorbers to maximise absorption of solar radiation and to reduce re-radiation losses, hence increasing thermal efficiency of collectors. Their use in practical collectors was first demonstrated in 1955 by Gier and Dunkel [86].

An ideal selective absorber surface is one with an absorptance of unity in the wavelength range of the solar spectrum $(0.3-2.5\mu\text{m})$ and an absorptance of zero for wavelengths longer than about $3\mu\text{m}$. For opaque materials, the spectral absorptance $\alpha(\lambda)$ is related to the spectral reflectance by Eq. (2.25). However, ideal selective absorbers do not exist. In practice, one talks of an efficient selectively solar-absorbing coating for the photothermal conversion of solar energy. Such absorbers are used as the primary component in the construction of solar collectors. The basic requirements of a practical selective surface for a solar collector are [87]:

(a) high solar absorptance, α

(b) low thermal emittance, ε

(c) long term stability at desired operating temperature

(d) above-normal operating temperature stability

(e) stability against atmospheric corrosion

(f) low cost

In utilizing selective surfaces, the above properties must be taken into consideration.

3.7 Solar radiation measurement techniques and estimation

Most instruments for measuring solar energy fall into two categories: *photoelectric* and *bolometric* devices. The first group includes devices with receiving elements or sensors whose electrical characteristics change in the presence of solar radiation. *Photovoltaics* such as silicon and selenium cells, which generate a voltage when solar energy is incident on them, fall in this group. Their short-circuit current property is used to measure the intensity of the incident radiation. Some investigators, however, categorise the instruments either as *pyroheliometers*, which measure the beam irradiance G_b^* and *pyranometers* or *solarimeters,* which measure total irradiance G_{tc}. In this categorisation, only the active cavity radiometer (ARC) gives an absolute reading. In this instrument, the solar beam falls on an absorbing surface area A, whose temperature rise is measured and compared with the temperature rise in an identical (shaded) absorber heated electrically. *Photoconductive* detectors such as cadmium sulphide or cadmium selenide, change resistance in response to electromagnetic radiation. When connected across a battery, the current in the circuit becomes a measure of the intensity level. Vacuum tube devices known as photo-tubes, which have specially coated elements that emit electrons when light is incident on them are use to determine the intensity when the conductivity of the tube changes as a result of the production of the photoelectrons.

Although solid state photoelectric devices are durable, compact, inexpensive to fabricate, and are minimally affected by ambient conditions, they nevertheless have some major shortcomings. First, they do not always produce a signal that is linear in the insolation level; many tend to saturate or level off at high intensity levels. Second, photoelectric devices do not have a spectrally flat response over the solar spectrum. This means that equal amounts of energy arriving in different spectral regions produce

different signals. In particular, if a device is sensitive only to the visible spectrum, it will not detect the presence, or the change in the infrared solar energy.

The second category includes the bolometric devices. These instruments generally absorb the radiation in a black absorber and use the heat generated to produce a change in the state of the receiver. This change is measured and related to the insolation level. A typical bolometric instrument used in the United States is the *black and white pyranometer* whose receiver consists of two adjacent flat surfaces, one black and one white (or silvered). Each surface has a thermal sensor (usually a thermocouple) fixed to it. The sensors generate a voltage signal that is directly proportional to the temperature differences between the black and white surfaces. When solar energy is incident, the black surface absorbs the radiation and becomes warmer than the white one, which reflects the radiation and remains near the ambient temperature. The greater the insolation level is, the greater the temperature difference and the larger the voltage signal.

The steady-state temperature difference between the surfaces depends on the degree of solar heating of the black surface and also on the heat loss rate to the environment. Because the heat loss is not a simple function of the temperature, there is no *apriori* reason to expect a linear relationship between the radiant intensity and the voltage signal. Pyranometers that are generally calibrated in Wm^{-2} per milivolt assume such linearity. The output of the pyranometer depends on both the temperature and the wind conditions of the surroundings. Consequently correction charts are usually required when a pyranometer is used under environmental conditions other than those for which the unit was originally calibrated. To protect it from the elements, the receiver is generally covered with a glass dome transparent to solar radiation.

Bolometric instruments that operate on the principle of Ångström or electrical compensation avoid many of the difficulties encountered with the black and white pyranometers. In electrical compensators, a black surface is exposed to sunlight and its temperature noted. The same (or similar) surface is shielded from the sun and is heated electrically until the same temperature is reached. The electrical power supplied (which is then equal to the absorbed solar power) is measured.

A portable field instrument using the electrical compensation is the *autobalancing radiometer*. The receiver of this instrument is composed of two identical black surfaces. Each is a rectangular wafer consisting of a substrate with a black conductive coating such as graphite. The coating acts not only as a black absorber but also as an electrical joule heater. Each wafer has a thermal sensor to detect any temperature difference between them. Furthermore, each wafer is covered with a glass dome and the interior space partially evacuated. The dome is transmissive to solar radiation but opaque to thermal radiation. The wafer chosen as the heater has its dome silvered; the other becomes the solar wafer and will receive radiation. When the receiver is exposed to solar radiation, the exposed solar wafer becomes warmer than the heater wafer that is shielded from sunlight by its silvered dome. The thermal sensors detect this temperature difference. A direct voltage is applied across the Ohmic coating of the heater wafer until the joule heating brings the wafers to the same temperature. In the balanced state, both heaters are being heated equally-one wafer by solar energy and the other by joule heating. The incident flux is then determined from the equation

$$\text{flux} = \frac{V \times I}{\bar{a} \times A}, \tag{3.18}$$

where V and I represent the voltage and current applied to the heater at balance, A is the area of each wafer, $\overline{a}$ is a correction factor representing the product of the absorptivity of the coating and the transmissivity of the glass dome over the solar wafer. If the coatings were perfectly black and the glass perfectly transparent to solar radiation, we would have $\overline{a}=1$. In operation, an electronic control unit adjusts the voltage to keep the system in balance and the unit performs the necessary computations as required by Eq. (2.46).

Knowledge of solar radiation values in a region is essential to study and design the economic viability of systems which use solar energy. In order to use solar energy, the most important variable is the mean daily global radiation, but measurements of this variable are made in only a few places. This situation can be solved by using correlations which estimate solar radiation from more available meteorological parameters , such as sunshine duration. The pioneering work of Ångström [88] established a means to estimate the total radiation-income of the day, H, from hours of sunshine, S, expressed in a percentage of the greatest possible time of sunshine, S_0, of the form

$$H = H_c[c_0 + (1-c_0)S/S_0] \tag{3.19}$$

where H_c is the radiation-income corresponding to a perfectly clear day and c_0 is the proportion of the radiation received on a completely overcast day as defined by Black *et. al.* [89]. Owing to the practical difficulty associated with the determination of a precise value of H_c in the absence of local radiation measurements, Prescott [90] modified the Ångström equation to obtain the total radiation, H, on a horizontal surface. The modified equation often referred to as the global radiation reads as follows:

$$H = H_0(c_1 + c_2\, S/S_0) \tag{3.20}$$

where H_0 is the total radiation incident on a horizontal surface in the absence of atmosphere, referred to as extraterrestrial radiation, and c_1 and c_2 are empirical constants. For the purpose of finding the constants c_1 and c_2 by regression analysis, Eq. (3.20) can be transformed into the Ångström-Prescott-Page equation form given by

$$\frac{H}{H_0} = c_1 + c_2 \, S/S_0 \tag{3.21}$$

where the ratio H/H_0 is referred to as the cloudiness index by Liu and Jordan [91] and Iqbal [92], atmospheric transmissivity by Hay [93] and clearness index by Khogali *et. al.* [94] and Duffie and Beckman [7]. This simple form of the relation has received almost a world-wide acceptance for application [95-141]. However, Page [95] pointed out that the linear-type equation based on climatological means cannot necessarily be expected to be applicable to extreme values for particular days, as it overestimates the total radiation on cloudless days , i.e. when $S/S_0 = 1$, and on overcast days, i.e. when $S/S_0 = 0$. This fact was later confirmed by Benson *et. al.*, [141] and Michalsky [142] who considered the relationship on the basis of individual records. The former study showed a significant concave downward curvature of the data points with discontinuity of H/H_0 at $S/S_0 = 0$, hence a quadratic form for the relationship between daily global/extraterrestrial radiation and the actual/maximum possible hours of sunshine greater than zero must be found. Many investigators [143-152] suggested and adopted the second-order polynomial form of the relation

$$H/H_0 = c_3 + c_4 \, S/S_0 + c_5 (S/S_0)^2 \tag{3.22}$$

as a reasonable functional form where c_3, c_4, c_5 are the regression constants.

In search for models for global solar radiation all over the world, the modified version of the Ångström's correlation used by Page [95] has been the most convenient and widely used correlation for estimating the global radiation. The original Ångström equation has undergone several transformations resulting in a host of different forms. More recently İnci *et. at.* [153, 154] have given the modified Ångström equation as

$$\frac{\overline{H}}{\overline{H}_0} = a + b\left(\frac{\overline{n}}{\overline{N}}\right), \tag{3.23}$$

where $\overline{H}$ and $\overline{H}_0$ are, respectively, the monthly mean daily global radiation in MJ/m^2 on a horizontal surface and that at the top of the atmosphere; $\overline{n}$ and $\overline{N}$ are monthly means of hours of sunshine and length of the day in hours, respectively. The length of the day in hours is calculated from

$$H = \frac{2}{15}\cos^{-1}(-\tan\phi\tan\delta) \tag{3.24}$$

where δ is the declination defined as the angle formed by the line from the centre of the earth to the centre of the sun on a particular day and the plane containing the earth's equator, and ϕ the latitude of the place. The declination has values in the range $-23.45^0 \le \delta \le 23.45^0$, where places in the northern part of the equator have positive values while those in the southern part are denoted by negative values. a and b in Eq. (3.23) are the climatological Ångström regression coefficients and as reported by Glover and McCulloch [155] depend on the way the global radiation and sunshine data are grouped together.

Many investigators who have followed in the same line of research using the Ångström-type equation have tried to refine the measurement of solar radiation

techniques. They have used their methods to obtain data for specific locations to help in the establishment of the correct form of solar technologies that are appropriate for those locations. More recently, researchers such as Almorox *et al.*,[156] have concentrated their work in Spain whereas Tiba *et al.*, [157] established a new relationship between monthly global irradiation and sunshine hours from a database of Brazil and Righini *et. al.* [158] have provided an approach to drawing global solar irradiation contour maps for Argentina.

The *Bird Clear Sky Model*, a broadband algorithm which produces estimates of clear sky direct beam, hemispherical diffuse, and total hemispherical solar radiation on a horizontal surface was developed by Richard Bird in Colorado State (USA) in 1981 [159]. The model is based on comparisons with results from rigorous radiative transfer codes. It is composed of simple algebraic expressions with 10 user provided inputs. Model results should be expected to agree within ± 10% with rigorous radiative transfer codes. The model computes hourly average solar radiation for every hour of the year, based on the 10 user input parameters; however, variable atmospheric parameters such as Aerosol optical depth, ozone, water vapour are fixed for the entire year. Later, the model was modified to compute clear sky spectral direct beam, hemispherical diffuse, and hemispherical total irradiances on a prescribed receiver plane - tilted or horizontal - at a single point in time. For tilted planes, the user specifies the incidence angle of the direct beam or the tilt and azimuth of the plane. The wavelength spacing is irregular, covering 122 wavelengths from 305 nm to 4000 nm. Aerosol optical depth, total precipitable water vapor (cm), and equivalent ozone depth (cm) must be specified by the user. No variations in atmospheric constituents or structure are available. There is no separate computation of circumsolar radiation and the direct beam spectral irradiance is assumed to contain the

circumsolar radiation within a 5° solid angle. There are no smoothing functions provided in the model [160].

Other workers such as Maxwell and Christian Gueymard [161, 162] later developed algorithms, which use empirical relationships between the global and direct clearness indices (K_t, K_n), respectively defined as the direct beam transmittance and the effective global horizontal transmittance to estimate the direct beam component in addition to providing Gaussian or triangular smoothing functions with user-defined parameters. The clearness indices (K_t, K_n) are related to I_n (direct normal irradiance at the surface of the earth), I_t (total global horizontal irradiance), I_0 (extraterrestrial direct normal irradiance) and z (solar zenith angle) through different mathematical expressions, depending on which model is used to calculate them. For example, in the Aerospace Direct Insolation Prediction Model (ADIPA), developed by Randall and Whitson [163] and a simplified and modified version of this model called the Ersatz Typical Meteorological Year (ETMY) uses the expressions

$$K_n = I_n / I_0 \tag{3.25}$$

and

$$K_t = I_t / (I_0 \cos z) \tag{3.26}$$

More literature on the prediction of the direct components of solar radiation includes Ezekwe and Exeilo [164], Aliyu and Sambo [165], Adeyemo [166], Aksoy [167], Nguyen and Pryor [168] and Luhanga and Nijegorodov [169].

3.8 Solar energy collection

Before any solar energy can be used in a form capable of, say, generating electricity or providing hot water, it must first be collected. The Carnot efficiency, η, of a heat engine operating between high and low temperatures, T_H and T_L is given by:

$$\eta = \frac{T_H - T_L}{T_H}. \tag{3.27}$$

If high efficiencies are to be attained, T_H must be as high as possible and for radiation, the temperature T which can be reached for an incoming power density w is given by Eq. (2.38). As we have seen, a body which re-emits all the radiation incident upon it is known as a blackbody and has $\varepsilon = 1$. One, which emits no radiation, has an emissivity of zero. Highly polished aluminium and powdered carbon have emissivities of 0.04 and 0.9 respectively. A blackbody also absorbs all radiant energy incident upon it and is said to have an absorptivity, α, of unity. A real body will only absorb a fraction of the incident radiation and so has a value of α less than unity. Typically, α and ε have values of about 0.8 to 0.9 and both depend on the wavelength of the radiation.

Consider as an example a solar collector which is capable of absorbing 80% of the solar radiation in which it is placed, i.e. $\alpha = 0.8$, and has an emissivity for these wavelengths of 0.5, then for the favourable conditions where the available daytime energy is $800\,\mathrm{Wm}^{-2}$ we can calculate the total energy absorbed using Eq. (3.10) as

$$\alpha w = \sigma \varepsilon T^4 \tag{3.28}$$

or

$$0.8 \times 800 = 5.67 \times 10^{-8} \times 0.5 \times T^4. \tag{3.29}$$

If we let $T = 388\text{K}$ or 115^0C which is just more than the normal boiling point of water and assuming a perfect heat engine at an ambient temperature of 293K, then the efficiency will be

$$100(388 - 293)/388 = 24.5\%. \tag{3.30}$$

There are two possible ways of increasing the temperature. It is possible to use a collector material with a high value of α and a low value of ε. This is known as a selective absorber and is capable of achieving high temperatures, albeit at greater capital cost. If α becomes 0.9 and $\varepsilon = 0.04$ for example, T becomes equal to 750K which is a much more attractive temperature.

An alternative method is to use a focusing device such as a parabolic reflector to increase the effective power density. Any device that can increase the radiation density is useful as a radiation collector.

Our sense of vision and the process of photosynthesis in plants have evolved within the range of those wavelengths of sunlight that our atmosphere does not absorb, which is between 300nm and 1,100nm [170]. The net radiation to the sky at temperature T_s due to a surface with emittance ε and temperature T is obtained from equation (3.12) as

$$Q = \varepsilon\sigma A\left(T^4 - T_s^4\right) \tag{3.31}$$

T_s is the equivalent blackbody sky temperature.

Several relations have been proposed to estimate T_s for clear skies. These are:

$$T_s = 0.0552T_a^{1.5} \tag{3.32}$$

by Swinbank [171] whose equation relates sky temperature to the local air temperature and

$$T_s = T_a\left[0.8 + \frac{T_{dp} - 273}{250}\right] \tag{3.33}$$

by Bliss [172] where T_a and T_{dp} are the ambient and dew point temperature respectively. Brunt [173] give an equation relating the sky temperature to the water vapour pressure whereas Berdahl and Martin [174] used extensive data from the United States to relate the effective sky temperature to the dew point temperature, dry bulb temperature and hour from midnight t by the following equation

$$T_s = T_a\left[0.711 + 0.0056T_{dp} + 0.000073T_{dp}^2 + 0.013\cos(15t)\right]^{\frac{1}{4}} \tag{3.34}$$

where T_s and T_a are in degrees Kelvin and T_{dp} is the dew point temperature in degrees Celsius. The experimental data covered a dew point range from -20^0C to 30^0C. The range of the difference between the sky and air temperature is from 5^0C in hot, moist climate to 30^0C in cold dry climate.

The amount of heat absorbed by air can then be given by

$$C \cdot M \cdot \Delta T = \varepsilon\sigma A\left(T^4 - T_s^4\right), \tag{3.35}$$

where $\sigma = 5.6697 \times 10^{-7}\ \mathrm{W/m^2K^4}$ is the Stefan-Boltzmann constant, C is the specific heat capacity of the air at the stated temperature, M is the mass of the air and ΔT is the temperature difference. Substitution of Eq. (3.32) into Eq. (3.35) yields

$$C \cdot M \cdot \Delta T = \varepsilon\sigma A\left\{T^4 - (0.0552T_a^{1.5})^4\right\}, \tag{3.36}$$

and by employing Eq. (3.33), Eq.(3.35) may also be written as

$$C \cdot M \cdot \Delta T = \varepsilon\sigma A\left[T^4 - \left(T_a\left\{0.8 + \frac{T_{dp} - 273}{250}\right\}\right)^4\right], \qquad (3.37)$$

whereas using Eq. (3.33) in Eq. (3.34) gives

$$C \cdot M \cdot \Delta T = \left\{T_a\left[0.711 + 0.0056T_{dp} + 0.000073T_{dp}^2 + 0.013\cos(15t)\right]\right\}^4. \qquad (3.38)$$

Eqs (3.36), (3.37) and (3.38) describe a three-state process in which there exists radiation exchange between the surface and the sky and in turn the heat radiated by the collector surface which is absorbed by the air above it.

3.9 Wind speed measurement techniques

Wind speed measurements are usually taken at a height of 10 meters above ground level (a.g.l). This is the standard height recommended by the World Meteorological Organisation [15, 175]. However, in agrometeorological stations wind speeds are taken at a height of 2 above ground level. Most wind machines have their hub heights above this level or the standard meteorological height [15]. Thus, we require making extrapolations of average wind speeds so that they correspond to the hub height of the wind machine whenever wind speeds are measured at a different height. There are two method commonly used to extrapolate wind speed to higher distances above the standard heights. These methods are the logarithmic law, which is based on a combination of theoretical and semi-empirical techniques, and the power law, which is purely empirical.

The logarithmic law uses the mixing length theory and assumes that the stress and wind directions are constant with height and that the mixing length is zero at the

boundary layer which, increases with height. The logarithmic wind law expressing wind speed U as a function of height Z is of the form [15]:

$$U = \frac{U_*}{k} \ln \frac{Z}{Z_0} \tag{3.39}$$

where U_* is the friction velocity with a typical value of 0.2 to 0.4 ms^{-1}, $k \cong 0.4$ is the Von Karman's constant and Z_0 is the roughness length defined by Huschke [176] as a measure of the roughness of a surface over which a fluid is flowing, and must be determined empirically. It is sometimes taken as 15% of the average height of the roughness elements. Estimates of Z_0 range from much less than 1cm for relatively smooth land and ocean surfaces to meters for forests and urban areas [177]. This law gives reasonable results in the lower 50 to 60 meter layer in simple terrain during naturally stable conditions when mechanical turbulence predominates [15].

The other extrapolation method commonly used is the power law, which is expressed as:

$$\frac{u_1}{u_2} = \left(\frac{Z_1}{Z_2} \right)^a \tag{3.40}$$

where u_1 and u_2 are the wind speeds at heights Z_1 and Z_2 above the surface and a is the power law exponent, sometimes called the vertical component. It has been found that the power law exponent a strongly depends on the time of the day, wind stability and the surface roughness [178]. It has also been found that the magnitude of a ranges from 0.05 in the tropics to 0.4 in the temperate latitudes in winter [178, 179]. Under natural stability (e.g., at high wind speeds) and for open flat terrain, a is assumed to be 1/7 [12, 15]. This law is sometimes therefore called the 1/7 th power law. Low values of a apply

to exposed sites with relatively smooth surfaces in the prevailing direction of wind while high values are applicable to more complex terrain with pronounced surface roughness, particularly urban and forested areas [180].

3.10 Weibull statistics for wind speed measurement

The knowledge about the continuity of wind energy supply in a year is more important than the total amount of energy in a year. However, sites with annual average wind speed greater than or equal to $8\,ms^{-1}$ are considered good for electricity generation while those sites with average wind speed less than $5\,ms^{-1}$ are not good [12].

In order to explore the wind energy for any particular site, meteorological data on wind speed are required so that hourly mean speeds throughout the year are available. It is necessary to investigate the expected frequency distribution of the wind speed at that site [181, 182]. Frequency distribution of wind speed shows, for example, the number of hours per month or per year in which a certain value of wind speed has occurred. The frequency distribution of wind speeds therefore gives much more detailed information in comparison with annual or monthly average value [10]. Frequency distribution of wind speed is very useful in assessing the use of wind energy for power generation because, it helps in answering such questions as how long is a wind power plant not generating power in case of lack of wind and which is the range of the most frequent wind speeds [183]. From such distribution, one can be able to ascertain whether the available wind power is worth harvesting or not.

The data from meteorological stations can be used to draw some important curves such as the wind speed distribution curves which show the number of hours that certain wind speed is higher than the upper boundary of the wind speed interval and the wind

speed cumulative distribution curves, which show the number of hours that a certain wind speed was lower than the upper boundary of the wind speed interval. Histogram of wind speed frequency distribution can be drawn from which a cumulative frequency curve can be estimated. The cumulative frequency curve can then be used to assess the potential of wind energy at the site where the wind data was collected.

Usually, mathematical functions are found which approach these curves as closely as possible. Several such functions exist and they include; the Rayleigh distribution, the Bivariate normal, the Gamma distribution and the Weibull distribution [184, 185]. It has been found that the Weibull function approaches the frequency distribution curves much more closely than any of the functions mentioned above [181, 182, 185]. Furthermore, the Weibull function has been found more useful and appropriate for wind energy studies [17, 184]. The Rayleigh distribution function, which is a special case of the Weibull distribution, is sometimes used.

The cumulative distribution function $F(v)$, (or the wind speed duration curve) is related to the time fraction or the probability $P(v \leq v')$, that the wind speed v is smaller than or equal to a given wind speed v' by the relation [181, 184, 185].

$$F(v) = P(v \leq v'). \tag{3.41}$$

By using probability laws, the probability that the wind speed v is larger than or equal to a given wind speed v' can be expressed as:

$$1 - F(v) = P(v \geq v') \tag{3.42}$$

On the other hand, the probability density function $f(v)$, (or the wind speed frequency curve) is defined as [184, 185],

$$f(v) = \frac{dF(v)}{dv}. \tag{3.43}$$

From this definition, we can write

$$F(v) = \int f(v)dv . \tag{3.45}$$

The average speed $\bar{v}$ can be found by [12, 184]

$$\bar{v} = \frac{\int_0^\infty vf(v)dv}{\int_0^\infty f(v)dv} \tag{3.46}$$

The Weibull distribution function is a unimodal two parameter family of distribution functions. In the Weibull distribution, the probability density function (PDF) $f(v)$, for the wind velocity v is expressed as [12, 184, 186, 187]

$$f(v) = \frac{k}{c}\left(\frac{v}{c}\right)^{k-1} \exp\left[-\left(\frac{v}{c}\right)^{k}\right] \tag{3.47}$$

and the cumulative distribution function as

$$F(v) = 1 - \exp\left[-\left(\frac{v}{c}\right)^{k}\right] \tag{3.48}$$

where $v[\mathrm{ms}^{-1}]$ is the wind speed, $c[\mathrm{ms}^{-1}]$ is the Weibull scale parameter and $k[-1]$ is the Weibull shape parameter. The average wind speed $\bar{v}$ in Eq. (3.46) can be expressed as a function of k and c by using Eq. (3.47). Thus, for the Weibull distribution, the expression for the average wind speed $\bar{v}$ in Eq. (3.46) now becomes

$$\bar{v} = \frac{\int_0^\infty vv^{(k-1)} \exp\left[-\left(\frac{v}{c}\right)^{k} dv\right]}{\int_0^\infty v^{(k-1)} \exp\left[-\left(\frac{v}{c}\right)^{k} dv\right]}. \tag{2.76}$$

By letting $t=(v/c)^k$ (from which we get $v=ct^{1/k}$) and differentiating t with respect to v, (we get $dt=\left(k/c^{k-1}\right)v^{k-1}dv$) and substituting these into Eq. (3.48), we arrive at the expression for the average wind speed in the form

$$\bar{v}=c\int_0^\infty t^{\frac{1}{k}}\exp(-t)dt\,. \tag{3.49}$$

Note that after substitution, the denominator becomes unity. Eq. (3.49) can be expresses in the form of a standard integral called the factorial or gamma function defined as:

$$\Gamma(n)=\int_0^\infty y^{(n-1)}\exp(-y)dy \tag{3.50}$$

where y is any variable.

By relating the gamma definition Eq. (3.50) with Eq. (3.47), we notice that Eq. (3.47) can now be written as

$$\bar{v}=c\Gamma\left(1+\frac{1}{k}\right)=c\Gamma\left(\frac{1}{k}!\right) \tag{3.51}$$

taking into account that the Gamma function satisfies $\Gamma(1)=1$ and $\Gamma(n+1)=n\Gamma(n)$

The values of k and c can be estimated from different methods depending on which wind statistics are available and what level of sophistication in data analysis one wishes to employ [185]. The methods include the Weibull probability paper (or the least square fit to the observed distribution), the trends of k versus the wind speed, the mean wind speed and fastest mile, the standard deviation analysis and the median and quartile wind speeds.[185].

An example of data representation as velocity-duration curves or as velocity-frequency curves are shown in Figs. 3-3 and 3-4. The figures show three sets of velocity

data from three different sites A, B and C, which are at different heights with height at A greater than height at B and height at B greater than height at C.

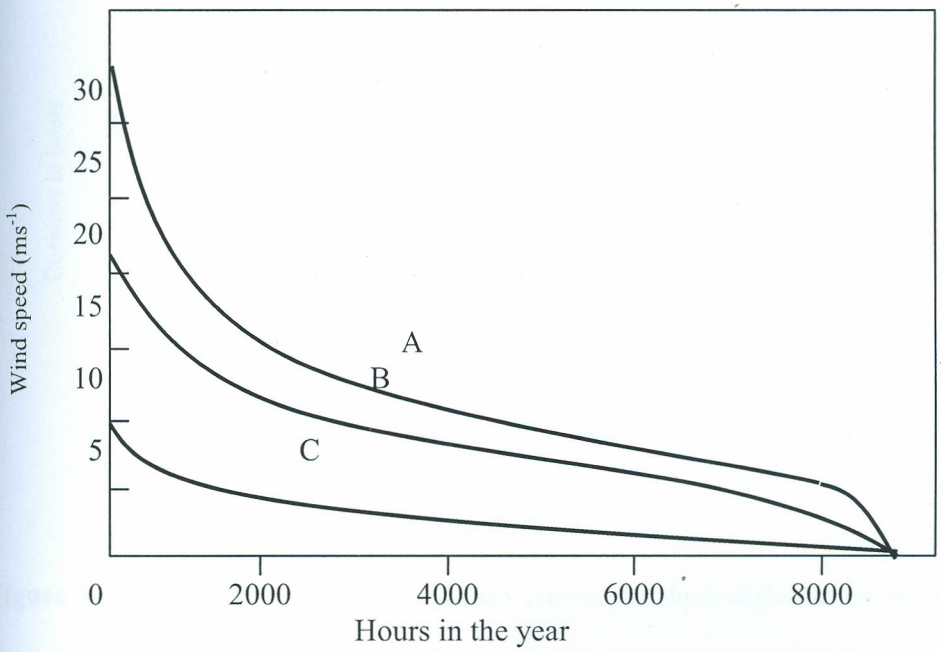

Figure 3-3. *Examples of velocity-duration curves for three different locations.*

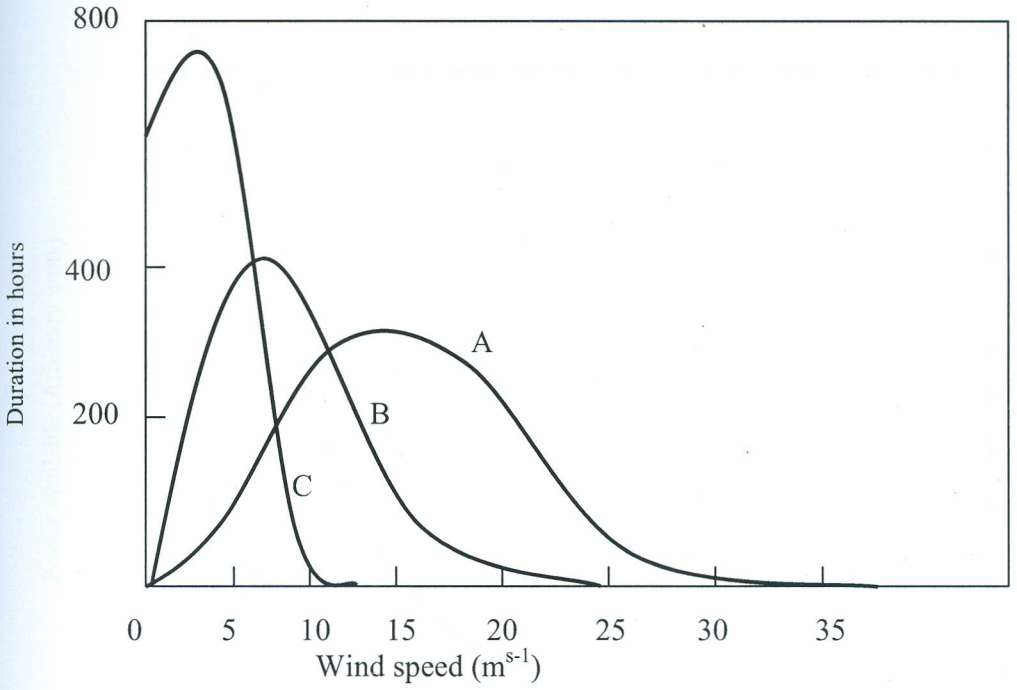

Figure 3-4. *Examples of velocity-frequency curves for three different locations of Fig.3-3.*

The average wind speeds for the three sites are A, B and C are 10.7, 7.2 and $2.8\,m\,s^{-1}$. Fig. 3-4 shows the number of hours in the year for which the speed equals or exceeds each particular value; Fig. 3-3 re-plots the same data to show the annual hours of duration of various wind speeds. The suitability of each site is illustrated in Fig. 3-5, where the velocities of values of Fig. 3-3 have been cubed to give the power on an arbitrary scale as the ordinate. The superiority of a site like A is apparent.

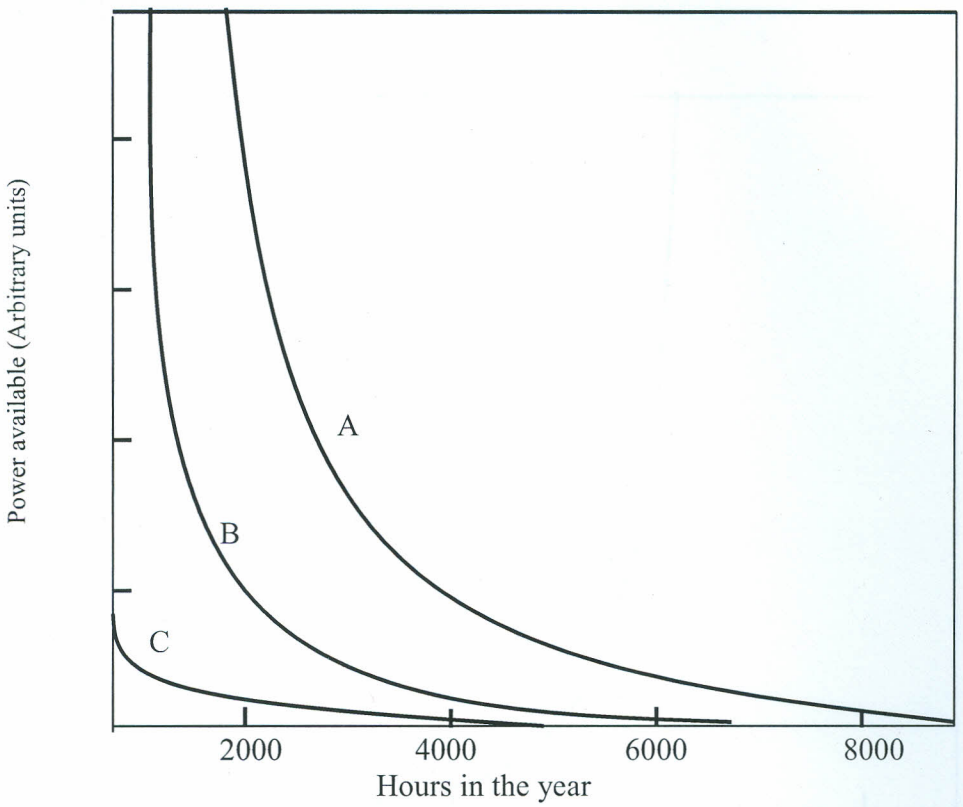

Figure 3-5. *The potential power output for the three sites A, B and C of Fig. 3-3.*

The load on a windmill structure increases with the square of the wind velocity, so that if advantage is to be taken of an exposed site, for example, the support must be capable of withstanding that load. As the device must be able to generate power in calm conditions as well as when the wind is strong, these considerations must inevitably lead to a compromise in design.

To avoid wind damage, a windmill should not be used in winds with speeds greater than the upper limit of 20.6 ms^{-1}. Figure 3-6 shows for example, a hypothetical curve indicating the proportion of the year with wind speeds greater than this speed as a function of mean annual speed. Thus, for a good site with an average speed of 11.6 ms^{-1}

say, winds over 20.6 ms^{-1} will persist for 8% of the year, at which times the device cannot be safely used.

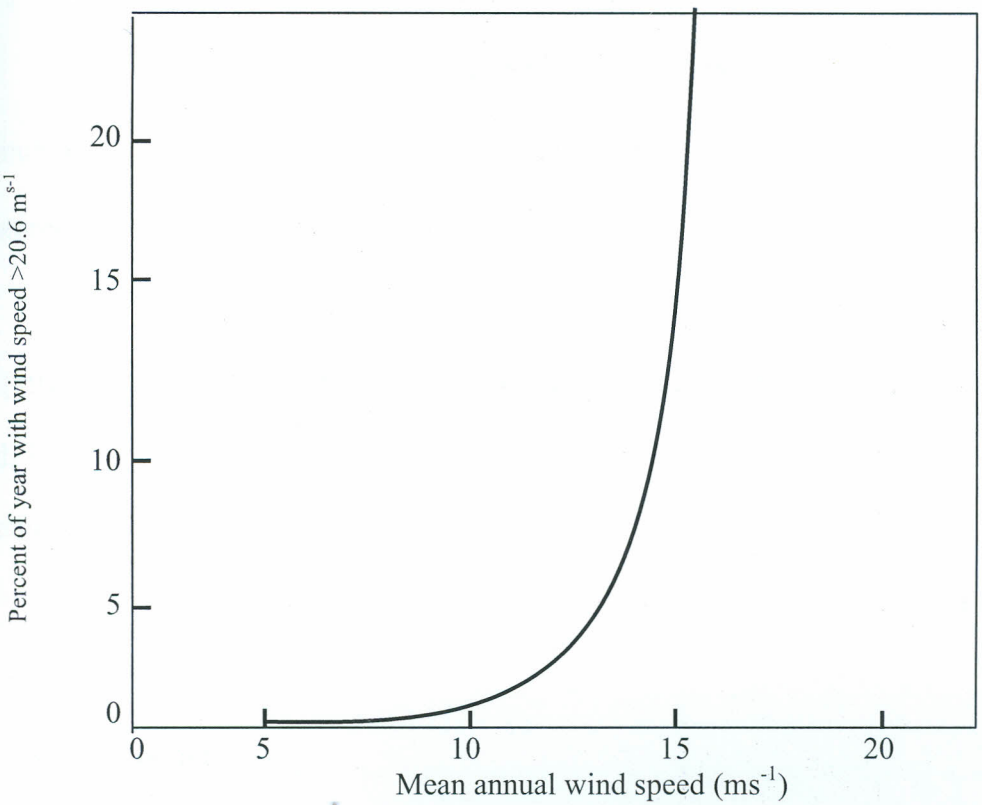

Fig.3-6. *Hypothetical curve of duration of high-speed winds as a function of mean annual wind speed.*

3.11 Wind power: energy calculations

During the last 15 years or so, advanced computational methods have been developed to gain the data to use in estimation of wind energy potential and micro sitting [188-190]. A precise prediction of the wind speed at a given site is essential for the determination of regional wind energy resources. Because of aerodynamic reasons, the power output of a wind turbine is proportional to the third power of the wind speed.

The power available from the wind, that is air in motion, is calculated on the basis that power is energy per unit time and the kinetic energy for any particle is $0.5mu^2$ where

m is its mass and v is the velocity. The volume per unit time of wind moving with velocity u through an area A is Au and the mass per unit time is ρAu where ρ is the density of air. Hence, available power is given by

$$\text{Power} = 0.5(\rho Au)u^2 = 0.5\rho Au^3 \text{ W}. \tag{3.52}$$

Substituting $\rho = 1.2 \text{kg m}^{-3}$ for average ambient conditions and considering unit area gives the theoretical maximum per area power as

$$\text{Power} = 0.6u^3 \text{ W m}^{-2}. \tag{3.53}$$

Betz [191] showed that the theoretical maximum efficiency of a windmill was 59% though later work by Shepard *et. al.* [192] raises this figure to 60%. Thus the normal maximum power per area is

$$P = 0.36u^3 \text{ W m}^{-2} \tag{3.54}$$

3.12 Solar chimney

The solar chimney electric power plant principle involves air being heated by solar radiation under a low transparent or translucent roof open at the periphery; the roof and the natural ground below it form a solar air collector. In the middle of the roof is a vertical tower with large air inlets at its base. The joint between the roof and the tower base is airtight. Since hot air is lighter than cold air, it rises up the tower. Suction from the tower then draws in more hot air from the collector, and cold air comes in from the outer perimeter. Continuous 24 hours operation can be achieved by placing tight water-filled tubes or bags under the roof. The water heats up during daytime and releases its heat at night. These tubes are filled only once, no further water is needed. Thus solar radiation causes a constant updraft in the tower. The energy contained in the updraft is converted

into mechanical energy by pressure-staged turbines at the base of the tower, and into electrical energy by conventional generators [43-45].

The fundamental dependencies and influence of the essential parameters on power output of a solar tower are presented here in a simplified form. Generally speaking, power output P of the solar tower can be calculated as the solar input $\dot{Q}_{solar}$ multiplied by the respective efficiencies of collector, tower and turbine(s):

$$P = \dot{Q}_{solar} \times \eta_{coll} \times \eta_{towr} \times \eta_{turbine} = \dot{Q}_{solar} \times \eta_{plant} . \tag{3.55}$$

The solar energy input $\dot{Q}_{solar}$ into the system can be written as the product of global horizontal radiation G_h and the collector area A_{coll} as

$$\dot{Q}_{solar} = G_h \times A_{coll} . \tag{3.56}$$

The tower (chimney) converts the heat-flow produced by the collector into kinetic energy by convection current and to potential energy by the pressure drop at the turbine. Thus, the density difference caused by the temperature rise in the collector works as a driving force. The column of air in the tower is less dense than the air in the surrounding atmosphere. These two air masses are connected at the base (inside the collector) and at the top of the tower, and thus acquires a lift. The total pressure difference Δp_{tot} is produced between the base (collector outlet) and the ambient given by

$$\Delta p_{tot} = g \int_0^{H_{tower}} (\rho_a - \rho_{tower}) dH . \tag{3.57}$$

Thus Δp_{tot} increases with tower height.

The pressure difference Δp_{tot} can be subdivided into a static component Δp_s and dynamic component Δp_d. Neglecting friction losses we can write

$$\Delta p_{tot} = \Delta p_s + \Delta p_d \tag{3.58}$$

The static pressure difference drop at the turbine and the dynamic component of the total pressure difference describes the kinetic energy of the airflow. With the total pressure difference and the volume flow of air at $\Delta p_s = 0$, the total power, P_{tot}, contained in the flow is now given by

$$P_{tot} = \Delta p_{tot} \times v_{tower,\max} \times A_{coll} \tag{3.59}$$

from which the efficiency of the tower can be established as

$$\eta_{tower} = \frac{P_{tot}}{\dot{Q}}. \tag{3.60}$$

Actual divisions of the pressure difference into static and dynamic component depends on the energy taken up by the turbine. Without turbine, a maximum flow speed of $v_{tower,\max}$ is achieved and the whole pressure difference is used to accelerate the air which, is then converted into kinetic energy according to Eq. (3.52):

$$P_{tot} = \frac{1}{2}\dot{m}u^2_{tower,\max} \tag{3.61}$$

where $\dot{m}$ implies a density mass profile with height and time.

Using the Boussinesq approximation [193, 194] whose basis is that there are flows in which the temperature varies little, and therefore the density varies little, yet in which the buoyancy drives the motion. Thus, the variation in density is neglected everywhere except in the buoyancy term. If we let ρ_b denote the density at the bottom where temperature is T_b, then for small temperature difference between the top and bottom layer we can write

$$\rho = \rho_b[1 - \gamma(T - T_b)] \tag{3.62}$$

where γ is the coefficient of volume expansion. For liquid the coefficient of volume expansion is in the range 10^{-3} to 10^{-4}. For temperature variation of moderate amount, we have

$$\frac{|\delta\rho|}{\rho_b} = \frac{|\rho - \rho_b|}{\rho_b} = \gamma|T - T_b| << 1 \tag{3.63}$$

but the buoyancy term $g(\rho - \rho_b)$ is the same order of magnitude as the inertia, acceleration or the viscous stress so it is not negligible. For this reason, the speed reached by free convection current in the tower can be expressed as

$$u_{tower,\max} = \sqrt{2 \times g \times H_{tower} \times \frac{\Delta T}{T_0}} \tag{3.64}$$

where ΔT is the temperature rise between the ambient and collector outlet (=tower inflow).

The tower efficiency is given in Eq. (3.60) becomes [46]

$$\eta_{tower} = \frac{g \times H}{c_p \times T_0} \tag{3.65}$$

This equation explains one of the basic characteristics of the solar tower; the efficiency is fundamentally dependent only on the height. For heights of 1000 m the deviations from the exact solution, caused by the Boussinesq approximation [193, 194], is negligible.

Using Eqs. (3.55), (3.56) and (3.65) we find that the solar tower power output is given by

$$P = G_h \times A_{coll} \times \frac{g \times H}{c_p \times T_0} \times \eta_{coll} \times \eta_{turbine} \tag{3.66}$$

which in terms of the dimensions of the plant is seen to be proportional to the collector area and the tower height.

As electrical output of the solar tower is proportional to the volume included within the tower height and the collector area, the same output may result from a large tower with small collector area and vice versa. As soon as friction losses in the collector are included in a detailed simulation, the linear correlation between power output and the product 'collector area times tower height' is not strictly valid any more. Still, it is a good rule of thumb as the collector diameter is not too large.

3.13 *Solar pressure-staged wind tunnel* electric power plant

The principle underlying the power generating system of *solar pressure-staged wind tunnel* technology compared to a natural process is now presented. In nature, it is solar power that creates wind power. Consider the example of the sea breeze in which the sun heats both land and sea, but the land heats up more quickly and reaches a higher temperature than the sea. The air over the land becomes hotter than the air over the sea and the hot air rises, creating an area of lower air pressure (close to the surface). Air moves from the area of higher pressure over the sea to the area of lower pressure over the land. The cool sea air heats up as it moves over the land and so it rises, creating a cycle. The result of this cycle is a steady wind moving from the sea to the land. In this example from nature, the land is acting like a solar collector, changing sunlight into heat. The heated land heats the air and creates a wind. Wind turbines can be used to harvest this wind energy. A *solar pressure-staged wind tunnel* power plant would imitate this same type of system that occurs in nature. The *solar pressure-staged wind tunnel* power plant would have a greater degree of control and predictability. This will result in a more reliable wind with a higher average-wind speed directed within tunnels housing turbines.

Solar pressure-staged wind tunnel electric power plant is still an experimental method that can be used to produce electric power from a solar/wind hybrid system. The system depicted in Figure 3-7 shows only a single tunnel for simplicity, however, up to four or more tunnels can be joined to the collector. The system consists of a large solar collector composed of a thermally selective material which absorbs heat from sunlight and the solar collector heats the air above it which then rises, as a result cooler air moves in to replace the rising hot air and a cycle begins.

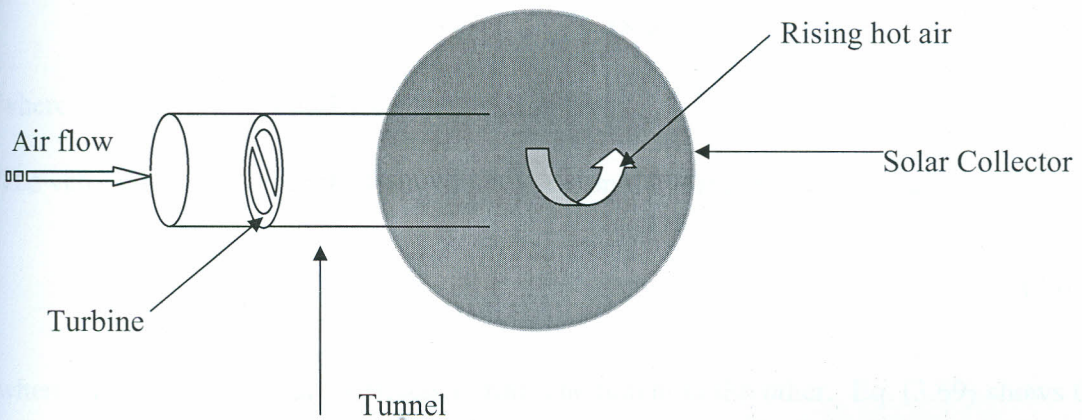

Fig. 3-7. *Schematic showing a proposed solar pressure-staged wind tunnel electric generating power plant.*

In the *solar pressure-staged wind tunnel* power plant, the solar collector continually heats the air, which rises and is replaced by cooler air from the surrounding environment. The heated rising air decreases the air pressure above the collector. The result is that the rising hot air over the collector creates a lower air pressure region than the cooler air over the land away from the collector. A large diameter pipe (or "air tunnel") is positioned to connect the lower air pressure region near the centre of the collector to the higher air pressure region a short distance away from the collector. Air then moves from high to low air pressure region through the air tunnel. Inside the air

tunnel, pressure-staged wind turbines convert the wind's mechanical energy into electricity. Using Eq. (3.52), available power from the wind in a tunnel depend on the wind velocity u according to the relation

$$P = \frac{1}{2}\dot{m}u^2 \tag{3.67}$$

According to Conte [37], the available wind power P_1, per square meter cross-sectional area depends on the cube of the wind velocity and density, hence Eq. (3.67) may be rewritten as

$$P_1 = 0.5 \times \rho \times u^3 \tag{3.68}$$

where v is the velocity and ρ is the air density.

The velocity of air within the tunnel impinging on the turbine blades is expressed as [37]

$$u = \sqrt{\frac{2}{3}\frac{\Delta p_{\text{tot}}}{\rho}} \tag{3.69}$$

where Δp_{tot} is the pressure difference from one tunnel to the other. Eq. (3.69) shows that the inverse square root of the air density affects the velocity [195]. Equation (3.69) can be solved for the total pressure difference Δp_{tot} giving

$$\Delta p_{tot} = u^2 \cdot \rho \cdot \frac{3}{2} \tag{3.70}$$

Equation (3.70) assumes that the wind turbine extracts the theoretical maximum power by reducing the pressure across the turbine Δp_s by two thirds of the pressure difference Δp_{tot} [46].

Since velocity is cubed in Eq. (3.68), overall, a greater air density provides less power and higher air temperature generally result in lower air density, which then provide higher air velocity and greater power. To find the power available for any cross-sectional

area of the tunnel which is assumed to house a turbine of the same diameter, the available power in the wind (P_1) in Eq. (3.68) is multiplied by the cross sectional-area to obtain the total power that a turbine of a particular diameter would generate at specified air velocity (u) and air pressure difference (Δp_{tot}) and through the air tunnel. Air density is assumed to be 1.165 kg/m^3 at 30 °C and standard atmospheric pressure.

For any area A_i m^2 swept by the turbine blade, the blade length of the turbine is given by

$$r_i = \sqrt{\frac{A_i}{\pi}} \text{ meters} \tag{3.71}$$

which is obtained by using the formula for the area of a circle $A = \pi r^2$

We now look at the wind flow dynamics within the tunnel. This very important effect could be used to increase the wind velocity in the tunnel by designing the main tunnel to have "wind injectors" or "booster tunnels" as shown in Fig. 3-8.

It is proposed that by incorporating "booster/injector tunnels" the wind velocity can be increased in the main tunnel by an amount δ, where δ is a constant greater than unity and would only be as a result of the effect of the "booster/injector" tunnels. By using Eq. (3.69), the velocity in the main tunnel would take the form

$$v = \delta \sqrt{\frac{2}{3}\frac{\Delta p_{\text{tot}}}{\rho}} \tag{3.72}$$

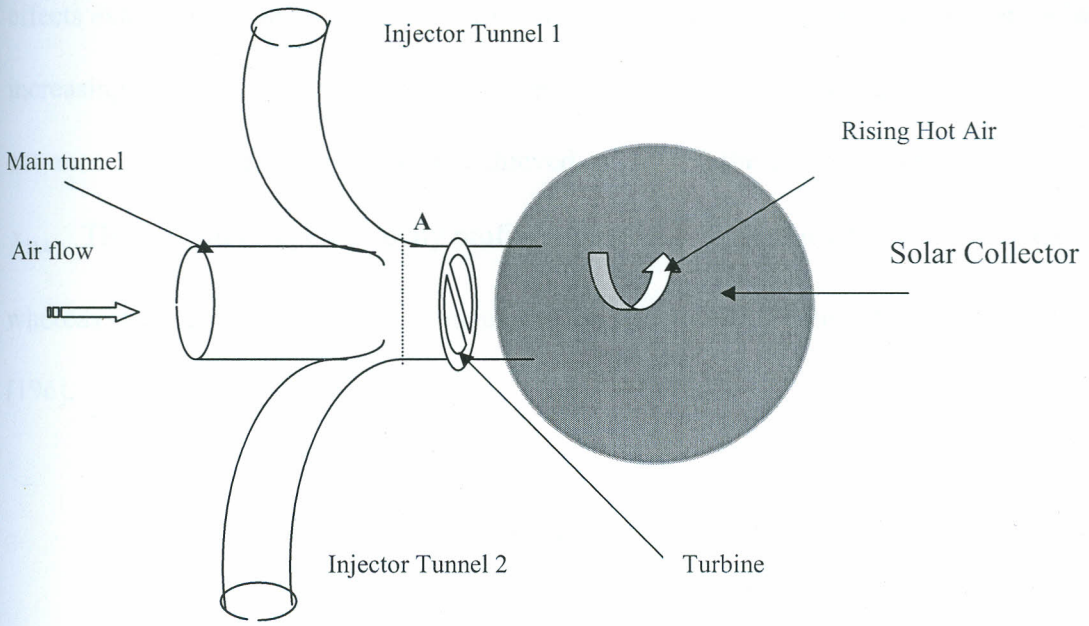

Fig. 3-8. *The modified wind from the sun power plant incorporating "injector/booster tunnels"*

Theoretically, Newton's third law of motion can be used to describe the flow of air inside the main tunnel. The mass of air at pint **A** as shown in Fig.3-8 is assumed to be moving with a certain prescribed velocity u_1. As air rushes in to the main tunnel through the booster/injector tunnels, the mass of air at point **A** is pushed forward by the mass of air from the injectors. If there is no loss due to friction, then the velocity of air in front of point A towards the collector should increase to u_2 say, where $u_2 > u_1$.

We now make theoretical analysis of airflow within a tunnel. We consider laminar flow of fluid in a tube of radius, r_o, (Fig. 3-9), where the fluid enters the tube with a uniform velocity. Assuming air to be a fluid, on contact with the surface, viscous effects come into play and become important with increasing distance x along the path of flow. This development occurs at the expense of a shrinking inviscid flow region and concludes with boundary layer merger at the centreline. Following this merger, viscous

effects extend over the entire cross section and the velocity profile no longer changes with increasing x. The flow is then said to be *fully developed*, and the distance from the entrance at which this condition is achieved is termed the *hydrodynamic entry length*, $x_{\mathrm{fd},h}$. The fully developed velocity profile is parabolic for laminar flow in a circular tube whereas it is *flatter* due to turbulent mixing in the radial direction for a turbulent flow [196].

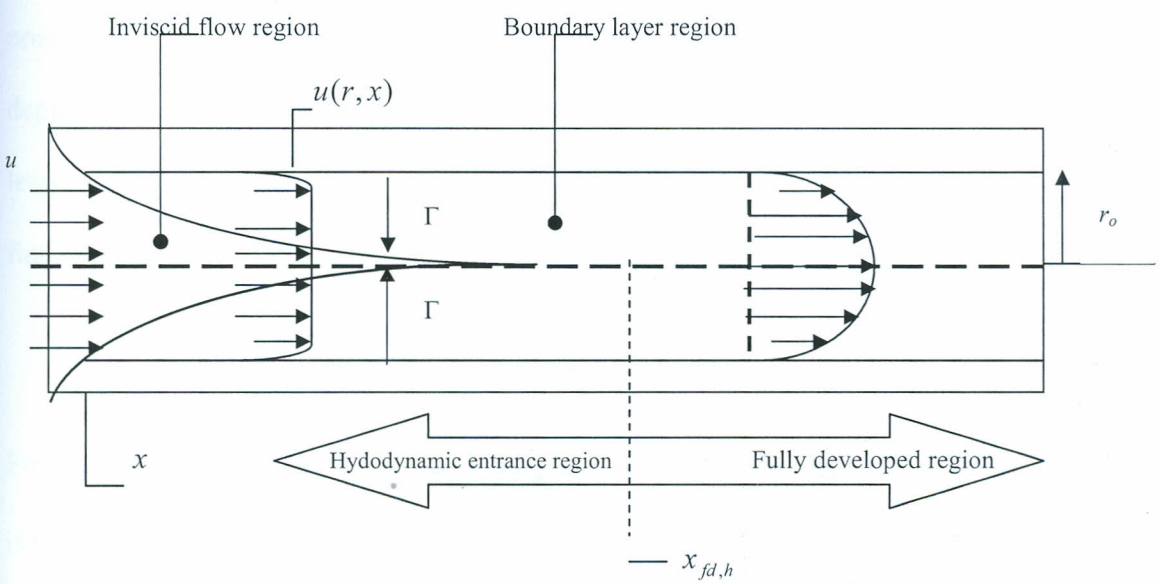

Figure 3-9. *Laminar, hydrodynamic boundary layer development in a circular tube (wind tunnel)*

The Reynolds number for flow in a circular tube is defined as

$$\mathrm{Re}_D \equiv \frac{\rho u_m D}{\mu}, \tag{3.73}$$

where u_m is the mean fluid velocity over the tube cross section, D is the diameter of the tube and μ is the viscosity (in $\mathrm{kg}\,s^{-1}\cdot\mathrm{m}$) of the fluid of mass density ρ. In a fully developed flow, the critical Reynolds number corresponding to the onset of turbulence is

$$\mathrm{Re}_{D,c} \approx 2{,}300 \tag{3.74}$$

although much larger Reynolds number ($\mathrm{Re}_D \approx 10{,}000$) are needed to achieve fully turbulent conditions. For laminar flow ($\mathrm{Re}_D \approx 2{,}300$), the hydrodynamic entry length may be obtained from an expression of the form [196]

$$\left(\frac{x_{\mathrm{fd},h}}{\mathrm{D}}\right)_{lam} \approx 0.05\,\mathrm{Re}_D\,. \tag{3.75}$$

Equation (3.75) is based on the presumption that the fluid enters the tube from a rounded nozzle and is hence characterised by a nearly uniform velocity profile at the entrance as depicted in Fig. 3-9. Although there is no satisfactory general expression for the entry length in turbulent flow, it is approximately independent of Reynolds number and as a first approximation [196] is given by

$$10 \le \left(\frac{x_{\mathrm{fd},h}}{\mathrm{D}}\right)_{turb} \le 60\,. \tag{3.76}$$

For the purposes of calculations for a fully turbulent flow, the approximation $(x/D) > 10$ is usually used.

Since there is no well-defined free stream due to velocity variation over the cross section, it is necessary to work with the mean velocity u_m when dealing with internal flow. This velocity is defined in such away that, when multiplied by the fluid density and the cross-sectional area of the tube A_c, it provides the rate of mass flow through the tube. Hence,

$$\dot{m} = \rho u_m A_c\,. \tag{3.78}$$

For steady, incompressible flow in a tube of uniform cross sectional area, $\dot{m}$ and u_m are constants that do not depend on x. Employing Eqs. (3.74) and (3.78) for the flow in a circular tube ($A_c = \pi D^2 / 4$), the Reynolds number reduces to

$$\mathrm{Re}_D = \frac{4\dot{m}}{\pi D \mu} \tag{3.79}$$

Since the mass flow rate may also be expressed as the integral of mass flux (ρu) over the cross section

$$\dot{m} = \int_{A_c} \rho u(r,x) dA_c \,, \tag{3.80}$$

it follows that, for incompressible flow in a circular tube, an expression can be found for the mean velocity by using Eq. (3.78) and (3.80) as follows:

$$u_m = \frac{\int_{A_c} \rho u(r,x) dA_c}{\rho A_c} \tag{3.81}$$

Now, $A_c = \pi r_o^2$ therefore,

$$u_m = \frac{2\pi\rho}{\rho\pi r_o^2} \int_0^{r_0} u(r,x) r dr = \frac{2}{r_o^2} \int_0^{r_o} u(r,x) r dr \,. \tag{3.82}$$

Equation (3.82) may be used to determine the mean velocity u_m at any axial location x from the knowledge of the velocity profile $u(r)$ at that location.

For a fully developed velocity profile [196]

$$u(r) = -\frac{1}{4\mu}\left(\frac{dp}{dx}\right) r_o^2 \left[1 - \left(\frac{r}{r_o}\right)^2\right] \tag{3.83}$$

where $\frac{dp}{dx}$ is defined as the pressure gradient. From this result the mean velocity of the flow may be calculated by substituting Eq. (3.83) into Eq. (3.82) and integrating to obtain

$$u_m = -\frac{r_o^2}{8\mu}\frac{dp}{dx} \tag{3.84}$$

Substituting this result into Eq. (3.83), the velocity profile is then

$$\frac{u(r)}{u_m} = 2\left[1-\left(\frac{r}{r_o}\right)^2\right] \tag{3.85}$$

Since u_m can be computed from the knowledge of the mass flow rate, Eq.(3.80) can be used to calculate the pressure gradient.

3.14 Solar thermal technology

We shall consider water-heating systems because other systems for other fluids can be modelled along the same line as those for water.

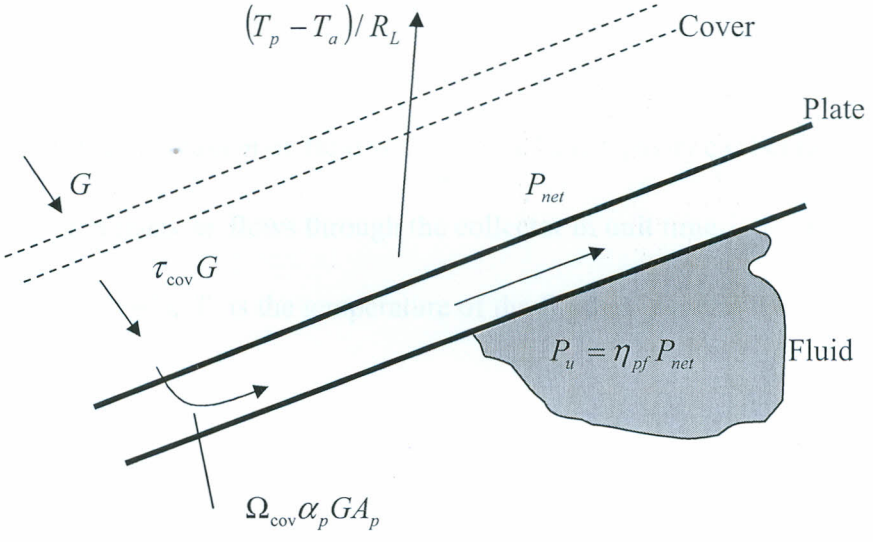

Fig. 3-10. *Heat transfer from solar radiation to a fluid in a collector.*

In Fig. 3-10, [12] the radiant flux striking the plate is $\Omega_{cov}A_pG$ where G is the irradiance on the collector, A_p is the exposed area of the plate and Ω_{cov} is the transmittance of any transparent cover that may be used to protect the plate from wind.

Only a fraction α_p of this flux is actually absorbed. Since the plate is hotter than its surrounding, it loses heat at a rate $(T_p - T_a)/R_L$ where R_L is the resistance to the heat loss from the plate with temperature T_p to the outside environment at temperature T_a. The net heat flow into the plate is given by

$$P_{net} = \Omega_{cov}\alpha_p A_p G - \{(T_p - T_a)/R_L\} = \eta_{sp} A_p G \qquad (3.86)$$

where η_{sp} is the capture efficiency (<1). Eq. (3.86) is known as the Hottel-Whillier equation.

In general, only a fraction η_{pf} of P_{net} is transferred to the fluid at temperature T_f. In a well-designed collector the temperature difference between the plate and the fluid is small, and the transfer efficiency η_{pf} is only slightly less than unity. Thus, the useful output power from the collector is

$$P_u = \eta_{pf} P_{net}$$

$$= mcdT_f/dt \text{ if a static mass } m \text{ of fluid with specific heat capacity c is being heated}$$

$$= \dot{m}c(T_2 - T_1) \text{ if a mass } \dot{m} \text{ flows through the collector in unit time.} \qquad (3.87)$$

In the second case of Eq. (3.87), T_1 is the temperature of the fluid as it enters the collector and T_2 as it leaves the collector.

These equations are most commonly used to determine the output P_u for a given irradiance G. The parameters A, Ω, α of the collector are usually specified, leaving R_L to be calculated using thermal resistance formulas.

There are many more uses of solar heat than just heating water. However, the theory of heat transfer and storage are quite similar to those of water heating systems.

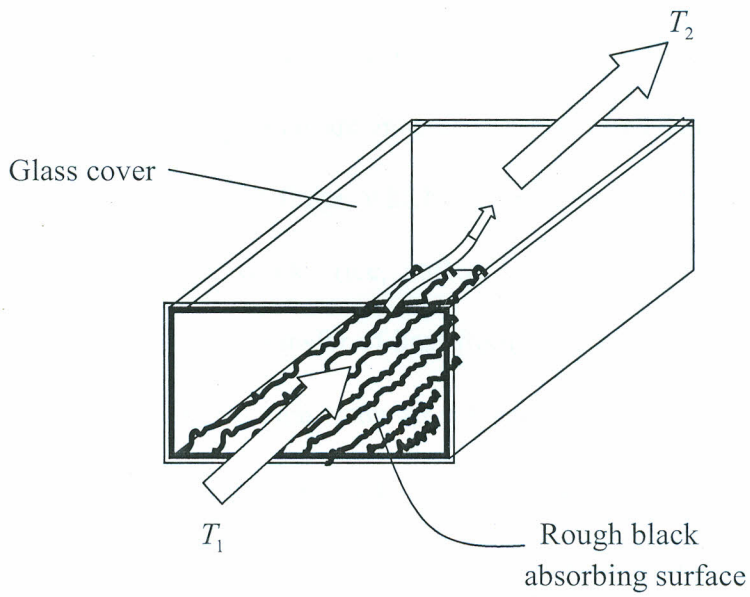

Fig. 3-11. *A simple design of air heater.*

For the design shown in Fig. 3-11, the useful heat flow into the air is given by

$$P_u = \rho c Q(T_2 - T_1) \tag{3.88}$$

where $Q = Au$ is the volumetric flow rate at velocity u, ρ is the density of the fluid, c the specific heat capacity and $T_2 - T_1$ is the temperature difference between the outlet and the inlet. The density of air is 0.001 that of water, and so for the same energy input, air, can be given a much greater volumetric flow rate Q. Since the thermal conductivity of air is much lower than that of water for similar circumstances, the heat transfer from the plate to the fluid is much poorer. Therefore air heaters of the type shown in Fig. 3-11 are often built with roughened or grooved plates, to increase surface area and turbulence available for heat transfer to the air. An alternative strategy is to increase the contact area by using porous or grid collectors. The analysis of internal heat transfer is complicated, because the same molecules carry the useful heat and the convective heat loss, i.e. the

flow "within" the plate and from the plate to the cover is coupled. The usual first approximation is to ignore this coupling and use Eq. (3.86) as for water heaters.

Most agricultural crops which are intended to be stored before use have to be dried first. Otherwise, insects and fungi, which thrive in moist conditions, render them unusable. Examples include wheat, rice, coffee, copra (coconut flesh), maize, and timber. All crop drying involves transfer of heat from the crop to the air around it. It is important to determine first how much water air can accept as water vapour by the use of psychometric charts, which show plots of the saturation humidity, χ_s, or some related measure of humidity against temperature T. The *absolute humidity* (or "vapour concentration"), χ, is the mass of water vapour in $1\,\mathrm{m}^3$ of air. At a particular temperature T, if we try to increase χ beyond saturation, (e.g. by blowing in steam), liquid water condenses. The ratio χ/χ_s is called the relative humidity, and ranges from 0% (completely dry air) to 100% (saturated air). Many other measures are also used [197].

If unsaturated air is passed over wet material, the air will take up air from the material. The water has to be evaporated and the heat to do this comes from the air and material. The air is thereby cooled. In particular, if a volume V of air is cooled from T_1 to T_2 in the process of evaporating a mass m_w of water, then

$$m_w \Lambda = \rho c V (T_1 - T_2) \tag{3.89}$$

where Λ is the latent heat of vaporization of water and ρ and c are the density and specific heat capacity of air at constant pressure at the mean temperature, for moderate temperature differences.

The basic problem in designing a crop drier is therefore to determine a suitable temperature (T_1) and volume (V) to remove a specified amount of water (m_w). The temperature (T_1) must not be too high, because this would make the grain crack and so allow bacteria and parasites to enter, and high humidity at elevated temperature for extended time will encourage microbial growth.

Another major use of energy in colder climates is to heat buildings in winter as opposed to cooling them in hot climates during summer. What is considered as a comfortable air temperature depends on the humidity, the radiation flux, the wind speed and on how much clothing one is wearing. Therefore the aim is to keep the inside (room) temperature T_r in a comfortable range (say $15-20^0$ C) while using the minimum artificial heating P_{boost}, even when the ambient temperature T_a drops to 0^0 C or less. The heat balance of the inside of the building is given by equation like Eq. (3.86), namely

$$mc\frac{dT_r}{dt} = \Omega\alpha GA + P_{boost} - \frac{(T_r - T_a)}{R} \tag{3.90}$$

where R is the loss resistance.

For cooling foodstuffs etc., at least in small quantities, there are also available commercial compression refrigerators and freezers powered by solar cells via batteries. These are economically attractive for remote areas from conventional electricity supplies.

In the last category of solar thermal systems we briefly discuss water desalination systems. To support communities in desert areas there is need to supply fresh water for drinking, crop growth and general purposes. Many desert regions have supply of salt water under the ground, and it is usually much cheaper to distil this water than to transport fresh water from afar. Since deserts usually have high insolation, it is reasonable to use solar energy to perform this distillation.

We finally in this section consider a different category of solar thermal systems known as solar concentrators. Solar concentrators are the collection of devices which increase solar radiation flux on the absorber surface as compared to the radiation flux existing on the entrance aperture. Fig.3-12 show schematic diagrams of the most common concentrating solar collectors. [198]. Optical concentration is achieved by the use of reflecting or refracting elements positioned to concentrate the incoming solar radiation flux onto a suitable absorber. Due to the apparent diurnal motion of the sun, the concentrating surface, whether reflecting or refracting will not be in a position to redirect the solar radiation on the absorber throughout the day if both the concentrator surface and absorber are stationary.

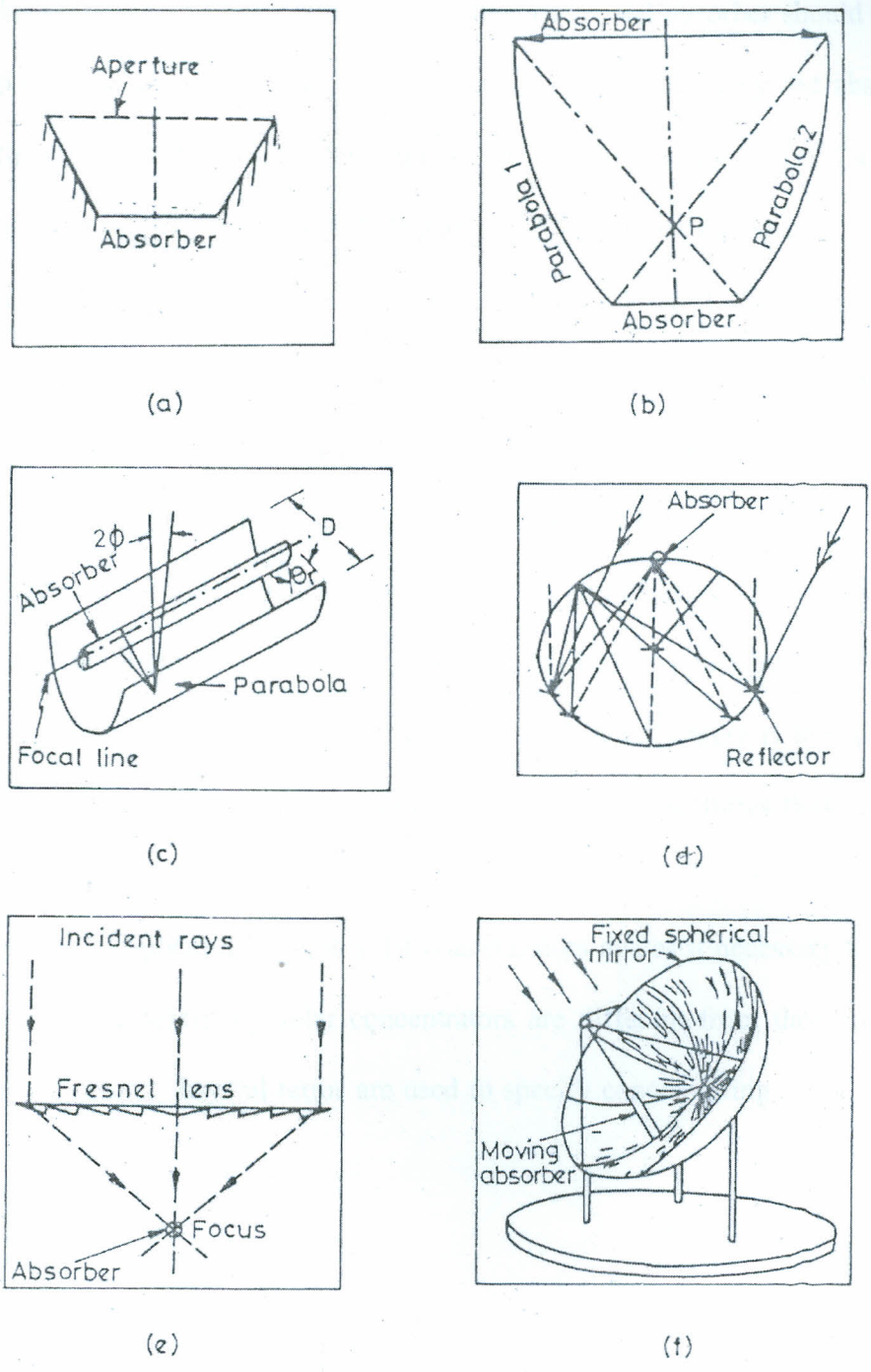

Fig. 3-12. *Schematic diagrams of the most common solar concentrators: (a) Flat plate absorber with plane reflectors (V trough), (b) compound parabolic concentrator, (c) Cylindrical parabolic trough, (d) Russel's fixed mirror solar concentrator, (e) Fresnel lens, (f) Hemispherical bowl.*

Ideally, the total system consisting of mirror/lens and absorber should follow the sun's apparent motion so that the sun rays are always captured by the absorber. In general, therefore, a solar concentrator consists of (i) a focussing device (ii) a blackened metallic absorber provided with a transparent cover and (iii) a tracking device for continuously following the sun. Temperatures as high as $3{,}000^0$ C can be achieved with solar concentrators and they find applications in both photo-thermal and photovoltaic conversion of solar energy. The use of solar concentrators may lead to advantages such as increase in energy delivery temperatures, improved thermal efficiency due to reduced heat loss, reduced cost due to replacement of large quantities of expensive material(s) for constructing flat plate solar collector systems by less expensive reflecting and/or refracting elements and a smaller absorber tube. Additionally there is the advantage of increased number of thermal storage options at elevated temperatures thus reducing the storage cost.

The use of optical devices in solar concentrators makes it necessary that some of the parameters characterizing solar concentrators are different from those used in flat plate solar collectors. Several terms are used to specify concentrating collectors. These are:

(i) Aperture area

(ii) Acceptance angle

(iii) Absorber area

(iv) Geometrical concentration ratio

(v) Local concentration ratio

(vi) Intercept factor

(vii) Optical efficiency

(viii) Thermal efficiency.

The aperture area (A_a), is defined as the plane area through which the incident solar radiation is accepted whereas the acceptance angle $(\theta_{\max})$ defines the limit to which the incident ray path may deviate from the normal drawn to the aperture plane and still reach the absorber. A concentrator with large acceptance angle needs only seasonal adjustments while one with small acceptance angle must track the sun continuously.

The absorber area (A_{abs}), is the total area that receives the concentrated solar radiation. It is the area from which useful energy can be removed and the geometrical concentration ratio (C), or the radiation balance concentration ratio of a solar concentrator is defined as the ratio of the collecting aperture area to the area of the absorber. Mathematically this is given by

$$C = \frac{A_a}{A_{abs}} \tag{3.91}$$

The brightness concentration ratio or the local concentration ratio is a quantity that characterizes the nonuniformity of illumination over the surface of the absorber. It is the ratio of the radiation flux arriving at any point on the absorber to the incident radiation flux at the entrance aperture of the solar concentrator.

The intercept factor (γ) for a concentrator-receiver system is defined as the ratio of energy intercepted by the absorber of a chosen size to the total energy reflected/refracted by the focussing device, that is,

$$\gamma = \frac{\int_{-\omega/2}^{+\omega/2} I(x)dx}{\int_{-\infty}^{+\infty} I(x)dx}, \tag{3.92}$$

where $I(x)$ is the solar flux at a certain position (x) and ω is the width of the receiver. For a typical concentrator-receiver design its value depends on the size of the absorber, the surface area of the concentrator and solar beam spread.

The optical efficiency (η_0), of a solar concentrator-receiver system is defined as the ratio of the energy absorbed by the absorber to the energy incident on the concentrator's aperture. It includes the effect of mirror/lens surface shape and reflection/transmission losses, tracking accuracy, shading, receiver cover transmittance of the absorber and solar beam incidence effects.

In a thermal conversion system a working fluid may be a liquid, a vapour or gas is used to extract energy from the absorber. The thermal performance of a solar concentrator is characterized by its thermal efficiency, which is defined as the ratio of useful energy delivered to the energy incident on the aperture of the concentrator.

The instantaneous efficiency of a solar concentrator may be calculated from an energy balance on the absorber. The useful energy delivered by a concentrator is given by

$$q_u = \eta_0 I_b A_a - U_L (T_{abs} - T_a) A_{abs} \tag{3.93}$$

where I_b is the direct beam on the concentrator, U_L is called the overall heat loss coefficient for the collector of the concentrator and is the sum for the heat loss from the bottom, U_b, the sides, U_s, and the top, U_t, i.e.,

$$U_L = U_b + U_s + U_t . \tag{3.94}$$

The other symbols have their usual meanings as previously defined.

The instantaneous efficiency, which is defined as the useful rate of energy delivered to the working fluid divided by the energy incident at the concentrator aperture, may then be written as

$$\eta = \frac{q_u}{I_b A_a} = \eta_0 - \frac{U_L (T_{abs} - T_a)}{I_b C}. \tag{3.95}$$

The linear approximation of heat loss factor made in Eq. (3.94) is valid for small operating temperatures only. At high operating temperatures, where the radiation loss term dominates the convective losses, energy balance may be written as

$$q_u = \eta_0 I_b A_a - U_L (T_{abs}^4 - T_a^4) A_{abs} \tag{3.96}$$

where U_L now takes into account the accompanying convective and conduction losses also, hence Eq. (3.95) may now be modified as

$$\eta = \eta_0 - \frac{U_L (T_{abs}^4 - T_a^4)}{I_b C}. \tag{3.97}$$

Since the absorber surface temperature is difficult to determine, it is convenient to express the efficiency in terms of the inlet fluid temperature T_i by means of the heat removal factor F_R as

$$\eta = F_R \left[\eta_0 - \frac{U_L (T_i - T_a)}{I_b C} \right]. \tag{3.98}$$

Equation (3.98) is a first order steady state expression for the instantaneous efficiency of a solar concentrator. The instantaneous efficiency of a solar concentrator receiver system is dependent on two types of quantities, namely the concentrator receiver design parameters and the parameters characterizing the operating conditions. The optical efficiency, heat loss coefficient and heat removal factor are the design dependent

parameters while the solar flux, inlet fluid temperature and the ambient temperature define the operating conditions.

3.15 Thermophysical properties of opaque bulk materials

When a sample bulk opaque material is heated by absorption of photon flux from a solar simulator and cools by radiation, the solar absorptance and hemispherical emittance and their ratio can be calculated from the measured rates of heating and cooling. During the heating and cooling to an equilibrium temperature of the specimen, the following heat equations [199] apply

$$\alpha = \frac{mC_p}{A_1 I_s}\left(\frac{dT}{dt}\right)_{heating} \tag{3.99}$$

and is used when the sample is exposed to solar radiation, where α, is the absorptance, m is the mass of the sample, C_p, is the specific heat, and $\left(\frac{dT}{dt}\right)_{heating}$ its heating rate. A_1 is the irradiated area of the sample and I_s is the irradiation intensity. In this equation, the radiation losses are neglected by assuming that $T \approx T_2$, the ambient temperature.

When radiation source is turned-off, the sample cools and heat is emitted by the sample. The equation governing the emitted radiation is

$$\varepsilon = \frac{mC_p}{A_2\sigma(T^4 - T_2^4)}\left(\frac{dT}{dt}\right)_{cooling} \tag{3.100}$$

where $\left(\frac{dT}{dt}\right)_{cooling}$ is the cooling rate at temperature T of sample, T_2 is the temperature of the surrounding (ambient), A_2 is the total area of the sample and σ is the Stefan-Boltzmann constant.

Under constant irradiance from solar simulator, an equilibrium is reached when heating and cooling rates are equal and sample attains a stagnation temperature, T_1. When equilibrium is attained, then

$$\frac{\alpha}{\varepsilon} = \frac{A_2\sigma(T_1^4 - T_2^4)}{I_s A_1}. \tag{3.101}$$

This model has the advantage of yielding the absolute values without the need for any comparison standard. It also gives the value of $\frac{\alpha}{\varepsilon}$ as a function of temperature.

Using an integrating sphere without ports as employed in this work, if one considers reflection of heat inside the sphere, simple calculations show that if the initial radiation is reflected only once from the inside of the sphere, then a sample placed in the middle of the sphere will receive from any direction 98% reflection of the original heat energy [200]. Continuing this calculation on 98% reflection of energy at any time, a second reflected radiation will posses 96.04% of the original radiation and a third beam reflected from the wall of the sphere will have 94.12% of the original energy. A fourth reflected beam possesses 92.24% of the initial radiation and a fifth reflected beam has 90.39% of the original radiation. Further calculation and simulation show that after several reflections inside the sphere, the amount of radiation which still fall on the sample in this configuration is more than 50% of the original radiation. (Fig. 3-13). It is thus reasonable to assume that the sample is heated uniformly and also radiates uniformly. Hence, when A_1 (the irradiated area of the sample) equals A_2 (the total area of the sample) Eq. (3.101) reduces to:

$$\frac{\alpha}{\varepsilon} = \frac{\sigma(T_1^4 - T_2^4)}{I_s}. \tag{3.102}$$

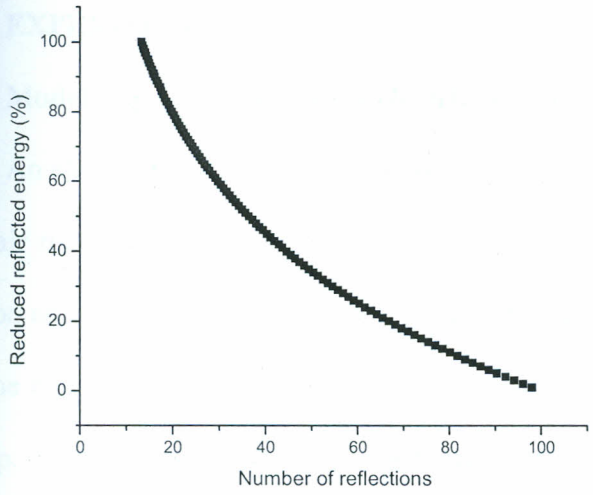

Fig.3-13. *Reflected energy versus the number of reflections.*

CHAPTER FOUR

4.0 EXPERIMENTAL

4.1 Modelling of solar chimney electric power plant

An electric power station using solar chimney is based simply on the principle that warm air rises. Air underneath a glass ceiling or transparent plastic is heated by solar radiation and rises through a chimney. The warm air that has just risen is replaced by air from the edge of the glass or plastic, which flows inwards, and will then itself begin to heat up. In this way, the sun's heat radiation is converted into kinetic energy of constantly rising air to drive turbine built into the chimney. The turbine then converts the wind power by means of a generator into electrical energy. We design and model an appropriate solar chimney that can be constructed in rural villages in developing countries where the grid is absent or inaccessible. The design and simulation of the solar chimney electric power generating plant considers the parameters that would maximise the power production but minimise the dimensions of the chimney.

We start by analysing the heat balance equation for a solar chimney electric power plant illustrated in Fig. 4-1. The heat energy transferred from a patched surface of the collector is given by

$$W_1 = hA(T_s - T_H) \tag{4.1}$$

where T_s and T_H are the temperatures at the surface covered by a selective material and at any position H in the covered area A and h is the convective transfer coefficient.

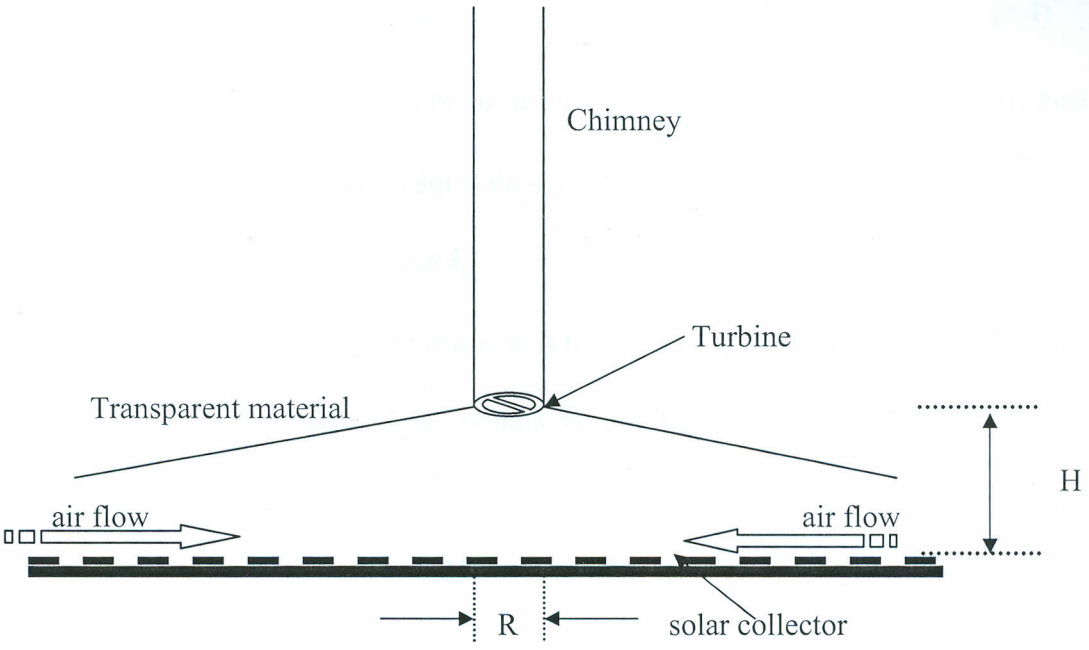

Fig. 4-1. *Solar chimney electric power generator.*

The convective coefficient is given by

$$h = h(R_e, P_r, k, L).$$

In the case of a turbine [84],

$$h = 0.036 \frac{k}{L} P_r^{\frac{1}{3}} R_e^{0.8} \tag{4.2}$$

where k is the thermal conductivity of the air, L is the width of the surface, R_e and P_r are the Reynolds and Prandt numbers, respectively [7, 200, 201].

For a square collector of sides L, the area is given by $A = L^2$ and equation (4.1) becomes

$$W_1 = hL^2(T_s - T_H). \tag{4.3}$$

On the other hand heat transferred from the patched area to air under the canopy is given by

$$W_2 = \dot{m} C_p (T_m - T_s) \tag{4.4}$$

where T_m is the temperature of mass of air inside the chimney, and C_p is the specific heat capacity at constant pressure and m dot is the mass flow rate (kg/s) given by

$$\dot{m} = \rho_a u A_p \tag{4.5}$$

where ρ_a is the ambient density of the air, u is the velocity with which the mass flows.

The cross-sectional area of the opening around the square patch of side L is given by

$$A_p = 4LH\ .$$

This allows Eq. (4.4) to be rewritten as

$$Q_2 = 4\rho_a u C_p LH(T_m - T_s)\,. \tag{4.6}$$

For a circular chimney of radius R, the velocity $\bar{u}$ at which air impinges on the rotor blades of the air turbines can be obtained by equating the air inflow into the collector and the outflow from the chimney resulting in

$$\pi R^2 \bar{u} = 4LHu \tag{4.7}$$

resulting in

$$u = \frac{\pi R^2 \bar{u}}{4LH} \tag{4.8}$$

hence the heat transfer to the air under the chimney is

$$W_1 = Q_2 = \rho_a \pi R^2 \bar{u} C_p (T_m - T_s)\,. \tag{4.9}$$

Combining Eqs. (4.3) and (4.9), we obtain

$$h = \frac{\pi \rho_a C_p R^2 \bar{u}}{L^2} \left(\frac{T_m - T_s}{T_s - T_H} \right). \tag{4.10}$$

Transposition of Eq. (4.10) gives

$$\bar{u} = \frac{hL^2}{\pi \rho_a C_p R^2}\left(\frac{T_s - T_H}{T_m - T_s}\right). \tag{4.11}$$

Substituting known values for the constants in Eq. (4.11), we obtain the expression for the velocity V, at which the air impinges on the rotor blades as

$$\bar{u} = \left(\frac{0.036}{\pi}\right)^5 \left(\frac{\pi}{4}\right)\left(\frac{L^5 k^5}{\xi^{\frac{5}{3}} H^4 \nu^{\frac{7}{3}} C_p^5 \rho_a^5 R^2}\right)\tau^5 \tag{4.12}$$

where

$$\tau = \left(\frac{T_s - T_H}{T_m - T_s}\right) \tag{4.13}$$

ν is the kinematic viscosity, ξ the thermal diffusivity of the air and k the thermal conductivity of the air at a given temperature.

If it is assumed that the area swept by the rotor is the same as the cross-sectional area of the chimney, then using Eq. (4.7), the instantaneous electric power P_i produced by a single turbine is readily derived as

$$P_i = \frac{16}{27}\left(\frac{1}{2}\rho_m \pi R^2 \bar{u}^3\right) \tag{4.14}$$

where ρ_m is the density of the air at temperature T_m and the factor of $\frac{16}{27}$ (called the Betz criterion) gives the ideal limit for the extraction of power and can be applied to all turbines set in an extended fluid stream.[12, 202, 203].

From Eqs. (4.12) and (4.14), the instantaneous electric power is

$$P_i = 3.0\times10^{-31}\beta\left(\frac{L^{15}}{H^{12}R^4}\right)\tau^{15} \tag{4.15}$$

where at $300K$ and one atmosphere

$$\beta = \left(\frac{\rho_m k^{15}}{\xi^5 C_p^{15} \nu^7 \rho_a^{15}} \right) = 1.493 \times 10^{-12}. \qquad (4.16)$$

Equation (4.15) shows that the instantaneous electric power depends mainly on the dimensions of the solar chimney for a given temperature ratio, τ. Thus the equation can be treated as generic. However, except for the ambient density ρ_a, all other parameters in Eq. (4.16) vary with τ, hence β is a function of τ hereafter expressed as $\beta(\tau)$. Substituting known constants [41, 42, 50] in Eq. (4.15) for dry air at one atmospheric pressure and ambient temperature ($T = 300K$), the expression for the instantaneous power reduces to

$$P_i = 4.48 \times 10^{-43} \times \left(\frac{L^{15}}{H^{12} R^4} \right) \tau^{15} \qquad (4.17)$$

Using known values of ρ_m, k, ξ, C_p ν and ρ_a [201] one can show that $\beta(\tau)$ does not change significantly from the value obtained at $300K$ and at one atmospheric pressure. The upper and lower limits of τ can, however, be determined through differentiation of equation (4.13).

For $T_s > T_H$ and $T_m > T_s$, Eq. (4.13) can be written as

$$\tau = (T_s - T_H) \frac{1}{T_m} \left(1 - \frac{T_s}{T_m} \right)^{-1}. \qquad (4.18)$$

Assuming that $T_m >> T_s$ we can use Binomial expansion on $\frac{1}{T_m}\left(1 - \frac{T_s}{T_m}\right)^{-1}$ in the product of Eq. (4.18) to obtain

$$\tau = (T_s - T_H) \frac{1}{T_m} \left[1 - \frac{T_s}{T_m} + \left(\frac{T_s}{T_m} \right)^2 - \left(\frac{T_s}{T_m} \right)^3 + \left(\frac{T_s}{T_m} \right)^4 - \left(\frac{T_s}{T_m} \right)^5 + \cdots\cdots \right]. \qquad (4.19)$$

Obviously the upper limit of τ is determined by the limit of the expanded binomial term since the surface temperature is fixed by the characteristics of the collector and the temperature at a height H is in turn fixed by the height. Given fixed values of T_s and T_H the upper limit is obtained by taking the maximum value of the binomial series for particular values of T_m. Expanding the bracket in Eq. (4.19) we get

$$\tau = \frac{T_s}{T_m} - \frac{T_s^2}{T_m^2} + \frac{T_s^3}{T_m^3} + \cdots\cdots - \frac{T_H}{T_m} + \frac{T_H T_s}{T_m^2} - \frac{T_s^2 T_H}{T_m^3} + \cdots\cdots . \tag{4.20}$$

Differentiating Eq. (4.20) with respect to T_m term by term and ignoring terms in $\frac{1}{T_m}$ above second order we get

$$\frac{d\tau}{dT_m} = \frac{T_H}{T_m^2} - \frac{T_s}{T_m^2} . \tag{4.21}$$

$\frac{d\tau}{dT_m} = 0$ gives the minimum value of τ when $T_s = T_H$. This is the equilibrium state when the surface temperature equals the temperature at the turbine level. However, the maximum value of τ approaches an asymptotic value as T_m approaches T_s, that is when $T_m - T_s$ approaches zero. The physical meaning of this condition is that the temperature of the air mass approaches the temperature of the solar collector surface as heat is transferred from the collector surface to the air mass as can be deduced from Eq. (4.13). Assuming reasonable typical temperatures for the collector surface, air mass and a reasonable height as $T_s = 330\text{K}$, $T_H = 313\text{K}$, $T_m = 334.4\text{K}$, we find that $\tau \approx 4.25$.

4.2 Modelling of *solar pressure-staged wind tunnel* electric power generating plant

The solar chimney power plant modeled in the last section operates on similar principles to the *solar pressure-staged wind tunnel* power plant. Fig. 4-2 shows a proposed model of *solar pressure-staged wind tunnel* power plant.

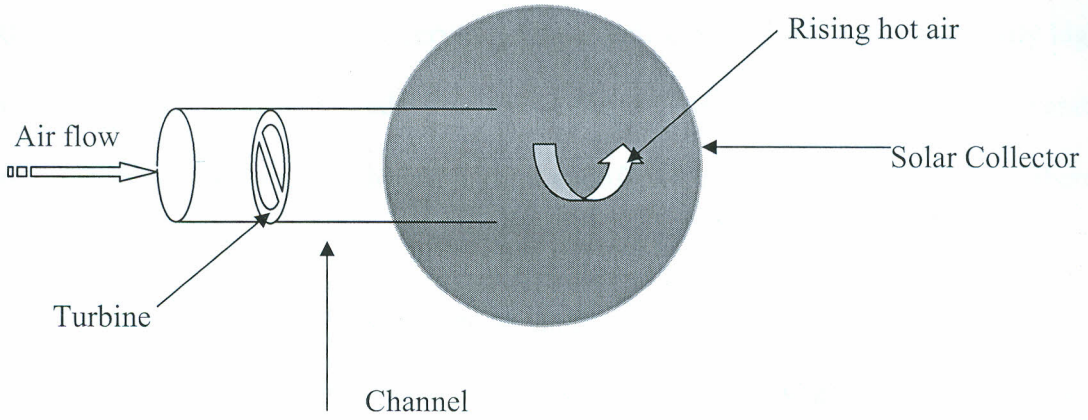

Fig. 4-2 *Schematics of the original proposed solar pressure-staged wind tunnel electric power plant.*

The plant to be simulated consists of a solar collector composed of material capable of absorbing solar radiation to increase its temperature. The hot collector material in turn heats the air above it creating a low-pressure region. Due to the pressure difference, air from the high-pressure region around the collector will rush through tunnels extending into the collector to drive turbines strategically placed to generate electricity through generators. Up to four tunnels can be placed on one collector.

The mechanism of the model described in Fig. 4-2 can be compared to the mechanism by which sea breeze is generated. In the case of the sea breeze, the temperature differences between two areas, land and sea creates wind. Similarly, the temperature difference between the solar collector and the surrounding land drives the system, producing wind. The solar collector must become significantly hotter than the

surrounding land in order to create wind. For a sea breeze, a typical temperature difference is 10° C resulting in a typical wind speed of 12 m/s [204]. The solar collector will tend to be hotter towards its centre and cooler towards its perimeter. A smaller solar collector loses some heat to its perimeter. A larger collector has less perimeter per unit area and so loses less heat to its perimeter, making the centre of the collector hotter than the perimeter. The centre of a very large solar collector will reach a significantly higher temperature than the outer edges of the collector. However, the crucial temperature difference is in the air, which will depend significantly on the collector surface thermal characteristics.

Both solar chimney power plant and *solar pressure-staged wind tunnel power* plant use a solar collector to heat air. They both generate wind from the rising of the heated air.

We will now model the *solar pressure-staged wind tunnel* electric power plant based on both theoretically generated data and existing information on certain parameters such as air densities at specific temperatures. According to Schlaich, [40] a solar chimney electric power plant with a solar collector of 400 meter in diameter and a 1,500 meter tall chimney will produce 600 GWh/y. The area of such a collector would be approximately 12.57 million square meters calculated by using $A = \pi r^2$.

Let us assume that the average solar radiation is X kWh/m^{2}y. The system's energy input can be determined by multiplying the area A m^2 of the solar collector by the average solar radiation giving $X \cdot A$ kWh/y. The energy input times the efficiency of the system gives the power output. The total efficiency would involve the efficiency of conversion of the sun's energy into useful heat and the efficiency of the wind turbine

itself which is taken as 0.5923 [203, 205]. For the *solar pressure-staged wind tunnel* power plant, the efficiency has not yet been determined. Even with a low overall efficiency, a sufficient amount of power can be obtained from such a system. Assuming an efficiency of 90% of conversion of light into heat and an efficiency of 59.23 for the turbine, the overall efficiency of the power generating plant will be 53.3%. Increasing the area of the solar collector will increase the power input, and, assuming certain degrees of efficiency, the power output would increase proportionately.

The air temperature above the solar collector is the result of the amount of energy from the sun, which is converted to heat by the collector and transferred to the air above. A scenario in which the amount of energy used to heat a certain amount of air is presented. To determine the amount of air, which can be heated on such a day, we use Eq. (4.22).

$$Q = C \cdot M \cdot \Delta T \tag{4.22}$$

In Eq. (4.22), Q is the heat added to the air by the solar collector, C is the specific heat capacity of the air, M is the mass of the air, and ΔT is the change in temperature. The energy input in Watt-hours can be converted to Joules. The conversion leaves us with the value for Q (heat added) in Joules as:

$$3600 \text{ seconds/hour} \cdot 0.9 \cdot R \cdot A \text{ Joules-hour/second} = 3240 \cdot R \cdot A \text{ Joules} \tag{4.23}$$

If the change in air temperature is a typical temperature difference needed to produce a strong sea breeze, then ΔT is about 10^0C. More air could be heated to a lower temperature, or less air to a higher temperature, with the same energy input. Also, in a real world system, it is not the case that an amount of air is heated to any particular temperature. However, there are gradations of temperature found in the volume of air

over the collector because the air is moving constantly and its temperature is changing over time. If we begin by calculating how much air the collector can heat to a particular temperature, we can find out whether enough air can be heated to drive the system.

The specific heat of the air will change over time, because the air is being heated and so undergoes changes in density, pressure, and temperature as it is heated. However, to simplify the calculations, we will choose a single conservative number for the specific heat of air within the range of densities, pressures, and temperatures, which the air will move through. The specific heat of dry air at constant pressure and at a temperature 30^0C is about 1,005 Joules/kg.C [206, 207].

Using Eq. (4.22) we get;

$$3240 \cdot R \cdot A \text{ Joules} = 1005 \text{ Joules/kg.C} \cdot M \cdot 10^0\text{C} \qquad (4.24)$$

Hence,

$$M = 0.3224 \cdot R \cdot A \text{ kg} \qquad (4.25)$$

Depending on the size of the collector and the solar radiation for a particular day, the amount of the air that the collector can heat by 10^0C is given by Eq. (4.25).

The volume of the air heated can be determined by dividing mass by density. The density of air at 30^0C is 1.165kg/m^3, but the air is now 40^0C, so the density has changed to 1.127kg/m^3 [38].

The volume of the heated air is then given by:

$$\text{Volume} = 0.2861 \cdot \text{R} \cdot \text{A m}^3 \qquad (4.26)$$

Eq. (4.26) gives the volume of air heated by 10^0C on a day with solar radiation of R Wh/m^2. The calculation provides an estimate of the amount of air the system can effect. Since the heat being added to the air is due to the heating of the collector by the

sun's energy, the heat balance equation must be evaluated due to the radiation exchange between the surface and sky.

We now simulate the power output of *solar pressure-staged wind tunnel* electric power plant. Since velocity is cubed in Eq. (3.52), overall, a greater air density provides less power and higher air temperature generally result in lower air density, which then provide higher air velocity and greater power. To find the power available for any cross-sectional area of the channel which is assumed to house a turbine of the same diameter, the available power in the wind (P_1) in Eq. (3.68) is multiplied by the cross sectional-area. This allows us to compute the output power. The total air pressure difference (Δp_{tot}) and air velocity (u) through the air channel, to power available in the wind per square meter (P_1) to the swept area of the wind turbines and total power output (P_2) can then be compared. Air density is assumed to be 1.165 kg/m at 30 degrees Celsius and standard atmospheric pressure. Total power output (P_2) is simply the product of the power of the wind per square meter and the total swept area (A) of the turbines. Note that total power output is the theoretical maximum, actual power output will be less than is theoretically possible. Thus, the total power output can be expressed as

$$TOTAL\ POWER\ OUTPUT = P_1 \times SWEPT\ AREA \tag{4.27}$$

For any area A_i m^2 swept by the turbine blade, the blade length of the turbine is given by

$$r_i = \sqrt{\frac{A_i}{\pi}} \text{ meters} \tag{4.28}$$

which is obtained by using the formula for the area of a circle $A = \pi r^2$. In simulating the power output, we use a range of values of the radius r from Eq. (4.28) in Eq. (4.27) to calculate the total power output for different turbines.

4.3 Determination of thermophysical properties of opaque bulk materials

The calorimeter, a closed integrating sphere made from two half-spheres of hard plastics, whose inside is painted white with barium sulphate was used in this work. Four (4) thermocouples to measure temperatures were interfaced to a Fluke-2286/5 data logger through a temperature measuring card attached to the data logger as shown in Fig. 4-8. The complete integrating spherical calorimeter formed had a diameter of 10 cm. The spherical box chamber had a rectangular or entrance window (3.55 cm × 2.22 cm), a sample holder, a shutter, tungsten–halogen lamp (90 watts) attached to it. An external power supply was used to the lamp and a KIPP & ZONEN pyranometer was used to measure the global irradiance from the lamp.

Before the actual measurements were taken, all the four thermocouples were placed randomly on the sample and from the initial state; the readings were recorded after 200, 300 and 400 seconds with the readings being averaged every time the measurements were taken. These test runs were done five times. The thermocouples were then placed randomly in the sphere and the measurements taken again. Each time the measurements were taken, it was found that the average values varied from the measured quantities by $\pm 0.02^{o}$ C.

In the actual experiment, two of the four thermocouples were placed inside the calorimeter to measure the ambient temperature around the sample. The readings of the two thermocouples were automatically averaged at pre-set time intervals and the resulting average value of the temperature stored in a specified register in the data logger. The other two thermocouples were attached to the sample (one in front and the other at the back) to measure an average temperature of the sample at the same pre-set time interval

as the average ambient temperature. The data logger (programmed using machine language) displayed on its output screen and printed both the average ambient and sample temperatures every forty (40) seconds on thermal paper from an in-built printer.

The size of the aluminium sample used in the experiment was $5.0\,\text{cm} \times 2.55\,\text{cm} \times 0.1\,\text{cm}$ and weighed $3.40\,\text{g}$ while the copper sample used was $5.0\,\text{cm} \times 2.55\,\text{cm} \times 0.05\,\text{cm}$ and weighed $3.10\,\text{g}$. The samples were placed at the centre of the chamber facing the radiation at an angle depicted in Fig.3-3. The arrangement ensured that the reflected heat from the top surface was reflected severally within the spherical chamber before reaching the focus of the sphere, thus rendering uniform heating of the sample.

The data logger was calibrated using the internal calibration function between the temperature range set at $293\,\text{K}$ for the lower limit and $353\,\text{K}$ for the upper limit. Between these limits the internal program measures each temperature sensed by the thermocouples to either $\pm 0.1\,\text{K}$ or $\pm 0.01\,\text{K}$, depending on whether the temperature readings are programmed to be recorded to one or two decimal places. In the experiment, the internal program was set to give readings to two decimal places.

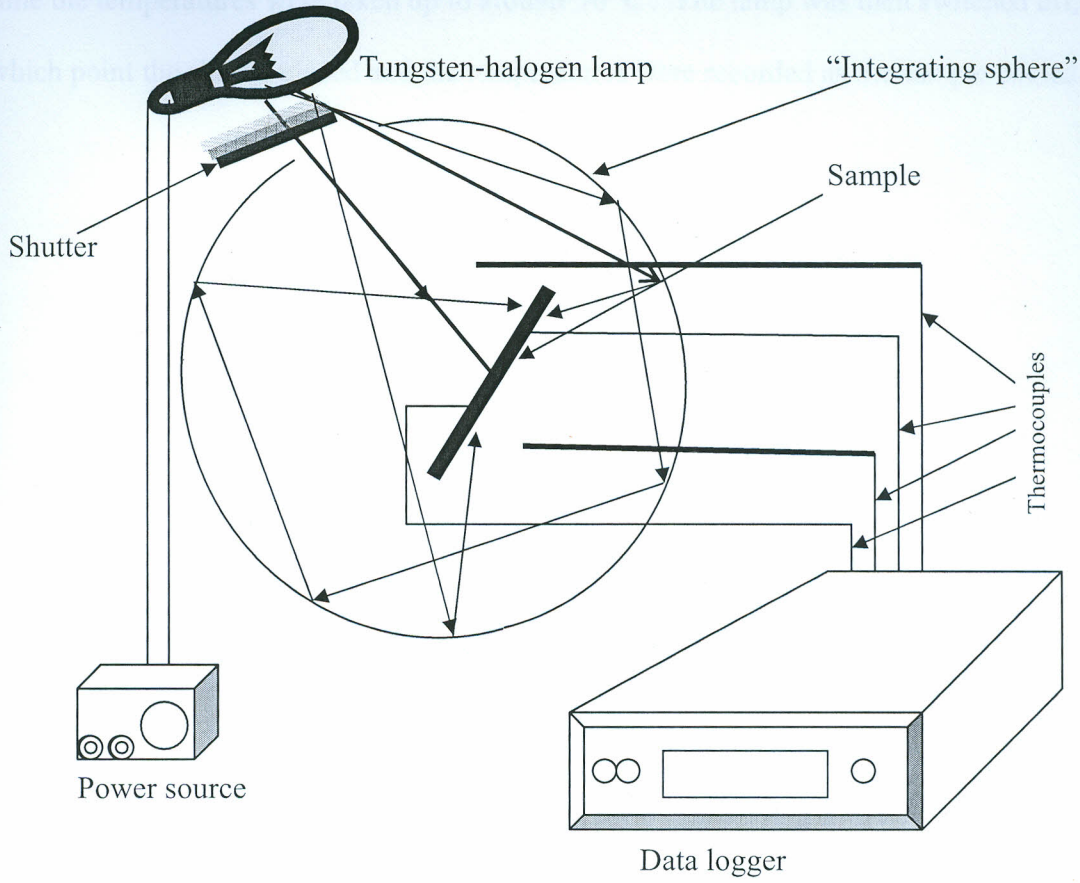

Fig. 4-3. *Experimental set-up for heating and cooling histories of aluminium and copper.*

Precaution had to be taken when measuring the global irradiance by making sure that the voltage and current supplying the lamp was not changed during the experiment, otherwise, different values would be obtained if the voltage was varied. This is comparable to the difference in the irradiance of the sun during different times of the day or even different times of the year.

In the first part of the experiment, by switching the lamp on, the shutter automatically opens and the data logger started recording the temperature rise of the sample (copper and aluminium alternately) to a steady state temperature.

In the second part of the experiment the same procedure was repeated but this time the temperatures were taken up to around 70^0C. The lamp was then switched off, at which point the shutter closed and the temperatures were recorded as the sample cooled.

CHAPTER FIVE

5 RESULTS AND DISCUSSION

5.1 Solar chimney

Using the value of $\beta(\tau)$ at 300K and one atmosphere, Eq. (4.17) was employed to obtain curves shown in Fig.5-1 by calculating and plotting the values of P_i versus τ for various dimensions of the solar chimney. Here τ is the temperature ratio arising from the difference between the collector surface temperature and the temperature of the turbine $(T_s - T_H)$ and the difference between the air mass temperature under the roof and the collector surface temperature $(T_m - T_s)$. The curves clearly show that there are specific threshold values of τ beyond which appreciable power ($\geq 10^3$ watts) can be generated by a solar chimney. Furthermore, beyond these threshold values of τ, the power from the chimney increases exponentially.

As in the case with the voltage-current ($I - V$) characteristics for different diodes in the forward direction where a threshold voltage V_γ exists beyond which the current rises rapidly, the $P_i - \tau$ characteristics shown in Fig.5-1 also show that there is a threshold value of τ above which appreciable energy can be generated by a solar chimney.

The curves show that the minimum threshold value of τ beyond which appreciable power (10^3 watts) can be generated by a viable solar chimney power generating plant with a surface of $360{,}000\,\mathrm{m}^2$ is approximately 2.9. The curves also show that the power increases rapidly after each threshold value of τ for each specified dimension of the chimney.

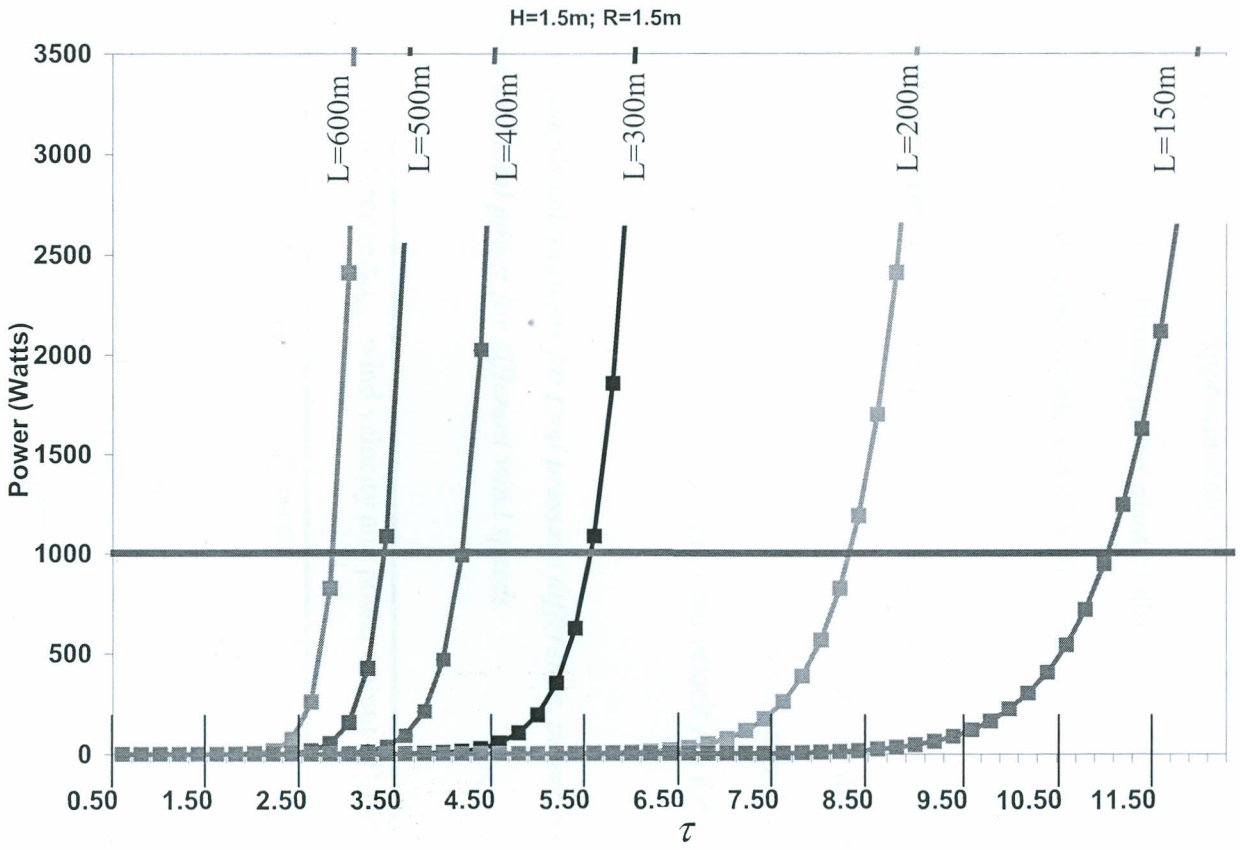

Fig.5-1. *Curves showing simulated power output for solar chimneys of different lengths when* $H = R = 1.5\text{m}$

The dimension of a reasonably sturdy solar chimney power plant that would generate energy of the order of 10^3 watts, for example, is $L = 150\text{m}$, $H = 1.5\text{m}$ and $R = 1.5\text{m}$. This specific dimension requires that $\tau = 10.9$. The length L can be reduced to 50m provided a value of $\tau = 32.9$ is attained inside the chimney. This is, however far beyond the highest attainable value of approximately 15. If a value of $\tau = 15$ can be attained inside the chimney, a solar chimney power plant of dimensions $L = 150\text{m}$, $H = 1.5\text{m}$ and $R = 1.5\text{m}$ would generate approximately 4.47×10^4 watts.

4.2 *Solar pressure-staged wind tunnel* electric power plant

Using Eq. (4.27) and Eq. (4.28) sample calculations of the pressure difference between the centre of the collector in a *solar pressured-staged wind tunnel* power generator are given in Table 5-1 for a few values of the velocity in the tunnel.

Table 5-1: ***Sample calculations for total pressure difference, power for different turbine vane areas and total power for different wind speeds.***

Pressure difference Δp_{tot}, wind velocity and power output (P_2) for sample areas					
Δp_{tot} (Pa)	v (m/s)	P_1 (Watts/m^2)	P_2 (MW) for A=10,000 m^2	P_2 (MW) for A=25,000 m^2	P_2 (MW) for A=50,000 m^2
10.92	2.5	9.10	0.091	0.228	0.455
43.69	5.0	72.81	0.728	1.820	3.640
98.30	7.5	245.74	2.46	6.14	12.99

The simulated power output for the designed *solar pressure-staged wind tunnel* power generating plant for different values of the parameters from Table 5.1 is presented on the curves shown in Fig. 5-2. These results show that if the minimum area swept by the turbine vanes is $10{,}000\,m^2$ then the wind velocity must be about $7.5ms^{-}$ in the tunnel so as to provide approximately 10 kW of electric power. It is also clear from the curves that for a particular wind speed, the power output increases with the cross sectional area swept by the wind. In other words, power increases as the size of the turbine is increased. This requires that the diameter of the tunnel be approximately 100 meters. The result offers an opportunity to estimate the size of turbines for any desired electric power requirement and output for a *solar pressure-staged wind tunnel* electric power plant.

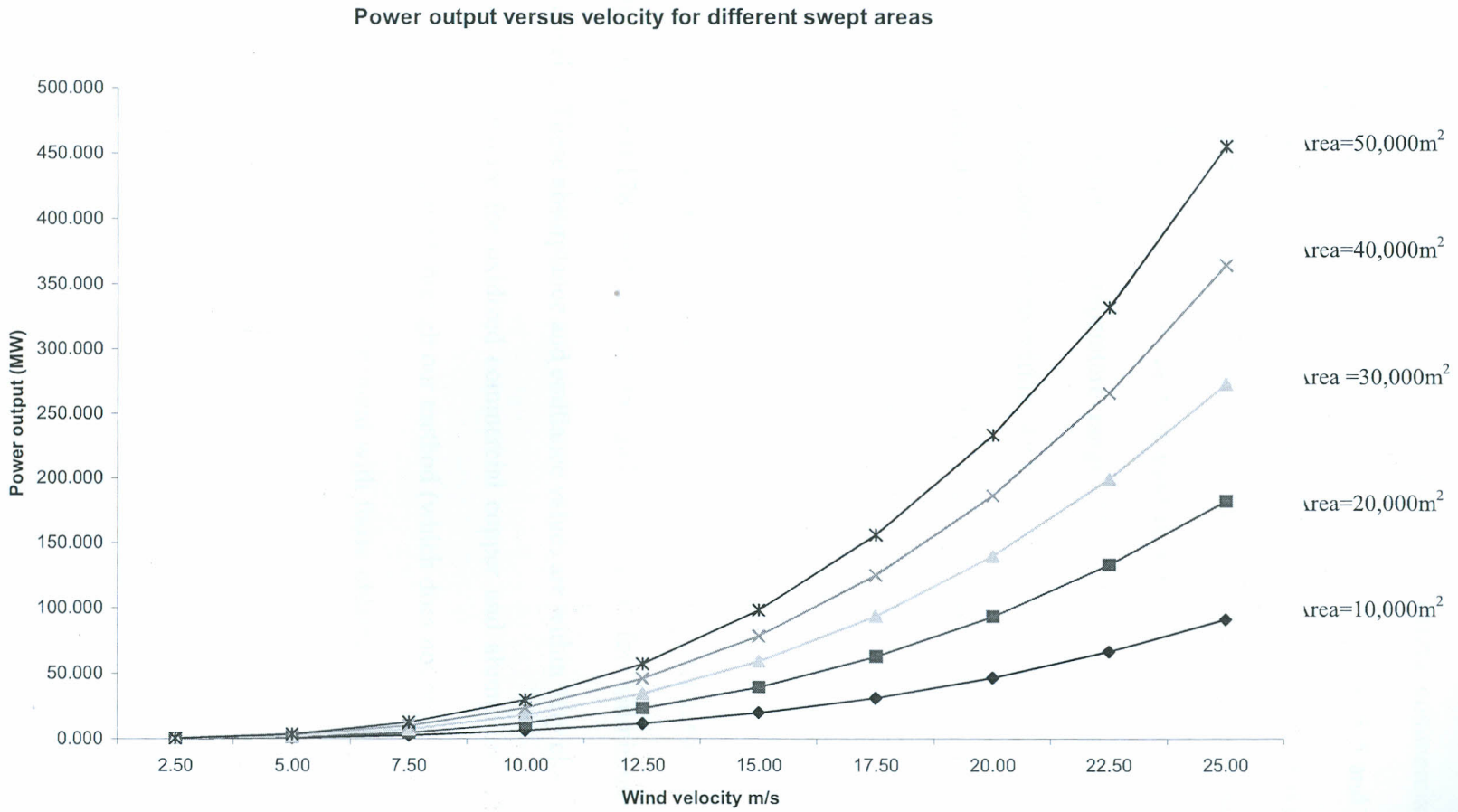

Fig.5-2. *Simulation of power produced by turbines of different diameters and specified wind velocities.*

5.3 Emittance and absorptance of some opaque bulk materials

Figures 5-3 and 5-4 show the graphs obtained for heating commercial samples of aluminium and copper to equilibrium temperatures whereas Figs. 5-5 and 5-6 show the heating and cooling curves. As can be seen from the first two graphs it was found that the steady state temperature for aluminium was 74.15°C whereas the ambient temperature was 73.00°C. When the same values were used in numerical calculations, it was found that, within experimental temperature range $304-347\,\mathrm{K}$, the emittance ε and the absorptance α are constants to within 4% for commercial aluminium [31]. Similar evaluations carried out for copper between the experimental temperature range $300-345\,\mathrm{K}$ also show that the two properties are constant within the same error range of 4%. However, results from the algorithm [29] using raw data have deviations as large as 19% [30] giving $\alpha = 0.123$ and $\varepsilon = 0.204$ for aluminium and $\alpha = 0.365$, $\varepsilon = 0.202$ for copper. By using data from Figs. 4-5 and 4-6, the values obtained for α and ε are $\alpha = 0.100$, $\varepsilon = 0.178$ and $\alpha = 0.325$ and $\varepsilon = 0.240$ for aluminium and copper respectively. These absorptance and emittance values are within very close range to those reported in literature for oxidized commercial copper and aluminium [29, 69, 31, 82, 208]. The values obtained through our method (which does not require that temperatures reach steady state) are in good agreement with those obtained when temperatures reach steady state [69].

Heating curves for aluminium to a steady temperature

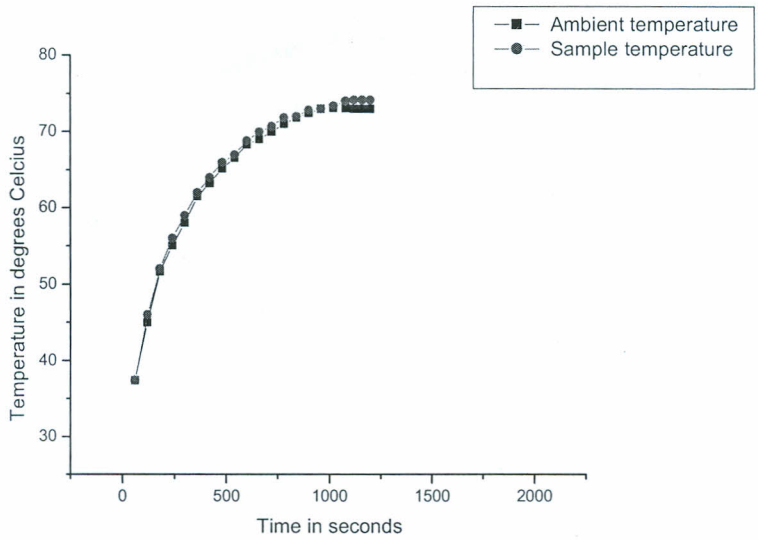

Fig. 5-3. *Graph showing the heating of aluminium up to a steady state temperature with superimposed ambient temperature.*

Heating curves for copper to a steady state temperature

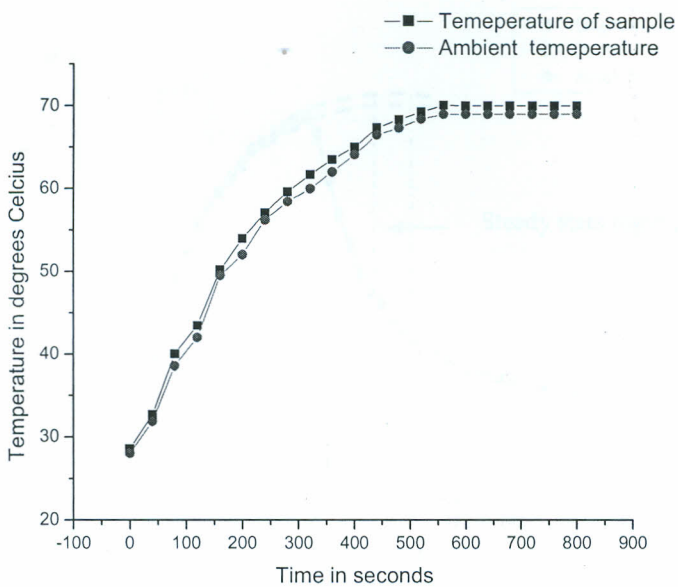

Fig. 5-4. *Graph showing the heating of copper to a steady state temperature with superimposed ambient temperature inside the enclosure.*

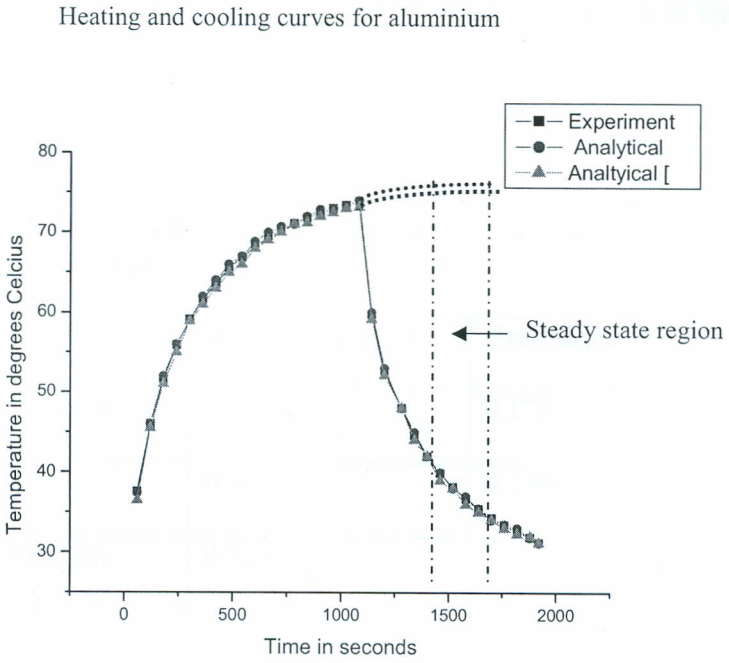

Fig. 5-5. *Graph of heating and cooling for aluminium with superimposed analytical data.*

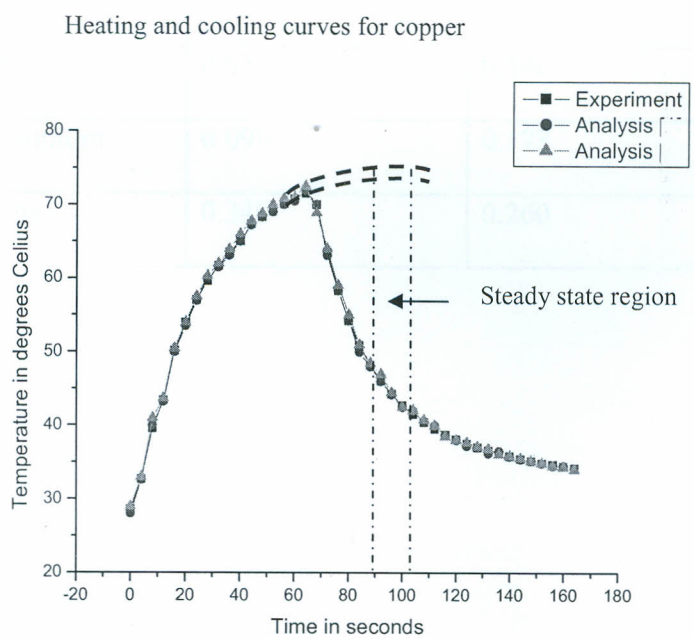

Fig.5-6. *Graph of heating and cooling for copper with superimposed analytical data.*

Table 5-2 summarizes the results and gives a comparison to known values of absorptance and emittance of aluminium and copper.

Table 5-2. ***Comparative values of absorptance and emittance for aluminium and copper from different sources***

Material	**Absorptance (α)**	**Emittance (ε)**	**Source of values**
Aluminium	0.100	0.176	Results in this work
Copper	0.325	0.240	
Aluminium	0.120	-	www.sheldahl.com [209]
Copper	0.300	-	
Aluminium	0.060	-	Jaworske, D. A [82]
Copper	-	-	
Aluminium	0.099	0.174	Otieno *et al* [29]
Copper	0.351	0.246	
Aluminium	0.099	0.178	Kola *et al* [31]
Copper	0.349	0.260	

CHAPTER SIX

6.0 CONCLUSION AND RECOMMENDATION FOR FUTURE WORK

6.1 Conclusion

Solar chimney power stations could make important contributions to the energy supply in Africa and Asia because more than enough space and (insolation) are available in these continents. Although countries such as Sudan, India and Ghana have shown real interest in the technology, all construction plans in these least developing countries have not come to fruition due to exorbitant costs. It is therefore inevitable to develop small power plants for small-scale and medium-scale industries [33].

It has been shown in this thesis that the plotted curves (Fig. 5-1) for simulated typical solar chimney electric power plants of various dimensions are similar to the $I-V$ characteristics of various diodes. The curves show that there exist threshold values of the temperature ratio (τ) arising from the difference between the collector surface temperature and the temperature of the turbine $(T_s - T_H)$ and the difference between the air mass temperature under the roof and the collector surface temperature $(T_m - T_s)$ at which significant power (10^3 W) can be produced by a solar chimney of specific dimensions. Above the threshold values, τ, the instantaneous electric power increases exponentially. It is thus reasonable to say that to generate appreciable power of practical significance, the temperature ratio τ has to be equal to or greater than 2.9. As the length L of the collector surface is increased and the height H of the turbine above the ground or radius R of the turbine reduced, the power generated by the solar chimney plant increases as shown in Fig. 5-1. It is readily deduced that even at 10% efficiency, a solar chimney power plant with the dimensions $L = 150\,\text{m}$, $H = R = 1.5\,\text{m}$, would produce

approximately 4.47×10^{3} W of power, which is sufficient to run a small scale industry or serve approximately fifty (50) households in a rural village. The dimensions $L=150\,\text{m}$, $H=R=1.5\,\text{m}$, give the minimum specifications such a solar chimney power plant that under the given design conditions would produce appreciable energy for the need stated.

A single solar chimney with a suitably large roof area and a high chimney can therefore be designed to generate from 1kW to 200 MW continuously 24 h a day.

Even though solar chimney seem to be a good method of producing electric power cheaply using applied basic physics principles, the results of the second aspect of the study which looked at designing a *solar pressure-staged wind tunnel* electric power plant show that the main parameters influencing appreciable power production are the size of the turbine vanes and the wind velocity inside the tunnel. Results of simulation given in (Fig. 5-2) show that if the minimum area swept by the turbine vanes is $10{,}000\text{m}^2$ then the wind velocity must be about 7.5ms^{-1} in the tunnel so as to provide approximately 10 kW of electric power. This requires that the diameter of the tunnel be approximately 100 meters. This result offers an opportunity to estimate the size of turbines for any desired electric power requirement and output for a *solar pressure-staged wind tunnel* electric power plant.

A novel technique using an integrating sphere calorimeter that has only one port for determination of thermophysical properties of bulk opaque materials from temperature histories of the sample has been designed and tested. The results obtained for the values for absorptance and emittance of commercial aluminium and copper compare well with those obtained using other techniques such as the well established Mathematica procedures [210]. The equations used in our work were tested experimentally and resulted in thermophysical values, which are in good agreement with

values obtained using other methods and calorimeter configurations [69-72, 74, 75, 76]. The experimental results summarised in Table 4-2 obtained from our "integrating sphere" calorimeter gave the absorptance for aluminium as $\alpha = 0.100$ and its emittance as $\varepsilon = 0.176$. For copper $\alpha = 0.325$, $\varepsilon = 0.240$ [80] all of which compare quite well with other known [31] experimental values of $\alpha = 0.099$ and $\varepsilon = 0.178$ for aluminium, $\alpha = 0.349$, $\varepsilon = 0.260$ for copper, respectively.

Based on the analysis of the results obtained in this work, it is reasonable to conclude that using the prescribed configuration of the integrating sphere calorimeter, and methodology, preparation of samples of specific form is not required as has been reported elsewhere in other methods [77, 31, 82, 83, 212]. There is also no need to know the exact mass of the sample because the mass does not appear in the determination of absorptance or emittance in our method.

6.2 Recommendations for future research

Research that has been done on power generation using solar chimney has concentrated on stand-alone systems. Works on solar chimney generating power plant hybrid model systems are rare. In this thesis either, no modelling of solar chimney hybrid system has been carried out. There is, however, need to carry out research to model and develop hybrid systems of solar chimney/solar photovoltaic, solar chimney/solar thermal, or solar chimney/diesel generators and any other viable combinations.

In this work, no cost comparative analysis has been carried out on different systems; hence this forms another area of research topic in renewable energy technologies.

Apart from Onyango, [103] no work has been done on solar energy insolation in Kenya over the past two decades; yet there is unlimited data dating back several years in meteorological stations and sub-stations which can be used to predict insolation and used to draw solar energy maps for many parts of the country. This is necessary for proper planning, implementation and maximum use of solar energy in the country.

Very little research on wind energy potential has been done in Kenya, therefore there is need to carry out more research in this area in order to come up with wind energy data that can be used to draw wind maps so as to make full use of the resource.

The economy of a country relies on energy in one way or another. One cannot talk about future economy without considering energy needs of the nation. There is need to know how many kilowatt hours the population will have and what will be the population by then and factor in the available energy options in order to make reasonable projections for future energy needs. The 2030 vision must therefore take into consideration these energy needs. In other words, there is need to establish the energy per capita for Kenya (energy requirement per person per year at present and for the future).

This therefore, calls for research into possibilities of using other forms of renewable energy such as mini-nuclear power stations based in different small towns and cities.

Solar photovoltaic research in Kenya has had a very uncoordinated trend and it is time documentation be put in place on what has been done, what is being done and what is planned to be done. There is need to develop proper energy policies, training and implementation of solar energy in Kenya. In this respect it is suggested that setting up an energy centre in any of the institutions of higher learning to advice and consult for the ministry of energy in the country. This will be an appropriate step in embarking on

national energy project, training manpower and assessing the energy needs of the country if we expect to achieve development goals as outlined in the 2030 vision development project paper.

Finally, it is suggested that more studies be carried out on materials for solar collector both for the solar chimney and *solar pressure-staged wind tunnel* electric power generating plants with the aim of increasing the efficiencies of the power generating plants and thus reducing the dimensions of the systems.

REFERENCES

[1] Buti, K. and Perlin, J. The golden thread: 2500 years of solar architecture.: Van Nostrand Reinhold Company, N.Y., (1980).

[2] http://images.wikia.com/solarcooking/images/5/51Sam.pdf. (September, 2006)

[3] McMullan, J.T., Morgan, R. and Murray, R.B. Energy Resources. Edward Arnold, London, (1976).

[4] http://www.en.wikipedia.org/wiki/Renewable_energy.(January, 2006)

[5] Onyango, F.N. Private communication.

[6] http://www.en.wikipedia.org/wiki/List_of_energy_development_topics (January, 2006).

[7] Duffie, A. and Beckman, W.A. Solar Engineering of Thermal Processes 2nd edition. John Wiley and Sons Inc., N.Y. (1991).

[8] Harker, J.H. and Backhurst, J.R. Fuel and Energy, Academic press, N.Y., (1981).

[9] Moran, J.M. and Morgan, M.D. Meteorology. 2nd edition. Macmillan Publishing Co. N.Y., (1989).

[10] Bansal, N.K., Kleeman, M., Meliss, M. Renewable Energy Sources and Conversion Technology. Tata McGraw-Hill Publishing Limited, New Delhi. (1990).

[11] Lutgens, F.K. and Tarbuck, E.J. The Atmosphere: An Introduction to Meteorology. 5th Edition. Prentice Hall, Inc., Englewood Cliffs, New Jersey, (1992).

[12] Twidel, J.W. and Weir, A.D. *Renewable Energy Sources*. E and F.N Spon, London, (1987).

[13] Iyer, V. *Scientific Notes* **VI**, No. 63. Indian Meteorological Department, (1948).

[14] Putman, P.C. Power from the Wind. Van Nostrand, N.Y., (1948).

[15] WMO Technical Note No. 175 *Meteorological Aspect of Utilisation of Wind as an Energy Source*. Edited by C. Aspliden *et al.*, WMO, Geneva (1981).

[16] Neil, G. D., Suruders, G. S. Wind Energy Development under the U.K Non-fossil Fuel and Renewables obligations. *Renewable Energy* **6**(7): 701-711 (1995).

[17] Justus, C.G., Hargraves, W.R., Mikhail, A. and Graber, D. Methods for estimating wind speed frequency distributions. *J. Appl. Meteorol.* **17:** 350-353 (1978).

[18] Doran, J.C. and Verhalek, M.G. A note on the vertical vertical extrapolation formulas for Weibull velocity distribution parameters. *J. Appl. Meteorol.* 17: 410-412 (1978).

[19] Sedafain, L. On the vertical extrapolation of mean wind power density. *J. Appl. Meteorol.* **19:** 488-493 (1980).

[20] Gupta, B.K. Weibull parameters for annual and monthly wind speed distributions for five locations in India *Solar Energy* **37:** 469-471 (1986).

[21] Hafzulla, A., Toprak, F., Ali, A. Z., Erdem, U. N. Stochastic generation of hourly mean wind speed data. *Renewable Energy* **29**(14)**:** 2111-2131 (2004).

[22] Satin, A.D., Sen, Z. First-order Markov chain approach to wind speed *modelling. Journal of Wind Engineering and Industrial Aerodynamics* **89:** 263-269 (2001)

[23] Kitagawa, T., Nomura, T. A wavelet-based method to generate artificial wind fluctuation data. *Journal of Wind Engineering and Industrial Aerodynamics* **91:** 943-964 (2003).

[24] Sfestos, A. A comparison of various forecasting techniques applied to mean hourly wind speed time series. *Renewable Energy* **21:** 23-35 (2000).

[25] Incecik, S. and Erdogmus, F. An investigation of the wind power potential on the western coast of Anatoalia. *Renewable Energy* **6**(7): 863-865 (1995).

[26] Ozerdem, B., Turkeli, H.M. Wind energy potential estimation and micrositting on Izmir Institute of Technology Campus, Turkey. *Renewable Energy* **30:** 1623-1633 (2005).

[27] Oludhe, C. and Ogallo, L. Vertical Variation of wind Power. Discovery and Innovation **2:** 73-80 (1990).

[28] http://www.afrepren.org/project/hbf/policy.pdf (January, 2007)

[29] Otieno, F.O., Kola, B.O. and Onyango, F.N. On-line determination of thermophysical properties in an absorption calorimeter. *Meas. Sci. Technol.* **8:** 239-244 (1997).

[30] Otieno, F.O. Analytical method for on-line determination of thermal properties of materials in an absorption calorimeter. *MSc. Thesis.* Department of Physics, University of Nairobi (1996).

[31] Kola, B.O., Mulwa, W. and Mate, P. A transient technique for determination of thermophysical properties in an absorption calorimeter. *Meas. Sci. Technol.* **6** 888-892. (1995).

[32] Willrath, H. and Smith, G.B. A new transient temperature emissiometer. *Solar Energy Materials* **4:** 31-46. (1980).

[33] Onyango, F. N., Ochieng, R. M. The potential of solar chimney application in rural areas of developing countries. *Fuel* ***85*****:** 2561-2566 (2006).

[34] Padki, M.M., Sherif, S.A. Solar chimney for power generation in rural areas. Seminar on Energy Conservation and Generation through Renewable Resources, Ranchi, India, 91-96 (1989b).

[35] Padki, M.M., Sherif, S.A. A mathematical model for solar chimneys. In Proceedings of 1992 Renewable Energy Conference, Amman, Jordan, Vol. 1, 289-294 (1992).

[36] Padki, M.M., Sherif, S.A. Solar chimney for medium to large scale power generation. In proceedings of the Manila International Symposium on Development and Management of Energy Resources, Manila, Philippines, 1, 432-437 (1989a).

[37] http://www.windfromthesun.com/pdf/WindfromtheSun.pdf. (January, 2007)

[38] http://en.wikipedia.org/wiki/Solar_updraft_tower (January, 2007)

[39] Gunther, H. In hundert Jahren-Die küngfige Energieversorgung der Welt, Kosmos, Gesellshcaft der Naturfeunde, Franckh'shce, Stuttgart (1931).

[40] Schlaich, J. The solar chimney: electricity from the sun. In: Maurer C, editor. Germany: Geislingen; (1995).

[41] Haaf, W., Friedrich, K., Mayr,G., Schlaich, J. Solar chimneys, part I: principle and construction of the pilot plant in Manzanares. *Int J Solar Energy* **2:** 3–20. (1983)

[42] Haaf, W. Solar chimneys, part II: preliminary test results from the Manzanares pilot plant. *Int J Solar Energy* **2:** 141–61. (1984).

[43] Schlaich, J., Bergermann, R., Schiel, W. Weinrebe, G. Design of commercial solar updraft tower systems-utilization of solar induced convective flows for power generation. *J. Solar Energy Eng.* **127:** 117–24 (2005).

[44] von Backström, T.W., Gannon, A.J. Compressible flow through solar power plant chimneys. *J. Solar Energy Eng.* **122:** 138–45. (2000).

[45] Schlaich, J., Bergermann, R., Schiel, W., Weinrebe, G. Sustainable electricity generation with solar updraft towers. *Structural Engineering International.* Vol. **3**. (2004).

[46] Schlaich, J. The Solar Chimney. Edition Axel Menges, Stuttgart, Germany (1995).

[47] Krisst, R.J.K. Energy transfer system. *Alternative Source Energy* **63:** 8–11, (1983).

[48] Kulunk, H. A. Prototype solar convection chimney operated under Izmit conditions. In: Proceedings of the 7th Miami International Conference on Alternative Energy Sources Veiroglu T.N. (ed.) Vol. 162, (1985).

[49] Pasurmarthi, N. Sherif, S.A. Performance of a demonstration solar chimney model for power generation. In: Proceedings of the 1997 35th heat transfer and fluid mechanics conference, Sacramento, California, USA 203–40, (1997).

[50] Schlaich, J. and Schiel, W Solar Chimneys. *Encyclopedia of Physical Science and Technology*, 3rd Edition, Academic Press, London (2001).

[51] Castillo, M.A. A new solar chimney design to harness energy from the atmosphere. Spirit of Enterprise: The 1984 Rolex Awards, 58-59 (1984).

[52] Ong, K.S. A mathematical model of a solar chimney. *Renewable Energy* **28:** 1047-1060 (2003).

[53] Dai, Y.J., Huang, H.B., Wang, R.Z. Case study of solar chimney power plants in North-western regions of China. *Renewable Energy* **28:** 1295-1304 (2003).

[54] Bernardes, dos S. M.A. and Weinrebe, A.Voβ. A. Thermal and technical analyses of solar chimneys. *Solar Energy* **75**: 511-524 (2003).

[55] www.visionengineer.com (July, 2008).

[56] Yang, J.K., Li, J., Xiao, B. Li, J.J., Zhang, J.F., Ma, Z.Y. A novel technology of solar chimney for power generation. *Acta Energinae Solaris Sinica* **24**(4):565-570, (2003).

[57] http://energy.seekingalpha.com/article/14935 (July, 2008).

[58] Koenigsberger, O.H., Ingersol, T.G., Mayhew, A. and Szokolay, S.V. Manual of tropical Housing and Building. Part I: Climate Design, Longmans, London. (1977).

[59] Kittler, R. Standardization of Solar Radiation with regard to prediction of Insulation and Shading of Buildings. Symposium Teaching the Teachers on Building Climatology, Stockholm, Paper 45, vol.2. (1975).

[60] Cole, R.J. Direct Solar Radiation data as Input into Mathematical Models Describing the Thermal Performance of Buildings-1. A review of Existing Relationships. *Building and Environment.* **11**(3)**:** 173-179 (1976).

[61] Burberry, P. Building for energy conservation: The Architectural Press Ltd., London (1978).

[62] Adelard, L., Pignolet-Tardan, F., Mara, T., Lauret, P., Garde, F. and Boyer, H. Sky temperature Modelization and Application in Building Simulation. *Renewable Energy.* **16**(1-4)**:** 418-430 (1999).

[63] Gan, G., Awbi, H.B. Numerical Simulation of the Indoor Environment. *Building and Environment.* **29:** 449-459 (1994).

[64] Shaviv, E. Computer Aided Conscious Building Design. *Solar Energy* **15**(1-4): 343-348 (1998).

[65] Yezioro, A. and Shaviv, E. Design Tools for Analyzing Mutual Shading Between Buildings. *Solar Energy* **52**(37): 27-37 (1994).

[66] Taheri, M. and Shafie S. A case study on the reduction of energy use for the heating of buildings. *Renewable Energy.* **7:** 673-678 (1995).

[67] Garg, H.P., and Kandpal, T.C. Laboratory Manual on Solar Thermal Experiments. Narosa, New Delhi. (1999).

[68] Maatouk, K. and Shigenao, M. Theoretical approach of a flat plate solar collector with clear and low-iron glass covers taking into account the spectral absorption and emission within glass cover layers. *Renewable Energy.* **30:** 1177-1194 (2005).

[69] Allen, L.C., Wallace, J., Deutsher, G. and Lindenfed, P. Measurement of optical absorption by calorimetry and analysis of solar collector *Am. J. Phys* **56(1):** 53-57 (1988).

[70] Beens, W.W., Sillkens, M. and Vester, J.L. An emmisiometer with high accuracy for determination of the total hemispherical emmitance of surfaces. *J.Phys. E: Sci. Instum* **13:** 873-876 (1980).

[71] Cheng, S.X., Ge, X.S., Li, J.A. and Feng, H.Q. A transient calorimeter pyreliometer of high accuracy. *Solar Energy* **45:** 79-83. (1999).

[72] Jaluria, Y. and Torrance, K.E. Computational heat transfer (Washington: Hemisphere. (1986).

[73] Choba, A.V., Pasichnyi, V. V., Pilipovskii, Yu.L. and Pereselentseva, L.N. Calculation of the thermophysical properties of tungsten-copper pseudoalloys, *Journal of Powder Metallurgy and Metal Ceramics*, **22**(8)**:** 639-644 (1983).

[74] Smith, G.B. and Willbrath, H. Calorimetric emissivities for solar-selective coatings on flat sheets. *J. Phys. E: Sci. Instrum.* **12:** 79-83. (1979).

[75] Pettit, R.B. and Sowell, R.R. Solar absorptance and emmitance properties of several coatings. *J. Vac. Sci. Technol.* **13(2):** 596-602. (1976).

[76] Timans, P.J. The experimental determination of the temperature dependence of the total emissivity of *GaAs* using a new temperature measurement technique *J. Appl. Phys.* **72(2):** 660-670. (1992).

[77] Faouzi, G., Taoufik, G., Marine, L., Rémi, C. and Jean, J.G. Influence of microroughness on emissivity *Journal of Applied Physics* **96:** 2656-2664 (2004).

[78] http://www.freepatentsonline.com/6424413.html (February, 2005)

[79] Lide, D. R. (ed.,) *Handbook of Chemistry and Physics,* 1994 72nd Edition, CRC Press, U.S.A.

[80] Ochieng, R.M., Onyango, F.N. and Owino, A.J. Determination of global absorptivity and emissivity of some opaque bulk materials using an integrating sphere calorimeter without ports. *Meas. Sci. Technol.* **18:** 2667-2672 (2007).

[81] http://www.oceanoptics.com/Products/ispref.asp (February, 2005)

[82] Cheng, S.X., Ge, X.S., Li, J.A. and Feng, H.Q. A transient calorimeter pyreliometer of high accuracy. *Solar Energy* **45:** 79-83. (1999).

[83] Willrath, H. and Smith, G.B. A new transient temperature emissiometer. *Solar Energy Matter* **4:** 31-46 (1980).

[84] Tiwari, G.N., Sangeeta, S. Solar Thermal Engineering Systems. New Delhi. Narosa Publishing House, (1997).

[85] Teddy, B. C. A comparative study of Copper and Nickel-pigmented anodised Aluminium coatings for solar energy absorption, PhD. Thesis, The University of Zambia, Lusaka, January (2004)

[86] Gier, J.T. and Dunkel, R.V. Trans. Int. Conf. Solar Energy, Vol II, Part I, Sec. A, 41-45 (1955).

[87] Tabor, H. In Solar Energy Conversion, edited by A.E. Dixin and J.D. Leslie, Pregamon, (1979).

[82] Ångström, A. Solar and terrestrial radiation *Qr. J Roy. Meteorol. Soc.* **50:** 121-129 (1924).

[89] Black, J.N., Bonython, C.W., Prescott, J.A. Solar radiation and the duration of sunshine. *Quarterly Journal of the Royal Meteorological Society* **80:** 231-235 (1954).

[90] Prescott, J.A. Evaporation from water surface in relation to solar radiation, *Transactions of the Royal Society of South Australia* **60:** 114-118 (1940).

[91] Liu, B.Y.H., Jordan, R.C. The interrelationship and characteristic distribution of direct, diffuse and total solar radiation. *Solar Energy* **4(3):** 1-19 (1960).

[92] Iqbal, M. Correlation of average diffuse and beam radiation with hours of bright sunshine. *Solar Energy* **23:** 169-173 (1979).

[93] Hay, J.E. Calculation of monthly mean solar radiation for horizontal and inclined surfaces. *Solar Energy* **23:** 301-307 (1979).

[94] Khogali, A. Ramadhan, M.R.I., Ali, Z.H.E., Fatah, Y.A. Diffuse solar irradiation in Yemen. *Solar Energy* **31(1):** 55-62 (1983).

[95] Page, J.K. The estimation of monthly mean values of daily total short wave radiation on vertical and inclined surfaces from sunshine records for latitudes 40^0 N - 40^0 S. Proceedings of U.N. Conference on New Sources of Energy, Paper No. 358/98, Vol. 4, 378-390 (1961).

[96] Abdalla, Y.A.G., Baghdady, M.K. Global and diffuse radiation in Doha (Qatar). *Solar and Wind Technology* **2**(3/4)**:** 209-212 (1985).

[97] Abdalla, Y.A.G., Faregh, G.M. Contribution to the study of solar radiation in Abu Dhabi. *Energy Conversion and Management* **28**(1)**:** 63-67 (1988).

[98] Davies, J.A., Estimation for insolation for West Africa. *Quarterly Journal of the Royal Meteorological Society* **91:** 359-363 (1965).

[99] Soler, A. On the correlation between normal direct radiation and global radiation for clear and over cast skies. *Solar Energy* **34:** 517-520 (1985).

[100] Frangi, J.P., Yahaya, S., Piro, J. Characteristic of radiation in the Sahel. Case study; Niamey, Niger. *Solar Energy* **49(3):** 159-166 (1992).

[101] Awachie, I.R.N., Okeke, C.E. Measurement of solar energy radiation at Nsukka and the determination of the regression constants. *Energy Conversion and Management* **28**(4): 295-302 (1988).

[102] Vignola, F., McDaniels, D.K. Beam-global correlation in the Pacific Northwest. *Solar Energy* **36:** 409-418 (1986).

[103] Onyango F.N. On the estimation of global solar insolation. *Solar Energy* **31:** 69-71 (1983).

[104] Alvi, S.H., Abdalla, Y.A.G. Estimation of solar radiation from Oman. *International Journal of Ambient Energy* **13:** 11-18 (1992).

[105] Tadros, M.T.Y. Uses of sunshine duration to estimate the global solar radiation over eight meterorological stations in Egypt. *Renewable Energy* **21:** 231-246 (2000).

[106] Udo, S.O. and Aro, T.O. Measurement of global solar global photosynthetically-active and downward infrared radiations at Ilorin, Nigeria. *Renewable Energy* **17**(1): 113-122 (1999).

[107] Can, E. and Osman, Y. Estimation of monthly average daily global radiation on horizontal surface for Antalya (Turkey). *Renewable Energy* **17**(1): 95-102 (1999).

[108] Rerhrhaye, A., Zehaf, M. and Flechon, J. Estimation of direct beam from seasonal correlations. *Renewable Energy* **6**(7): 779-785 (1995).

[109] Ododo, J.C., Sulaiman, A.T., Aidan, J., Yuguda, M.M. and Ogbu, F.A. The importance of maximum air temperature in the parameterization of solar radiation in Nigeria. *Renewable Energy* **6**(7): 751-764 (1995).

[110] Abdalla, Y.A.G., Al-Madani, H.M.N. A new method for estimating daily global solar radiation. *International Journal of Ambient Energy* **13:** 93-98 (1992).

[111] Samuel T.D.M.A. Estimation of global radiation for Sri Lanka. *Solar Energy* **47:** 333-337 (1991).

[112] Zeroual, A., Ankrim, M. and Wilkinson, A.J. Stochastic modelling of daily global solar radiation measured in Marrakesh, Morocco. *Renewable Energy* **6**(7): 787-793 (1995).

[113] Haught, A.F. Physics of solar energy conversions. *J. Solar Energy Engng.* **106:** 3-15 (1984).

[114] Badescu, V. The Lambertian geometric factor of the solar radiation flux emitted by a spherical source of black-body radiation. *Europhys. Lett.* **14**: 309-311 (1991).

[115] Cordon, F.M. and Hochman, N. On correlation between beam and global radiation. *Solar Energy* **32:** 329-336 (1984).]

[116] Luhanga, P.V.C. Solar u.v. radiation at Gaborone, Botswana. *Renewable Energy* **6**(7): 795-162 (1988).

[117] Jain, P.C. Comparison of techniques for the estimation of daily global irradiation and a new technique for the estimation of hourly global irradiation. *Solar and Wind Technology* **1**(2): 123-134 (1984).

[118] Khogali, A. and Al-Bar, O.F. A study of solar ultraviolet radiation. *Solar Energy* **48**: 79-87 (1992).]

[119] Babatunde, E.B. and Aro, T.O. Relationship between "clearness index" and "cloudiness index" at a tropical station (Ilorin, Nigeria). *Renewable Energy* **6**(7) 801-805 (1995).

[120] Maduekwe, A.A.L. and Chendo, M.A.C. Predicting the components of total hemispherical solar radiation from sunshine duration measurement in Lagos, Nigeria. *Renewable Energy* **6**(7): 807-812 (1995).

[121] Hay, J.E. A revised method for determining the direct and diffuse components of the total short-wave radiation *Atmosphere* **14**: 278-287 (1976).

[122] Bamiro, O.A. Empirical relation for the determination of solar radiation in Ibadan, Nigeria. *Solar Energy* **31**: 85-94 (1983).

[123] Sambo, A.S. The measurement and prediction of global and diffuse components of solar radiation for Kano in Northern Nigeria. *Solar Wind Technol.* **5**: 1-5 (1998).

[124] Ruth, D.W. and Chant, R.E. The relationship of diffuse radiation to total radiation in Canada. *Solar Energy* **18**: 153-154 (1976).

[125] Reindl, D.T., Beckman, W.A. and Duffie, J.A. Diffuese fraction correlations. *Solar Energy* **45**: 1-8 (1990).

[126] Al-Hamadani, N., Al-Riahi, M. and Tahir, K. Estimation of daily and monthly average global radiation for Fudhaliyah, Baghdad (Iraq). *Solar Energy* **42:** 81-85 (1989).

[127] Jain, S. and Jain, P.C. A comparison of the Ångström-type correlations and the estimation of monthly average daily global irradiation. *Solar Energy* **40**(2): 93-98 (1988).

[128] Gopinathan, K.K. An assessment on the availability of solar radiation intensity. *Renewable Energy* **4**: 125-129 (1991).

[129] Chou, M.D. Surface radiation in tropical pacific. *J. Climate Appl. Meteorol.* **24:** 83-92, (1985).

[130] Swartman R.K., Ogunlade, O. Solar radiation from common parameters. *Solar Energy* **11:** 170-172 (1967).

[131] Badescu, V. Verification of some very simple clear and cloudy sky models to evaluate global solar irradiance. *Solar Energy* **62**(4): 251-264 (1997).

[132] Alnaser, W.E., Al-Attar, R. Simple models for estimating the total, diffuse, direct and normal solar irradiation in Bahrain. *Renewable Energy* **18:** 417-432, (1999).

[133] Ahmet, A., Shafiqur, R. Global solar radiation in Northeastern Saudi Arabia. *Renewable Energy* **17:** 461-472 (1999).

[134] Elagib, N.A., Alvi, S.H., Mansell, M.G. Correlationship between clearness index and relative sunshine duration for Sudan. *Renewable Energy* **17:** 473-498 (1999).

[135] Reddy, S.J. An empirical method for the estimation of total solar radiation. *Solar Energy* **13:** 289-290 (1971).]

[136] Barra, A.O. Estimation of total solar radiation form meteorological data in the Italian climate area. *Solar Energy* **31:** 427-428 (1983).

[137] Rehman, S., Halawani, T.O. Global solar radiation estimation. *Renewable Energy* **12:** 369-385 (1997).

[138] Zuhairy, A., Sayigh, A.M. Simulation and modelling of solar radiation in Saudi Arabia. *Renewable Energy* **6:** 107-118 (1995).

[139] Jain, P.C. Global irradiation estimation for Italian stations. *Solar and Wind Technology* **3**(4): 323-328 (1986).

[140] Kuye, A., Jagtap, S.S. Analysis of solar radiation data for Port Harcourt, Nigeria. *Solar Energy* **49:** 139-145 (1992).

[141] Benson, R.B., Paris, M.V., Sherry, J.E., Justus, C.G. Estimation of daily direct, diffuse and global solar radiation from sunshine duration measurements. *Solar Energy* **32**(4): 523-535 (1984).

[142] Michalsky, J.J. Comparison of a National Weather Service foster sunshine recorder and the World Meteorological Organisation standard for sunshine duration. *Solar Energy* **48**(2): 133-141 (1992).

[143] Ahmed, I., Al-Hamadani, N., Ibrahim, K. Solar radiation maps for Iraq. *Solar Energy* **31**(1): 29-44 (1983).]

[144] Õgleman, H., Ecevit, A., Tasdemiroglu, E. A new method for estimating solar radiation from bright sunshine data. *Solar Energy* **33**(6): 619-625 (1984).

[145] Feuillard, T., Abillon, J.M., Bonhomme, R. Relationship between global solar irradiation and sunshine duration in Guadeloupe. *Solar Energy* **43**(1): 359-361 (1989).

[146] Singh, G.M., Bhatti, S.S. Statistical comparison of global and diffuse solar radiation correlation. *Energy Conversion and Management* **30**(2): 155-161, (1990).]

[147] Topcu, S., Dilmac, S., Aslan, Z. Study of hourly solar radiation in Istanbul. *Renewable Energy* **6**(2): 171-174 (1995).

[148] Akinoglu, B.G., Ecevit, A. Construction of a quadratic model using modified Ångström coefficients to estimate global solar radiation. *Solar Energy* **45**(2): 85-92 (1990).

[149] Tasdemiroglu, E., Sever, R. An improved correlation for estimating solar radiation from bright sunshine data for Turkey. *Energy Conversion and Management* **31**(6): 599-600 (1991).

[150] Maduekwe, A.A.L., Chendo, M.A.K. Predicting the components of the total hemispherical solar radiation from sunshine duration measurements in Lagos, Nigeria. *Renewable Energy* **6**(7): 807-812 (1995).

[151] Drake, F., Mulugetta, Y. Assessment of solar and wind energy resources in Ethiopia I. *Solar Energy* **57**(3): 205-217 (1996).

[152] Singh, O.P., Srivasta, S.K., Gaur, A. Empirical relationship to estimate global radiation from hours of sunshine. *Energy Conversion and Management* **37**(4): 501-504 (1996).

[153] Inci, T. T., Hasan, T., Duygu, E. Estimation of global solar radiation under clear sky radiation in Turkey. *Renewable Energy* **21:** 271-287 (2000).

[154] Inci, T. T., Hasan, T., Duygu, E. Estimation of global solar radiation from sunshine duration measurement in Elaziğ. *Renewable Energy* **19:** 587-595 (2000).

[155] Glover, J., McCulloch, J.S.G. The empirical relation between solar radiation and hours of sunshine in high altitude tropics. *Quarterly Journal of Royal Meteorological Society.* **84:** 56-60 (1958).

[156] Almorox, J., Benito, M., Hontoria, C. Estimation of monthly Ångström-Prescott equation coefficients from measured daily data in Toledo Spain. *Renewable Energy,* **30**: 931-936 (2005).

[157] Tiba, C., de Aguiar, R., Fraidenraich, N. Analysis of a new relationship between monthly global irradiation and sunshine hours from a database of Brazil. *Renewable Energy* **30:** 957-966 (2005).

[158] Righini, R., Grossi, G.H., Raichijk, C. Approach to drawing new global solar irradiation contour maps for Argentina. *Renewable Energy* **30**(8): 1241-1255 (2005).

[159] Bird, R. E. and Hulstrom, R. L. *Simplified Clear Sky Model for Direct and Diffuse Insolation on Horizontal Surfaces.* Technical Report No. SERI/TR-642-761, Golden, C.O: Solar Energy Research Institute, (1981).

[160] Bird, R. E. and Riordan, C. J. Simple Solar Spectral Model for Direct and Diffuse Irradiance on Horizontal and Tilted Planes at the Earth's Surface for Cloudless Atmospheres. *Journal of Climate and Applied Meteorology* Vol. **25**(1)**:** 87-97 (January 1986).

[161] Maxwell, E. L. *A Quasi-Physical Model for Converting Hourly Global Horizontal to Direct Normal Insolation.* Technical Report No. SERI/TR-215-3087, Golden, CO: Solar Energy Research Institute, (1987).

[162] Gueymard, C. A. Parameterized transmittance model for direct beam and circumsolar spectral irradiance. *Solar Energy.* **71**(5)**:** 325-346 (2001).

[163] Randall, C.M., Whitson, M.E.Jr. Hourly Insolation and Meteorological data Base Including Improved Direct estimates. Aerospace Report No. ART-78(7592)-1, El Segundo, CA: The Aerospace Corporation, (December 1977).

[164] Ezekwe, C.I. and Exeilo, C.O.C. Measured Solar Radiation in a Nigerian Environment Compared with Predicted Data. *Solar Energy.* **26:** 182-186 (1981).

[165] Aliyu, A.G. and Sambo, A.S. Development of a Model for computing the Total Component of Solar Radiarion in Sokoto. *Nigerian Journal of Renewable Energy.* **2**(2): 10-17 91991).

[166] Adeyemo, S.B. Estimation of Direct Solar Radiation Intensities. *Nigerian Society of Engineers Technical Transactions* **32**(1)**:** 1-11 (1997).

[167] Aksoy, B. Estimated Monthly average Global Radiation for Turkey and Comparison with Observation. *Renewable Energy.* **10**(4): 625 (1997).

[168] Nguyen, B.T. and Pryor, T.L. The Relationship Between Global Solar Radiation and Sunshine duration in Vietnam. *Renewable Energy* **11**(1)**:** 47-60 (1997).

[169] Luhanga, P.V.C. and Nijegorodov, N. Investigation of solar radiation in Botswana and some anomalous phenomenon observed. *Renewable Energy* **12**(4)**:** 401-408 (1997).

[170] Harris, B. University Physics, John Wiley: New York, (1991).

[171] Swinbank, W.C. *Quarterly Journal of Royal Meteorological Society* **89**: (1963).

[172] Bliss, R.W. *Solar Energy.* **5:** 103-109 (1961).

[173] Brunt, D. Notes on Radiation in the Atmosphere. *Quarterly J. Royal Meteorological Soc*, **58:** 389-396 (1932).

[174] Berdahl, P. and Martin, M. Emissivity of clear Skies. *Solar Energy*, **32**: 5 (1984).

[175] Ojosu, J.O. and Salawu, R.I. A survey of Wind Energy Potential in Nigeria. *Solar and Wind Technology* 7: (1990).

[176] Huschke, R.E. *Glossary of Meteorology.* American Meteorological Society. 45 Beacon St., Boston, Mass. 02108 (1980).

[177] Arya, S.P. Introduction to Micrometeorology. Academic, New York, (1988).

[178] Rizk, M. Wind Characteristics and the Available Wind Energy in Egypt. *Solar and Wind Technology* **4:** 45-52 (1978).

[179] Musgrove, P.J. Wind Energy Conversion: Recent Progress and Future Prospects. *Solar and Wind Technology* **4:** 37-49 (1989).

[180] Warne, D.F. *Wind Power Equipment.* E and F.N. Spon. London (1982).

[181] Lysen, E.H. Introduction to Wind Energy. Steering Committee for Wind Energy in Developing Countries. Amersfoort, Netherlands (1982).

[182] Faregh, G.M. Wind Energy Potential in Bahrain. *Energy Conversion and Management*, **34:** 321-327 (1993).

[183] Pashardes, S. and Christophides, C. Statistical Analysis of Wind speed and Duration in Cyprus. *Solar and Wind Technology* **55:** 405-414 (1995).

[184] Hennessey, J.P. Jr. A Comparison of Weibull and Rayleigh Distributions for Estimating Wind Power Potential. *Wind Engineering* **2:** 156-164 (1978).

[185] Stevens, M.J.M., Smulders, P.T. The Estimation of Parameters of the Weibull Wind Speed Distribution for Energy Utilisation Purposes. *Wind Engineering* **2:** 132-145 (1979).

[186] Jaramillo, O.A., Borja, M.A. Wind speed analysis in La Ventosa, Mexico: a bimodal probability distribution case. Renewable Energy **29:** 1613-1630 (2004).

[187] Nfaoui, H., Bahraui, J., Darwish, A.S. and Sayigh, A.A.M. Wind Energy potential in Morocco. *Solar and Wind Technology* **1:** (1991).

[188] Blanchard, M., Desrechors, G. Generation of auto-correlated wind speed for wind energy conversion system studies. *Solar Energy* **33:** 571-579 (1984).

[189] Chou, K.C., Corotis, R.B. Simulation of hourly wind speed and array wind power. *Solar Energy* **26:** 199-212 (1981).

[190] Bernard, J.C. An evaluation of three models designed for sitting wind turbines in areas of complex terrain. *Solar Energy* **46:** 283-294 (1991).

[191] Betz ADie Naturwissenschaften XV, N46, 10th November (1927).

[192] Shepard, M.L., Chaddock. J.B., Cocks, F.H. and Harman, C.M. Introduction to Energy Technology. Ann Arbor Science Publishers Inc., Michigan, (1976).

[193] Unger, J. Konvektionsströ. Teubner, Stuttgart (1988)],

[194] http://home.iitk.ac.in/~sghorai/NOTES/benard/node2.html (March, 2005)

[195] http://www.windpower.org/en/stat/units.htm (March, 2005)

[196] Incropera, F. P. and DeWitt, D. P., Fundamentals of Heat and Mass Transfer, John Wiley, New York, (1996).

[197] Monteith, J. Principles of Environmental Physics, Edward Arnold (1973).

[198] Garg, H.P., and Kandpal, T.C. Laboratory Manual on Solar Thermal Experiments. Narosa, New Delhi (1999).

[199] Solar Selective Coatings. In Reviews of Renewable Energy Resources Volume 2, edited by Sodha, M.S., Mathur, S.S., Malik, M.A.S. Wiley Western Limited New Delhi, India. (1984).

[200] http://www.oceanoptics.com/Products/ispref.asp (February, 2005)

[201] Welty, J.R., Wicks, C.E., Wilson, R.E. Fundamentals of Momentum, Heat, and Mass Transfer. Singapore: John Wiley (1995.).

[202] http://groups.yahoo.com/group/awea-wind-home/message/7677 (February, 2005).

[203] http://groups.yahoo.com/group/awea-wind-home/message/996 (February, 2005).

[204] http://www.met.tamu.edu/class/Metrl5l/tut/seabr/sea9.html (February, 2005).

[205] http://groups.yahoo.com/group/awea-wind-home/message/7677 (February, 2005).

[206] http://rredc.nrel.gov/solar/old data/nsrdb/atlas/redbook (February, 2005).

[207] Atlas for the Solar Radiation Data Manual for Flat-Plate and Concentrating Collectors. U.S. Solar Radiation Resource Maps. Values derived from the 1961-1990 National Solar Radiation Data Base (NSRDB).

[208] Lide, D.R. *Handbook of Chemistry and Physics,* 72nd edn Boca Raton, FL: CRC Press (1994).

[209] http://www.sheldahl.com (February, 2005)

[210] Wolfram S. *Mathematica: A System for Doing Mathematics by Computer* Addison-Wesley, N.Y., (1991).

[211] Timans, P.J. The experimental determination of the temperature dependence of the total emissivity of *GaAs* using a new temperature measurement technique *J. Appl. Phys.* **72(2):** 660-670 (1992).

[212] Singh, R.K., Prakash K. On Crystal Binding and Thermophysical Properties of Copper and Thallium Halides, *Journal of the Physical Society of Japan*, **51:** 141-150 (1982).